DYNAMIC RUPTURE PROCESS OF THE 1999 DÜZCE EARTHQUAKE

by

Feyza Nur BEKLER

B.S., Geophysical Engineering, Istanbul Technical University, 1997

M.S., Geophysics, Boğaziçi University, 2004

Submitted to the Kandilli Observatory and
Earthquake Research Institute in partial fulfillment of
the requirements for the degree of
Doctor of Philosophy

Graduate Program in Geophysics
Boğaziçi University
2018

DYNAMIC RUPTURE PROCESS OF THE 1999 DÜZCE EARTHQUAKE

APPROVED BY:

Assoc. Prof. Dr. Ali Özgün Konca (Thesis Supervisor)	……
Prof. Dr. Nurcan Meral Özel (Thesis Co-supervisor)	……...
Prof. Dr. Şerif Barış	……
Prof. Dr. Semih Ergintav	……
Assoc. Prof. Dr. Gülüm Tanırcan	……
Assoc. Prof. Dr. Serkan Irmak	……

Dedicated to my daughters

Zeynep Nur Bekler & Elif Nur Bekler

ACKNOWLEDGEMENTS

I would like to thank my thesis supervisor Prof. Dr. Nurcan Meral Özel, for making this dissertation possible. Prof. Dr. Özel has provided me with guidance, support, advice and an unwavering interest in my thesis scope. Perhaps most importantly she has taught me how to think critically and independently about my research.

I would like to mention Assoc. Prof. Dr. Gülüm Tanırcan who introduced me basic aspects of the theories and the codes used in this thesis here separately. She has been a very inspiring teacher.

I would like to express my gratitude to Assoc. Prof. Dr. Ali Özgün Konca for making his correction and suggestion with patience during my thesis especially at last period.

Special thanks Dr. Luis Dalguer for assistance and supplies with dynamic rupture codes.

I would also like to thank te my colleagues at the Regional Earthquake and Tsunami Monitoring Center of KOERI, for many insights, facilities, suggestions and encouragement throughout my years of research as a doctoral student. Many thanks to the Department of Geophysics for providing a good environment for research and education.

This work is dedicated to my parents, Tolga, Zeynep Nur, Elif Nur Bekler and my mother Hatice Kılıçer, father Metin Kılıçer (deceased) and brother Feyzullah Umut.

ABSTRACT

DYNAMIC RUPTURE PROCESS OF THE 1999 DÜZCE EARTHQUAKE

Rupture process of large magnitude earthquakes have been generally performed by using a kinematic approach. A typical set of input parameters for kinematic approach includes; fault length, fault depth, rupture velocity, slip distribution and rise time defining the slip velocity time function. Kinematic models have been quite successful in obtaining detailed slip distribution maps of large earthquakes. However, the kinematic models have their own disadvantages.

One major disadvantage is that the physics of the kinematic inversion scheme is incomplete. One uses representation theorem and Green's functions approach to obtain slip distribution without considering the forces and the frictional properties on the fault interface. In fact, it is not clear whether the kinematic models of earthquakes with the inverted slip and rise time distributions are physical plausible. This lack of physical constraint on physical properties and the force balance leads to lack of long-term behavioral property of the fault.

Dynamic modeling has been proposed as a new perspective to explain complexity of source parameters, rupture radiation pattern and slip distribution. One way of understanding the dynamic and kinematic mechanism of the earthquake source is to model how the rupture process improves. Hence, proper understanding of this process and appropriate modeling approaches play an important role in seismic hazard and seismic mitigation estimations. On the other hand, the modeling of a dynamic rupture process of an earthquake may provide information on how the limitations on the source can be understood.

In this thesis, a dynamic rupture model of the 1999 Düzce Earthquake is obtained in order to study the effects of dynamic parameters using outputs of kinematic inversion of slip model. The success of the dynamic process substantially depends on parameterization of the model input, which is described by the friction law and stress condition on a fault. These parameters of slip and rise time, obtained from the kinematic model, is then used as input for the dynamic code. In addition to Düzce earthquake, three more moderate earthquakes, namely Manyas, Gemlik and Ereğli earthquakes, were investigated with respect to those kinematic analyses. Slip distribution models on the fault plane indicate a simple circular rupture pattern with decreasing slip values for these earthquakes. For the Manyas earthquake, the model of rupture area was calculated to be 2.5 km in strike and 1.5 km in dip directions with maximum slip of 0.16 m. The static stress drop is about 8 MPa. The slip distribution geometry shows an almost circular pattern. Two asperities were modeled; for the Gemlik earthquake. One is larger asperity near the hypocenter and another is smaller and located to the deeper part of the fault plane towards the east. The best-fitting slip distribution from different parametric models is characterized a 0.18m slip and seismic moment is 9.70E15 Nm, stress drop is 12 Mpa. The result shows almost homogenously elongated asperities were modeled during the Ereğli earthquake. The maximum slip is estimated is 0.25 m near the hypocenter and total seismic moment found as 5.20E16 Nm that is slightly bigger than other two earthquakes occurred in southern Marmara region The static stress drop was calculated as 13 Mpa associated with strike slip faulting the Ereğli earthquake. The dynamic parameters are modified by trial and error to obtain a final slip distribution that is consistent with the rupture velocity and slip distribution obtained from the kinematic model. For the calculations of dynamic rupture simulation, a code named, Support Operator Rupture Dynamic Code (SORD) was used. Results will also be compared with previous findings stating that the Düzce rupture propagated with supershear velocity towards east. The reason of a strong forward rupture directivity effect is seen at a strong-motion record in the city of Bolu, in the east cannot be fully explained with previous simulations. Hence, our study is expected to provide important insight into the nature of the rupture-induced directivity and supershear rupture observed for Düzce earthquake.

ÖZET

1999 DÜZCE DEPREMİNİN DİNAMİK YIRTILMA İŞLEMİ

Büyük depremlerin neden olduğu yırtılma ve yer hareketlerinin simülasyonu işlemi genellikle kinematik bir yaklaşım kullanılarak elde edilmektedir. Kinematik yaklaşımda fayın boyu, derinliği, yırtılma hızı, kalıcı kayma miktarı ve kayma hızı zaman fonksiyonunu tanımlayan yükselme zamanı girdi parametreleri olarak kullanılmaktadır. Fay üzerinde kayma miktarının belirlenmesi öncelik taşıdığından, bu yaklaşım yırtılma işleminin fiziksel sonuçlarının araştırılmasına yönelik değildir. Bu yüzden kinematik yaklaşımın kaynak baskın yer hareketi olgusunun belirlenmesinde bir takım sınırlamaları olacağı değerlendirilmektedir. Dünya genelinde meydana gelen büyük depremlerin ters çözüm sonuçları depremlerin yırtılma süreçlerinin kinematik şekli ile tanımlanandan çok daha karmaşık olduğunu göstermektedir. Örneğin 1992'de oluşan 7.6 büyüklüğündeki Nikaragua depreminin yükselme zamanı 100 sn, aynı büyüklükteki 1993 Kushiro Oki depremininki ise 10 sn olarak hesaplanmıştır. Dinamik modelleme, kaynak parametrelerinin karmaşıklığınının, yırtılma yayılma örüntüsü ve kayma miktarı dağılımının açıklanmasında yeni ve etkili bir yol olarak önerilmektedir. Depreme ait yırtılma işleminin fiziksel olarak anlaşılması yer hareketinin tahmin edilmesi için olan sürecin gelişimine önemli katkı koyar, bu yüzden deprem risklerinin azaltılması ve deprem tehlike analizlerinde bu katkı önemlidir.

Depremlerin dinamik yırtılma sürecinin sayısal modelleri yer hareketi simulasyonlarında kaynağın fiziksel kısıtlamalarının ön görülmesini de sağlar. Bu modeller yüzeyde ve derin (gömülü) depremler arasındaki yer hareketi farklılıklarını açıklayan yırtılmaya bağlı yönlülük gibi kaynak-baskın yer hareketi olayının çalışılması için kritik potansiyele sahiptir. Son yıllarda yapılan çalışmalar, derin (gömülü) depremlerin yüksek frekanslarda yüzey depremlerinden daha güçlü yer hareketi ürettiğini göstermektedir.

Bu tez çalışmasında, 1999 Düzce depreminin kinematik ve dinamik modeli ele alınmıştır. Depremin dinamik modellemesinde yer hareketinde dinamik kaynak yırtılmasının etkileri araştırılmıştır. Bu şekilde depremin neden olduğu yapısal hasar dağılımının araştırılması da mümkün olacaktır. Fay üzerindeki gerilme durumu ve sürtünmeyi tanımlayan dinamik modelin parametreleştirilmesi, yakın alan kuvvetli yer hareketi kayıtlarının dalga formu ters çözümünden hesaplanan fay düzlemi üzerinde kayma dağılımı ile sınırlandırılmıştır.

Düzce depreminin kinematik analizi yanında Manyas, Gemlik ve Ereğli'de meydana gelen orta büyüklüklü 3 depremin de ayrıca kinematik çözümleri yapılmıştır. Bu depremlere ait fay düzlemi üzerinde yer değiştirme dağılımı azalan basit bir yırtılma düzeni göstermektedir. Manyas depremi için yırtılma alanı yanalda 2.5 km boyunca ve düşey yönde 1.5 km olarak sınırlandırılmış bulunmuştur. Yine bu deprem için kayma değeri 0.16 m ve gerilme düşümü de 8 Mpa olarak hesaplanmıştır. Gemlik depremi için de farklı modeller içinde en uygun kayma dağılım modeline göre ortalama 0.18 m kayma miktarı, 9.70E15 Nm sismik moment ve 12 Mpa da gerilme düşümü bulunmuştur. Ereğli depreminde ise hemen hemen doğu-batı uzanımlı türdeş bir kayma dağılımı dikkati çekmekte olup en büyük pürüzlülüğün de deprem odağına çok yakın olduğu izlenmiştir. Yanal atım karakterli Ereğli depremi için de en büyük kayma değeri 0.25 m toplam sismik moment 5.20E16 Nm ve gerilme düşümü de 13 Mpa olarak hesaplanmıştır. Kinematik çözüm sonrası elde edilen bu parametreler dinamik kod için girdi değerlerini oluşturmuştur. Ely ve dig. tarafından (2008) geliştirilen Support Operator Rupture Dynamic (SORD) kodu kullanılarak dinamik kaynak parametreleri belirlenmiştir. Düzce depreminin dinamik modellemesi ile düşük frekanslı hız yer hareketi, çalışma alanı içinde herhangi ağda herhangi bir noktada simule edilebilir. Bu simüle edilmiş hız yer hareketi ile uzun periyot yapısal hasar arasındaki ilişkisinin de incelenmesi mümkün olacaktır. Sonuçlar ayrıca daha önce Düzce depreminin doğuya doğru süper kesme hızı ile yırtılma yayılımı ile ilgili sonuçlar açısından da ele alınmıştır. Kayıtlarda doğu kesiminde (Bolu) gözlemlenen kuvvetli bir öne doğru yırtılma doğrultusunun nedeni, daha önceki simülasyonlarla tam anlamı ile açıklanabilir.

Bu nedenlerden dolayı bu tez çalışması, Düzce depreminde gözlemlenen süper kayma-yırtılma ve yırtılma eyletik yönlülüğün doğasını anlaşılmasında önemli bir kavramı beraberinde getirmiş olacaktır.

TABLE OF CONTENTS

ACKNOWLEDGEMENTS iv
ABSTRACT v
ÖZET vii
LIST OF FIGURES xi
LIST OF TABLES xvi
LIST OF SYMBOLS xvii
LIST OF ACRONNMYS/ABBREVIATIONS xviii
1. INTRODUCTION 1
1.1. Outline 1
1.2. Tectonic Framework of Marmara Region. 3
1.3. Seismicity 5
2. KINEMATIC RUPTURE PROCESS OF November 12, 1999 DÜZCE (Mw=7.1) EARTHQUAKE 8
2.1. Introduction 8
2.2. Representation of the Seismic Source 11
2.3. Constraints 13
2.4. Data Set 15
2.5. Flow Explanations 17
2.6. Discussions 18
3. RUPTURE PROCESS OF MODERATE EARTHQUAKES IN THE SOUTHERN MARMARA REGION 22
3.1. Introduction 22
3.2. Data 27
3.3. Velocity Model 29
3.4. Waveform Inversion 31
3.5. Estimation of Spectral Source Paramaters For Local Earthquakes In Southern Marmara Region 36
3.6. Discussions 42
4. DYNAMIC RUPTURE PROCESS: DATA AND METHODS 47
4.1. Introduction 47

4.2. Comparison between Kinematic and Dynamic Ruture Simulations 49
4.2.1. Kinematic Model 49
4.2.2. Dynamic Model 51
4.2.3. Numerical Comparison Between Kinematic and Dynamic Sımulation 52
4.3. Slip Weakening Behavior 54
4.3.1. The Slip-Weakening Law 55
4.3.2. The Rate-and-State-Dependent Friction Laws 57
4.4. SORD – A Support-Operator Method for Viscoelastic Wave Modeling in 3D Heterogeneous Media 59
4.4.1. Theoretical Formulation 59
4.4.2. Numerical Method 62
4.4.3. Perfectly Mached Layer 65
4.5. Dynamic Rupture Process 66
4.5.1. Stress Drop Calculation for Dynamic Rupture Process 66
4.6. Discussions 72
5. CONCLUSION 78
REFERENCES 81

LIST OF FIGURES

Figure 1.1. General tectonic view of Anatolian block and its surrounding tectonics motions. Red large arrows indicate main westward escapes of Anatolian Block and southwest motion of the Western Anatolian block those relative Eurasia (Taymaz, 2001)..……..…..……...4

Figure 1.2. Recent seismicity and historical earthquakes and active fault map of Marmara Region. Earthquake catalogs with magnitude M > 4.0 (1900-2016 taken from KOERI catalog. The pink lines indicate active faults in the Marmara Region (Şaroğlu et al., 1992; Barka, 1996; Ambraseys, 2002; Armijo et al., 2005).....6

Figure 2.1. (a) Source model of the Düzce Earthquake estimated from previous studies; (a) Slip distribution model by Yagi and Kikuchi (1999) with a teleseismic inversion of P waves (b) Slip distribution model by Utkucu et al., (2003) with a teleseismic inversion of P and SH waves (c) Distributed slip model by Bürgmann et al., (2002); (d) Distributed slip model by Umutlu et al., (2004); (e) Distributed slip model by Bouin et al., (2002); (f) Distributed slip model by Birgoren et al.,(2004)…….……...10

Figure 2.2. Schematic representation of the discretized observation equation in vector forms (Birgoren et all. 2004)…….……12

Figure 2.3. Map showing the epicenters (stars), the surface rupture (blue line), strong motion stations (triangles) and assumed fault plane (rectangle). (Bottom) Aftershock distribution for the first 4 days based on the aftershock catalogue from Bogazici University (Birgoren et all. 2004)……...…..16

Figure 2.4. The slip distribution for the Duzce earthquake faulting area. A band-pass filter with 0.1-1.0 Hz applied to the to the observed data. …...…….…..…19

Figure 2.5. The slip distribution for the Duzce earthquake faulting area. A band-pass filter with 0.01-0.5 Hz applied to the to the observed data…..…..…….....19

Figure 2.6. The slip distribution for the Duzce earthquake faulting area. A band-pass filter with 0.1-0.5 Hz applied to the to the observed data……..…20

Figure 2.7. Comparison between observed (black line) and synthetic velocity (m/s) seismograms for stations located at the western side of the hypocenter…20

Figure 2.8. Comparison between observed (black line) and synthetic velocity (m/s) seismograms for stations located at the eastern side of the hypocenter.....21

Figure 3.1. Recent seismicity and historical earthquakes and active fault map of Marmara Region. Red dots indicate earthquake locations (1970- Present) taken from KOERI. Historical earthquakes of $Ms \geq 6.8$ are for the period 1509 to 1999. Blue lines indicate active faults in the Marmara Region (Şaroğlu et al., 1992; Barka, 1996; Ambraseys, 2002; Armijo et al., 2005). Earthquakes of $6.8 \leq Ms \leq 7.4$ and which ruptured faults of 30 to more than 100 km in length are indicated by red stars ..……...…..……24

Figure 3.2. Location of the earthquakes and their fault plane solutions. The red triangles show the ERD station locations. Black lines indicate faults in the Marmara Region (Saroglu et al., 1992; Barka, 1996; Ambraseys, 2002; Armijo et al., 2005)……..……..25

Figure 3.3. Crustal Vp and Vs velocity models tested to calculate theoretical Green's function in this study……..……30

Figure 3.4. RMS misfits for 5 different earth structure model for both Gemlik and Manyas earthquakes. PREM (Preliminary Reference Earth Model); IASP91 (International Association of Seismology and the Physics of the Earth's Interior), KOERI (Kandilli Observatory and Earthquake Research

Institute), BEKLER (Bekler's explosion crustal model) and CS (Current Study)……..…..30

Figure 3.5. Comparison between observed (black line) and synthetic (red line) velocity (m/s) seismograms for the Manyas Earthquake.....32

Figure 3.6. Comparison between observed (red line) and synthetic (green line) velocity (m/s) seismograms for the Gemlik Earthquake …..…….……..33

Figure 3.7. Comparison between observed (red line) and synthetic (green line) velocity (m/s) seismograms for the Ereğli Earthquake …….……....34

Figure 3.8. The slip distribution of Manyas earthquake. The location of the source is represented by star symbol ……....35

Figure 3.9. The slip distribution of Gemlik earthquake. The location of the source is represented by star symbol ……..……...…….……35

Figure 3.10. The slip distribution of Ereğli earthquake. The location of the source is represented by star symbol ……..……..……36

Figure 3.11. An example of SH spectrum of broadband time history of earthquake recorded at ADVT on broadband instrument. along with fitted source model…….……40

Figure 3.12. Rupture Area-Seismic Moment relation. Red-filled circles indicate, source parameters estimated from theoretical relationship between certain source parameters taken from (Global Data) Mohammadioun and Serva (2001) and Wells and Coppersmith (1994). Black filled squares indicate, source parameters taken from Somerville et all., study (1999). Open circles indicate the source parameters obtained from this study, source parameters obtained from this study and Global Data are presented by triangles…....45

Figure 4.1. Dynamic parameters of the 2000 Tottori earthquake presented in the METI (2004) project: (a) Dynamic stress drop distribution; (b) strength excess distribution and (c) critical slip distance distribution. The start indicates the hypocenter location. (d) Slip weakening friction model; where τ_c is the static yielding stress, τ_0 the initial stress,τ_f final stress and D_c the critical slip distance.....53

Figure 4.2. Final slip distribution of the 2000 Tottori earthquake of the kinematic model of Iwata and Sekiguchi (2002)(left),and the dynamic model (right).....53

Figure 4.3. Contour plot of the rupture front of the 2000 Tottori (Japan) earthquake from kinematic (left) and dynamic (right) rupture models…….54

Figure 4.4. A graph of slip versus stress by means of weakening friction model…...57

Figure 4.5. A graph of exponential relationship between stress and slip velocity according to a typical rate-dependent friction law (velocity-weakening)..58

Figure 4.6. Slip vectors on a non-planar fault. Instead of classical source representation, vectors (unit normal $\hat{n}$) downward unit vector ($\hat{d}$) specify the strike and dip in coordinate system ($\hat{s}_1, \hat{s}_2 \times \hat{n}$).....62

Figure 4.7. Schematic diagram to prepare SORD input……..……...…….68

Figure 4.8. Interpolated final slip distribution of Düzce Earthquake……..……69

Figure 4.9. Initial stress drop of Düzce Earthquake……69

Figure 4.10 Schematic presentation of a fault plane geometry ……..……...69

Figure 4.11. Slip distribution and total rupture time by dynamic rupture process for the first process…….……72

Figure 4.12. Slip distribution and total rupture time by dynamic rupture process for the second process……73

Figure 4.13. Slip distribution and total rupture time by dynamic rupture process for the third process…..……...…….……73

Figure 4.14. Snapshots of dynamic slip distribution …….....……74

Figure 4.15. Comparison between kinematic (a) and dynamic (b) slip patterns. On the other and, almost similar distributions between initial stress drop (c) and dynamic stress drop (a) are remarkable …….…....……75

Figure 4.16. Total rupture time (a) and total rupture speed (b) obtained from dynamic process……76

Figure 4.17. Final dynamic rupture model. Strength excess distribution (a) and stress drop distribution (b) (Modified from Tanırcan et al., 2017)….....77

LIST OF TABLES

Table 2.1. Strong motion recording stations used in the waveform inversion of the 1999 Düzce earthquake……...……..…15

Table 3.1. Large (*Ms* ≥ 6.8) Earthquakes in the Marmara Region over 4 centuries (Barka 1996, Ambreseys 2002). *Ms* : surface-wave magnitude……...…..….23

Table 3.2. Parameters of the selected moderate earthquakes……...……25

Table 3.3. Name of the stations and their related information used during inversion of the waveforms…….28

Table 3.4. The slip values and stress drop……...……36

Table 3.5. The average values of spectral parameters of studied 3 earthquakes. M_0, Mw, Fc, Fmax, Sd, Sr and Nsta are seismic moment, moment magnitude, cut-off frequency, maximum frequency, stress drop, radius of source and number of stations, respectively……...……41

Table 3.6. The earthquake source information used in to create an empirical relationship…….....43

Table 4.1. Model Parameters of the underground structure for the SORD (model based on Mindevalli and Mitchell (1989)…….…70

Table 4.2. Initial dynamic parameter used in SORD processing…….…71

LIST OF SYMBOLS

β	Shear Wave Velocity
$_{ce}$	Chemical Effect of the fluid pressure
$\Delta\sigma$	Stress Drop
f	frequency, hz
$\lambda_{c,}$	Roughness
μ	Steady state friction
μ_s	Static friction
μ_d	Dynamic friction
ρ	Density
γ	Viscosity
$\hat{s}_1$	Strike Unit Normal
$\hat{s}_2$	Dip Unit Normal
Ω0	Low-Frequency Displacement Spectral Level
u	Slip
$\dot{u}$	Slip velocity
τ_f	Final Stress
τ	Shear Stress
Q	Seismic quality factor
τ_o	Shear Stress (Mpa)
T	Temperature
ta0	Initial stress
$\tilde{\tau}_i^s$	Trial Traction
u	Displacement vector
σ_n^{eff}	Effective Normal Stress
σ	Stress Tensor
σ_y	Yield Stress
σ_s	Static Stress Level

LIST OF ACRONYMS/ABBREVIATIONS

3-D	Three Dimensional
1-D	One Dimensional
ABIC	Akaike Bayesian Information Criterion
AFAD	Republic or Turkey Ministry of Interior Disaster and Emergency Management Authority
BB	Broad Band
D	Slip
Dd	Dynamic slip distribution
Dk	Kinematic slip distribution
D_c	Critical Slip Weakening Distance
fc	Corner Frequency
E-W	East-West component
ERD	Earthquake Research Department
FDM	Finite-Difference Method
IASP91	International Association of Seismology and the Physics of the Earth's Interior P & S Velocity Reference Earth Model
IRIGM	Université Joseph Fourier
KOERI	Kandilli Observatory and Earthquake Research Institute
Km	km
L	Fault length
LDEO	Lamont Doherty Earth Observatory of Columbia University
Mpa	Mega Passcal
MPI	Message Passing Interface
M_0	Seismic Moment
Mw	Moment Magnitude
MTWIT	Multi time window linear inversion scheme
Nm	Newton-meter
N-S	North-South component
NAFZ	North Anatolian Fault Zone

PML Perfectly Matched Layer

PREM Preliminary Reference Earth Model

Sec second

T Temperature

ta0 Initial stress

U Vertical component

Vr Rupture velocity

v velocity vector

V Slip velocity

V_0 Reference velocity

Vp P-wave velocity

Vs S-wave velocity

W Width

1. INTRODUCTION

1.1. Outline

Understanding the mechanism of earthquake source is a very complicated process. Some of the destructive earthquakes that have taken place in the last three decades have given substantial opportunities for seismologists in terms of the study of source rupture process, such as Kobe (1995), Chi-Chi (1999), Tottori (2000) earthquakes. The most important of these opportunities is to examine the dynamic and kinetic behavior of the source. Waveform inversion near field strong motion data has a wide range of applications associated with studying in kinematic source models (Hartzell and Heaton, 1983; Archuleta, 1984; Wald and Heaton, 1994; Yoshida et al., 1996; Sekiguchi et al., 2000; Iwata et al., 2004; Birgören et al., 2004). The kinematic inverse solution modeling results provide an overview of the parameters that define the source, primarily the slip distribution, seismic cycle, segmentation, pre-stress.

When earthquake source process is considered, a kinematic model that explains data sets fairly well may have physical irregularities in stress slip. When kinematic models are being constituted, it is assumed that the rupture is propagated at a constant speed during a certain interval. In the modeling procedure, time-dependent slip function is the major parameter (Peyrat et al., 2001).

Constant or variable (in a specific range) rupture velocity assumptions are done for kinematic models. The fundamental parameter is a key of time-dependent slip function. In this thesis, problems related to the physical mechanism of rupture have not been addressed.

Basically, anatomy of an earthquake can be defined as a shear crack which propagates as seismic waves. Stress and deformation provide remarkable insight of the dynamic characteristic of an earthquake on the fault plane. Aki and Richards (2002) remarked that understanding stress dependent medium properties can be explained by physical processing of seismic source.

Almost all of the earth structure is under compression from the dynamic loads above it. The compressive pressure from this overburden means that normal stress will almost always all be negative. For this reason, seismologists often resort to speaking of the "maximum compressive stress", which is the most negative, and the "minimum compressive stress," which is the least negative. The importance of the tectonics forces is that the simplest possible theory for the fracturing of rock predicts failure on the plane of maximum shear stress. In reality, this simple model might be modified, but it provides a useful insight into the process of rupturing.

One major advantage of dynamic modeling is that, if the physical properties of the fault zone and the forces acting on it are known at each time point, at least in principle, it becomes possible to predict the timing and the magnitude of earthquakes on that fault zone. Hence the dynamic approach can possibly lead to an understanding of the fault zones which provides a long term predictive power (Kaneko et al., 2010).

This thesis consists of 3 main chapters with respect to the theory and applications based on 1999 Düzce earthquake (Mw=7.4) and additionally three moderate size three earthquakes occurred in Southern Marmara Region, namely Manyas, Gemlik and Ereğli earthquakes. The purpose of this introductory chapter is to introduce the reader basic concepts in kinematic rupture process. Moreover, the theoretical background of kinematic process of seismic source area is presented and a flow chart of how the slip distribution of fault area for earthquakes considered in this thesis were obtained is given.

Chapter 3 introduces how the strong motion data recorded during the Manyas, Gemlik and Ereğli earthquakes were calculated. Multi time-window linear waveform inversion and the Green's Function calculation in modeling kinematic rupture process were performed. In addition, the spectral source parameters for those three moderate size earthquakes hit southern Marmara Region in order to compute seismic moment mainly.

Chapter 4 addresses an issue of dynamic rupture process to Düzce earthquake fault plane. In this chapter, stress drop and strength excess, rupture time and speed of the rupture as the fundamental parameters for the modeling of Düzce earthquake, are discussed.

1.2. Tectonic Framework of Marmara Region

The North Anatolian fault zone (NAFZ) spreads into three segments in the eastern Marmara region then runs to North Aegean regions. Because these strands are not continuous and are made up of small segments, there has been a conflict of ideas whether the southern strands should be considered within the North Anatolian fault zone representing a diffused boundary or internal deformation of the Western Anatolia. The boundary becomes diffused around the eastern Marmara and further west and south. The Marmara region is located in Pontids. The most active strands of the NAF zone pass the Marmara region through almost east west direction. The Marmara region, between the Bosporus and the Dardanelle's, crossed by the North Anatolian fault zone.

There are three main east-west trending features in the area. The area is partly under the influence of the right lateral strike slip motion, especially on the northern part (Straub et al., 1997). The recurrence interval in the middle and southern strands for large earthquakes is considerably lower than that is in the northern branch of NAFZ. The fault plane solutions of recent earthquakes and GPS measurements indicate that the dominant motion along these strands is strike-slip. In the general view of tectonics frame, all strike-slip fault segments strike ENE-WSW and/or NE-SW while the regional slip vector is almost E-W, causing a thrust component along the strike-slip segments. Seismic activities are mostly located the pull-a-part basins, thus normal faults, while strike-slip segments have almost no macro-seismic activity except aftershock activity. Although some sections of each strand have ruptured during twentieth century. There are some previously studies performed by several authors with respect to the tectonics setting of the Marmara region. Pınar (1943) indicated that two main strands of the North Anatolian fault crossed the Marmara Sea; the northern one running through the basins of Northern Marmara and the southern one running through the Gemlik and Ereğli. Pfannenstiel (1944) suggested the importance of the NE-SW trending ridges in the northern Marmara Sea and included NE-SW faults in his assumption. He also focused on the Plio-Qurternary evolution of the region and suggested that the lakes around the Marmara Sea were once (late Pleistocene) connected to the Marmara Sea. Crampin and Evans (1986) interpreted Northern Marmara as an E-W trending single graben and they also introduced a wedge shaped Marmara block by looking at seismicity patterns of the region. They considered that this Marmara block

escapes westward along the ophiolitic suture. Faulting structure and seismicity of the NAFZ in the Marmara region was studied by Barka and Kadinsky-Cade (1988). The details of each rupture segments have already been given by Barka and Kadinsky-Cade (1988). For the tectonics case of southern Marmara region, Pliocene deposits, which are located between Golcuk and south of the Sapanca Lake, are deformed by folding (Ikeda et al., 1991) and local thrusting. This suggest that the trends of the segments are slight oblique to the slip vectors. Straub (1996) reported that according to the GPS measurements in the area, the velocity vectors have an E-W trending, and this consistent with the fault plane solution of major earthquakes such as these in 1943, 1957, 1967. This results is consistent with the compressional deformation along the strike slip fault segments. GPS data show the most of the motion along the fault, about 10-15 mm/year, is taken up by the northern stand (Straub, 1986). This is consistent with both paleoseismological data and historical earthquake records. Stein et al. (1997) who modelled failure stress distributions of the migrating earthquakes along the north Anatolian fault between 1939-1967, reported that high failure stress accumulation on both strands of the fault, Sapanca-İzmit and Geyve-İznik. However, Barka (1992) claimed that the northern strand has more potential than the middle strand.

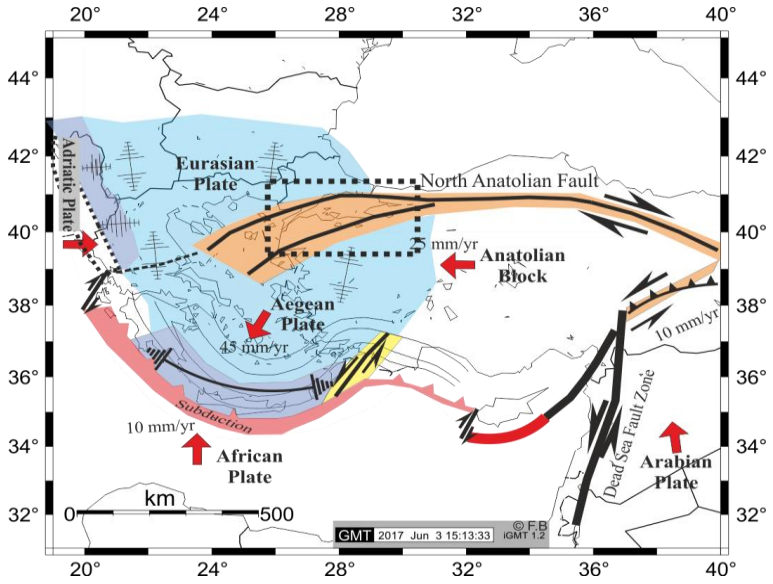

Figure 1.1. General tectonic view of Anatolian block and its surrounding tectonics motions. Red large arrows indicate main westward escapes of Anatolian Block and southwest motion of the Western Anatolian block those relative Eurasia (Taymaz, 2001).

Because of the obvious NE-SW extension on the area the crust was thinned. Observations of positive gravity anomaly in the coasts of the main Turkish mainland (Marmara and the NAF zone) suggest a contradiction between topography and gravity. These evidences make one to think that the area crust is thin or a denser material exist beneath the axis of gravity anomaly. In addition, seismic zone is very shallow (10-15 km) in the area (Crampin and Üçer, 1975; Eyidoğan and Jakson, 1985; Taymaz et al., 1991). Recently by using temporary microearthquake data Sellami et al., (1997) also show that the depth of most microearthquakes was found less than 15 km in Bursa. Pn velocities are found lower than the normal mantle velocities here. This suggests the existence of thin (i.e. hot) continental crustal material beneath the area. Recently relatively high velocity at the northern part of Marmara and lower velocity in the central and south of the area was found by using quarry blast source. This indicates thinning of the continental lithosphere from the north to south or at least presence of a stable mantle lid. By considering all these findings, it is obvious that beneath the study area crust is thin and thickens slightly towards the east and north, and becomes thinner towards the west and south.

1.3. Seismicity

Northwestern Anatolian presents prominent active tectonic pattern, including high seismicity and crustal deformation. Recent major earthquakes and microearthquake pattern in especially eastern Marmara around Adapazari and Düzce presenting current information on the earthquake activity in the western North Anatolian fault zone, also reach the conclusion that the majority of hypocenters is concentrated within upper 15 km of the crust, namely seismogenic zone. The earthquake mechanism solutions, strain rate calculations, GPS measurements (Straub, 1996; Reilinger et al., 1997) and neotectonic studies (Barka 1992) indicate that the Marmara region is under effect of the tectonics similarity and characteristics face of (NAFZ) The NAFZ splays into a number of branches in and around the Marmara Sea region. The northernmost branch forms a graben and follows the gulf of İzmit, connecting with the Çınarcık-Yalova pull-a-part basin in the Marmara Sea region. According to seismological studies (Crampin and Üçer 1975, Eyidoğan 1988, Üçer 1990) the Marmara region shows different seismotectonic characteristics than main part of the NAFZ and Aegean grabens. The Marmara region is known as seismically very active at both historical and instrumental periods.

The first descriptive catalogue of historical earthquakes in Turkey was prepared by Pınar and Lahn (1952). Later, Ergin et al. (1967) prepared a catalogue in the form of seismological meaning, including earthquakes between 1100-1964 Ad. Soysal et al. (1981) prepared a catalogue of historical earthquakes that occurred between 2100BC and 1900AD by studying the Selçuk, Byzantium and Ottoman documents. Ambraseys and Finkel (1991, 1995) have presented more reliable and complete earthquake records, especially for the destructive earthquakes which Affected many parts of the Marmara region, for the period between 0-1900AD. From these more reliable studies, it can be suggested that the recurrence interval of I_0=VIII earthquakes is about 100 years, while this value is about 250 years for I_0=IX earthquakes. The last I_0=VIII earthquake occurred in this region should be in 1984.

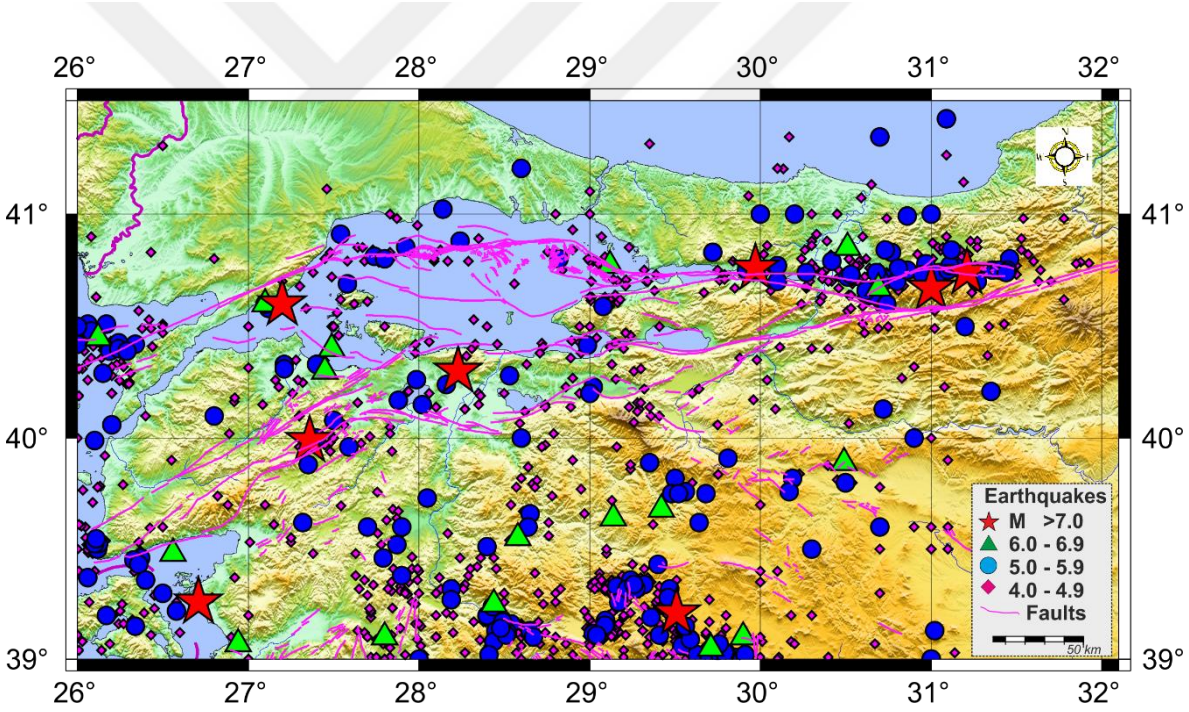

Figure 1.2. Recent seismicity and historical earthquakes and active fault map of the Marmara Region. Earthquake catalogs with magnitude M > 4.0 (1900-2016 taken from KOERI catalog. The pink lines present active faults in the Marmara Region (Şaroğlu et al., 1992; Barka, 1996; Ambraseys, 2002; Armijo et al., 2005).

At each side of the central Marmara ridge, there are two pull-apart basins, bounded by approximately E-W trending normal faults. A 1900-2016 seismicity map of the Marmara (Fig. 1.2) illustrates that the pull-apart basins have continuous seismic activity

while the ridges have very little or no activity, such as the gulf of İzmit, central Marmara Sea ridge and Gaziköy-Saros region. This can be interpreted that there are two different fault systems: normal faults forming southern and northern margins of the pull-apart units and strike-slip faults forming the ridges between the pull-apart structure. In terms of activity, Barka 1992 suggest that the pull-apart basins have earthquakes M<7, while the ridges have the ability of creating M>7 earthquakes. When focusing on the seismicity during the instrumental period, there have been several efforts made (Crampin and Üçer 1975, Alsan et al. 1975, Makropoulos and Burton 1981) to relocate earthquakes which occurred pre-1964, when ISC data become more reliable. In most cases, it was observed that these relocated epicenters are consistent with the macro-seismic epicenters. At the same time, magnitude determinations in recent catalogues are more homogeneous than in the previous studies, and most where determined as surface wave magnitude (Ms). In this study the earthquakes which occurred during the instrumental period (1900-2016). In the period between 1976-2016 data were collected with local networks. The northernmost cluster is the Gemlik Bay activity. It is associated with the southern zone of the western extensions of the NAFZ, i.e. that which passes through the İznik - Mekece valley, along the southern shore of lake İznik and which penetrates into Gemlik Bay near the town of Gemlik. This fault zone, which essentially shows a right lateral strike-slip mechanism to the east, is expected to have strong normal component inside Gemlik Bay.

2. KINEMATIC RUPTURE PROCESS OF THE NOVEMBER 12, 1999 DÜZCE (Mw=7.1) EARTHQUAKE

2.1. Introduction

The November 12, 1999 earthquake that occurred on the the Düzce Fault in the western segment of the North Anatolian Fault Zone has affected the Düzce and its surroundings considerably. This earthquake occurred 40 km east of the August 17, 1999 Kocaeli earthquake rupture area. Akyüz et al. (2002) reported that the earthquake caused a surface rupture of 40 km in length. On the hand, dramatically, this earthquake affected the part between Gölyaka and Bolu Mountain, causing 700 deaths and more than 1500 injured people.

The kinematic finite fault models for the modeling of the tearing mechanism of Düzce earthquake have been studied by many researchers. Yagi and Kikuchi (1999) examined this earthquake by teleseismic P-wave inversion. He found a single northward dip fault plane extending 10 km to the east and 20 km to the west (Fig. 2.1a). His results present a homogenous slip distribution and he announces a maximum slip found near the hypocenter.

Utkucu et al., (2003) inverted teleseismic P and SH waves in order to understand rupture characterization of Düzce earthquake on the model with dimension of 40×20 km^2 defined by sub-faults. According to Utkucu's model two asperities (Fig. 2.1b) have been calculated; larger one located at the east of the hypocenter (max slip is 5.96m) and a smaller asperity found at western shallow part of the Düzce fault (3.13 m slip with a average rupture propagation velocity of the as 2.5 km/sec

Bürgmann et al., (2002) used GPS and InSAR data in order to examine slip distribution model (Fig. 2.1c). This model has maximum strike slip is approximately 5m and traced close to the hypocenter. The most noticeable study was performed by Bouchon et al., (2001) by studying P and S wave arrival time differences recorded at strong motion data

belongs to ERDBOL station. He suggested rupture propagation towards eastwards direction with supershear velocity of 4.3 km/sec.

Umutlu et al., (2004) found the strike, dip and rake and seismic moment as 264^0, 64^0,172^0, $5.0x10^{19}$ N.m (Mw 7.1), respectively with a stress drop 7 MPa in average. They model of the slip distribution shown in Figure 2.1d leaks two asperities. The largest one has 2.6m slip, is located in the middle of the eastern asperity.

One of the researchers who investigated the rupture process of Düzce earthquake is Bouin and all. (2004) who used near field strong motion data and GPS measurement in combination in order to examined time and spatial behavior of Düzce earthquake (Fig. 2.1d). The most striking results of their study slip is bigger in the east part of the fault plane, but it has an important place in the west part of the fault plane. This study offers distinctively a normal slip is on the western part of the fault, however they found there is no slip in the eastern one except in the deep part. It can be deduced this outcome as slip distribution and observed surface slips are in agree along the surface rupture. According to Bouin et al. (2004) the main slip occurred in the central and eastern segments of the fault at very shallow depths.

The most detailed study was carried by Birgören et al. (2004) by inversing waveforms of near field strong motion data. This study results indicated also two asperities; while one is larger and located close to hypocenter, the smaller one is found near the free surface (Fig. 2.1f) in the eastern part of the fault plane. Near the hypocenter, the maximum slip of 5 m is estimated with the total moment as 1.3E19 Nm. According to models outputs, total rupture process almost took 9 sec.

On the other hand, supershear behavior of Düzce Earthquake is announced by focusing on rupture velocity, which is estimated from rupture progression. Velocities (the high first-time window front propagation velocity) were calculated as 4.8km/s and 2.9 km/s in the eastern and western part of the fault, respectively (Birgören et al., 2004).

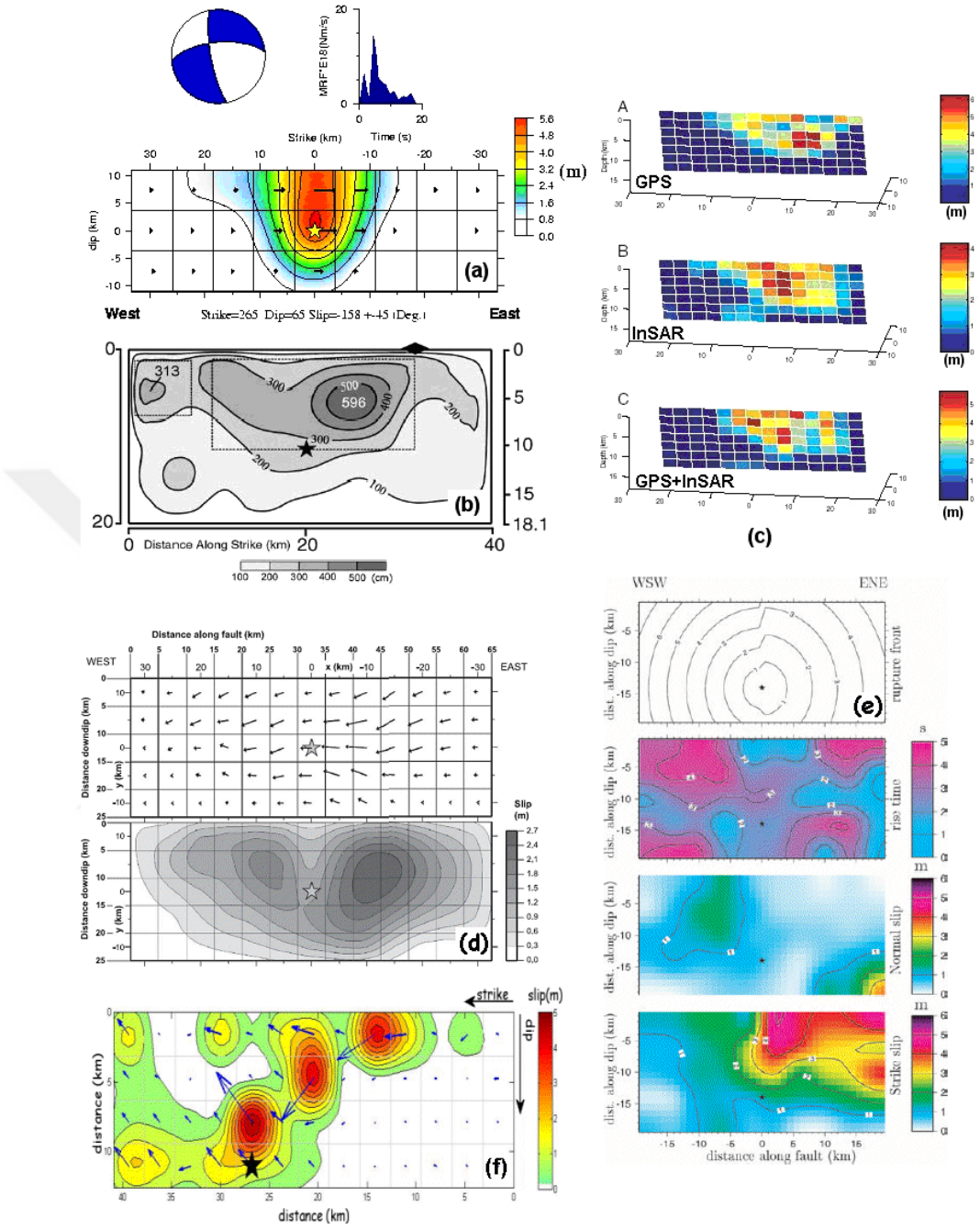

Figure 2.1. (a) Source model of the Düzce Earthquake estimated from previous studies; (a) Slip distribution model by Yagi and Kikuchi (1999) with a teleseismic inversion of P waves (b) Slip distribution model by Utkucu et al., (2003) with a teleseismic inversion of P and SH waves (c) Distributed slip model by Bürgmann et al., (2002); (d) Distributed slip model by Umutlu et al., (2004); (e) Distributed slip model by Bouin et al., (2004); (f) Distributed slip model by Birgören et al., (2004). Konca (2010).

2.2. Representation of the Source

According to the representation theorem, elastic displacement of a point in or on the earth is calculated by the convolution of dislocation over a faulting surface and partial derivatives of Green function. Therefore, earthquake faulting is represented as moment release vectors on the faulting surface (Sekiguchi and Iwata, 2002). Following Hartzell and Heaton (1983), moment release distribution over the faulting surface is achieved by discretizing the dislocations into time by time windows, in space by dividing to fault plane into subfaults and in slipping directions by assuming two orthogonal slip vectors on each sub-fault. Observation equation of n-th component of the ground motion u at position x (Asano et al., 2005; www.seismo.ethz.ch) and time t due to a unit impulse applied at position and time is expressed by Sekiguchi and Iwata, (2002) as follows;

$$u_n(x,t) = \sum_{itm=1}^{ntm} \sum_{is=1}^{ns} \sum_{if=1}^{nf} m(if,is,itm) \int \left[u_{unit_{is}}(\tau - \Delta t_{trig}) \right] \; c_{i(is)jkl}(\xi) n_j \;\; G_{kn,l}(x, t-\tau; \xi(if), 0) d\tau \tag{2.1}$$

and velocity wave field is expressed as;

$$\dot{u}_n(x,t) = \sum_{itm=1}^{ntm} \sum_{is=1}^{ns} \sum_{if=1}^{nf} m(if,is,itm) \int \left[u_{unit_{is}}(\tau - \Delta t_{trig}) \right] \; c_{i(is)jkl}(\xi) n_j \;\; G_{kn,l}(x, t-\tau; \xi(if), 0) d\tau \tag{2.2}$$

where

$$\Delta t_{trig} = \frac{R}{Vr} + \Delta tw(itm-1) \tag{2.3}$$

In the equation 2.1, *if*, *is* and *itm* are the parameters of function *m*. This gives the slip along the *th* direction at time of the the subfault *th*. $G_{kn,l}(x,t;\tau,\xi)$ is the derivative of Green's tensor in spatial domain at any *x* location of displacement along the *k -th* direction. Furthermore, ξ nf is the sub-faults numbers, l is direction, ns is the number of slip directions, ntm time window number and R is distance to hypocenter of the if -th sub-fault, and $[u_{unit_{is}}(\tau)]$ is the unit slip function, Vr is the 1st time window front velocity, c is the elastic constant tensor of Hook's law, Δtw is the time interval for time windows. Discretization of observed velocity wavefield equation results in the general form of the inverse problem as;

$$d = Am \tag{2.4}$$

where d is the observed velocity data vector, m is the model parameter vector and A includes the sub-fault synthetics given as followings

$$d_p = u_n(x,t) \tag{2.5}$$

$$m_q = m(if, is, itm)\ A_{pq} = \int \left[u_{unit_{is}}(\tau - \Delta t_{trig}) \right]\ c_{i(is)jkl}(\xi) n_j\ \ G_{kn,l}(x, t-\tau; \xi(if), 0) d\tau \tag{2.6}$$

$$p = (n-1)nt + (r-1)\Delta t \tag{2.7}$$

$$q = (itm-1)ns.nf + (is-1)nf + if \tag{2.8}$$

where $1 \le r \le nt$, $1 \le n \le ncmp$, $1 \le if \le nf$, $1 \le is \le ns$, $1 \le itm \le ntm$

Schematic illustration of the equation is given in Figure 2.2.

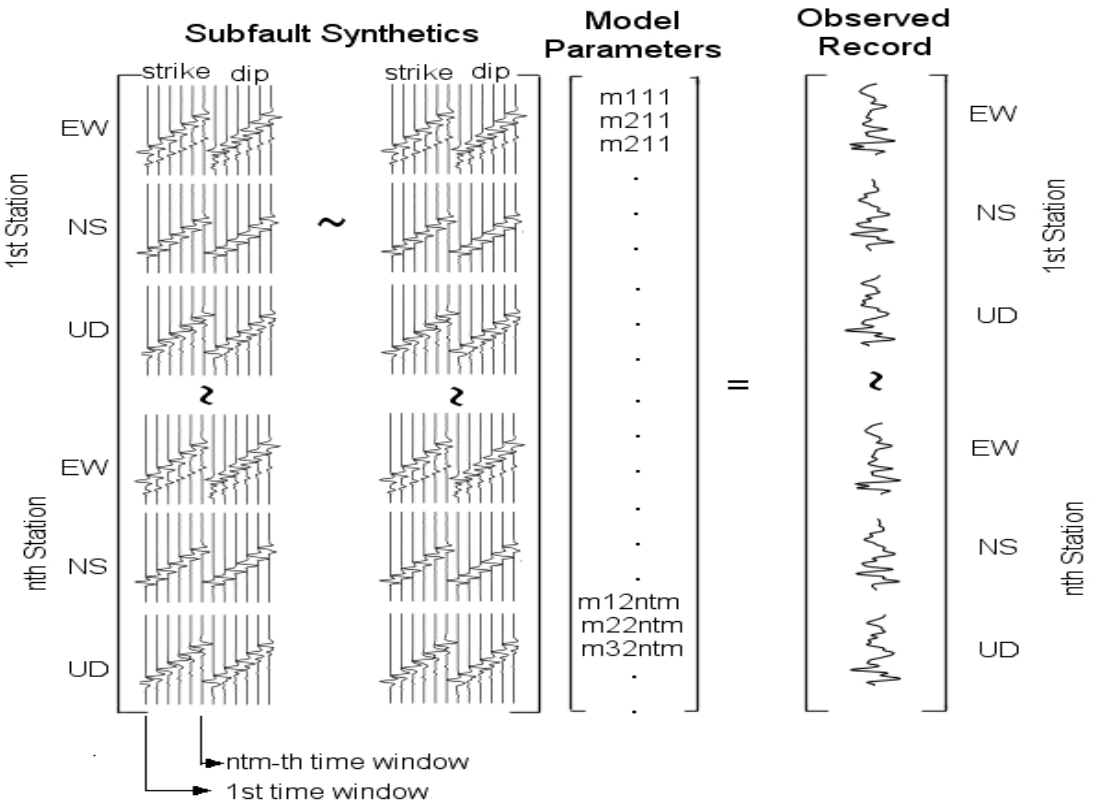

Figure 2.2. Schematic representation of the discretized observation equation in vector forms (Birgören et al., 2004).

2.3. Constraints

In order to stabilize the equation system certain constraints are necessary. Some of undetermined parameters adversely affects the slip pattern. Thus, non-negative and smoothing constraints are performed to get rid of uncomplimentary slip patterns.

Non-negative constraints: When using the least square model to fit the waveforms with the standard matrix, the analysis may fail due to the destructive interferences between adjacent sub-faults. In order to get reliable results from the inversion, rake angle variation is limited by non-negative least square inversion method introduced by Lawson and Hanson (1974).

Smoothing constraints: Smoothing constraint is necessary to avoid adding extra complexity to the model parameter for only marginal improvement of the fits to the data. In addition, smoothing constraint to the parameters help avoid drastic changes in model parameter estimations for small changes in data, especially when some of the parameters are not constrained well. Konca et al (2010) studied the kinematics of Duzce earthquake using InSAR, GPS and strong-motions and constrained the surface slip using SPOT images before and after the Izmit earthquake. Their study shows that surface slip reaches 3 m to the east of the hypocenter. In addition, they claim that rupture velocity was faster toward west reaching 4 km/s while toward east slower rupture velocity (~3km/s) was inferred.

Smoothing scheme used in this study was adapted from Sekiguchi et al., (2000). In this scheme, smoothing is assigned to every pair of model parameters, which are adjacent in time and space, with strength proportional to the inverse of the spatial-temporal distance between them.

$$S_{qq} = \left\{ \begin{array}{cc} \sum_{q'} & \frac{1}{r_{qq'}} \\ r_{qq'} \le \frac{Vs}{fh} & \end{array} \right\} m_n - \sum_{q'} \quad \frac{1}{r_{qq'}} m_{q'} \qquad r_{qq'} \le \frac{Vs}{fh} \qquad (2.9)$$

-

$$r_{qq'} = \left\| \left\{ trup_{if} - trup_{if'} + (itm - itm')\Delta twVs \right\} \right\| + \left\| rspace_{ifif'} \right\| \quad 2.10$$

where S is the smoothing matrix, | defines the first norms, rspace$_{ifif`}$ the distance between if-th and if'-th sub-fault in space, $V_s$ is the S-wave velocity at the sub-faults, $f_h$ the higher frequency limit of the analysis and q`=(itm`-1)ns.nf+(is`-1) nf+if` (www.seismo.ethz.com).

The smoothing matrix S, is constructed and included to the inverse problem together with hyper-parameter λ. The inversion is formulated as a least square problem subject to rake positivity and smoothing constrain as follows;

$$\begin{bmatrix} A \\ \lambda S \end{bmatrix} m = \begin{bmatrix} d \\ 0 \end{bmatrix} \quad 2.11$$

Optimal amount of smoothing is determined by a hyper-parameter λ. An ABIC-value (Akaike Bayesian Information Criterion, Akaike, 1980) is computed at the end of each inversion. The ABIC value is defined as follows;

$$ABIC = -2\log[\int P(d \mid m.\sigma)P(m,\sigma')dm] + 2N_{hp} \quad 2.12$$

$$P(d \mid m,\sigma) = (2\pi\sigma^2)^{-M/2} \exp\left[-\frac{\|d - Am\|^2}{2\sigma^2} \right] \quad 2.13$$

$$P(m,\sigma) = (2\pi\sigma'^2)^{-M_s/2} \exp\left[-\frac{\|Sm\|^2}{2\sigma'^2} \right] \quad 2.14$$

where N defines the number of model parameters and total number of hyper parameters are represented by N_{hp} . M and M_s are the number of data and the smoothing equations, respectively. P(d | m.σ) and P (m,σ') are likelihood functions for data distributions and a priori information of model parameters constructed by the smoothing constraints. The ratio σ/σ' is defined as λ. Gaussian-type distribution is automatically assumed for these likelihood functions, since the system is solved by the least-squares inversion method

(Sekiguchi and Iwata, 2002). The solution with the smallest ABIC-value is the final one where observed and synthetic waveforms fit each other the best.

2.4. Data Set

In this current thesis, study strong motion digital data were used. While data of stations governed by AFAD-ERD used in the current thesis, Birgören et al. (2004) used the same intuition and in additionally used IRIGM and LDEO data.

The station ERDBOL, which is installed in Bolu city located eastern Marmara region was only used due to the insufficient azimuthal coverage in the eastern part of the hypocenter. Table gives all the stations information used in waveform inversion of the Düzce earthquake. The number of stations used for this earthquake is inadequate, but the number of stations used in the modeling of the rupture process of the Kocaeli earthquake was higher. An initial fault plane model is taken as 40.95 km x 12.6 km dimension and fault geometry parameters are 265^0, strike and dip 65^0 solved by Regional Earthquake and Tsunami Monitoring Center (RETMC) of KOERI (formerly National Earthquake Monitoring Center). Other earthquake parameters are location and the depth of focus is given as 40.82^0N, 29.20^0 E and 10 km, respectively. Bilateral rupture propagation was assumed over a 40.95 km x 12.6 km rupture area.

Table 2.1. The list of strong motion stations used in the waveform inversion of the 1999 the Düzce earthquake.

Station Name	Location	Epicentral Distance (km)	Operated by
-CU1058-	40.75N-31.06E	12.25	Columbia Un. USA
-CU1059-	40.75N-30.87E	24.39	Columbia Un. USA
-CU1060-	40.78N-30.63E	44.70	Columbia Un. USA
-CU0362-	40.67N-30.67E	42.93	Columbia Un. USA

Table 2.1. The list of strong motion stations used in the waveform inversion of the 1999 the Düzce earthquake (cont.).

Station Name	Location	Epicentral Distance (km)	Operated by
-ERDSKR-	40.74N-30.38E	65.62	ERD-Turkey
-ERDBOL-	40.74N-31.61E	38.03	ERD-Turkey
-ERDDZC-	40.84N-31.15E	9.33	ERD-Turkey
-ERDMDR-	40.46N-31.18E	33.07	ERD-Turkey

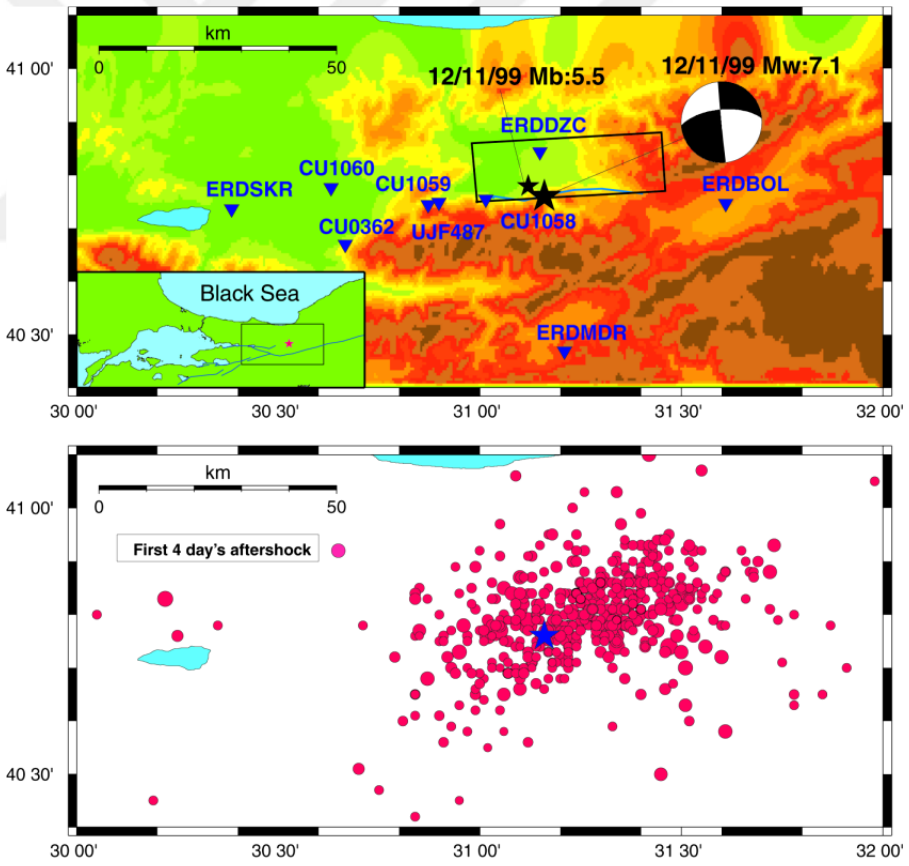

Figure 2.3. Location of the Düzce earthquake (blue star) and the strong motion stations (triangles) are shown with an assumed fault plane area (rectangle). The bottom figure indicates the aftershock distribution during the 4 days following the main event (Birgören et al. 2004).

From available strong motion recording stations, 8 stations in the range 65 km epicentral distance were used for the kinematic inversion process. Velocity seismograms were used as the basis of the algorithm used in the kinematic solution by converting strong motion digital data. The filters of 0.1-1.0 Hz, 0.1-0.5 Hz and 0.01-0.5 Hz are applied to the seismograms. Observed accelerograms were sampled with 100 Hz and those records resampled with 5 Hz to avoid local site effects. A time window of 1 sec before where we observed S-wave phase and 10 secs after S-wave portion were analyzed. Figure 2.1, 2.2, 2.3 show the slip distributions on the fault plane for different filter bands (0.1-1.0 Hz ,0.01 - 0.5 Hz, 0.1 - 0.5 Hz).

2.5. Flow Explanations

Kinematic inversion processing of an examined fault is run by the following shell scripts.

1. **Cut.Resample**
   Cut the original observed data and prepare by re-sampling.
2. **Zahyo.csh**
   Define the faulting area and type of fault by means of its strike, dip and rake. Stations used for calculations.
3. **Green.csh**
   Calculate the Green's functions by using a given crustal model parameter for each station.
4. **Conv.csh**
   Convolve the Green's functions by given a source type within each segment of fault area.
5. **Fil.gfun.csh**
   Apply band-pass filtering to convolved velocity seismogram for each station.
6. **Ruptlag.csh**
   Calculate lag time for a given rupture starting point in sub-fault coordinate by using rupture velocity.
7. **Rup.cut.csh**
   Calculate the timeshifts for each sub-fault and prepare new synthetics
8. **Smooth.csh**

Smoothing constrain for each segment. Each sub-fault is examined by 6 time windows by 0.5 s interval

9. **Gh1.csh**

   Prepare the output for least square inversion in case of inequality constrain

10. **Inversion inv8wei.stn3.csh**

    Make inversion for each time window, and calculate rise time and moment (N*m)
    In case of present sample; Half-rise time: 0.4 sn. Moment=0.1E18

11. **Syninv.csh**

    Prepare synthetic seismograms and put the files for each station into the syn directory.

While the rupture velocity is used a 2.8 km/s for the stations those located at the western part of the hypocenter, 4.8 km/s is used for the stations located at the eastern part of the hypocenter. Western stations are: 362, 160, 159, and SKR. Eastern Stations are : DZC, BOL, 158, and MDR.

2.6. Discussions

In the calculation of spatial and temporal distribution of spatial vectors on fault, multi-time window linear waveform inversion approach was used. Theoretical details of this technique given by Sekiguchi et al. (2000). Frequency range were selected as 0.1-0.5 during the source process. In order to do this, slip history discretization in space and time associated with sub-fault and time windows were implemented. The success of observational and synthetic waveforms matching depends on these. The discretized fault model is projected as number of 52 sub-fault with 3.15 km x 3.15 km cells. Discrete wave number method (Bouchon, 1981) and method of reflection-transmission coefficient matrix of Kennett and Kerry (1979) were performed synthetic seismogram computations. In general, rupture speed is less than the shear velocity of the ruptured fault. Arrivals of body waves generated from initial faulting hit the stations first than the sub-fault segmentation. In a relatively small area in the Duzce earthquake, bilateral rupture velocities are found as 2.8 km/s towards to West and 4.8 km/s towards to east of the fault plane. The seismic moment is obtained 1.3E19 N m.

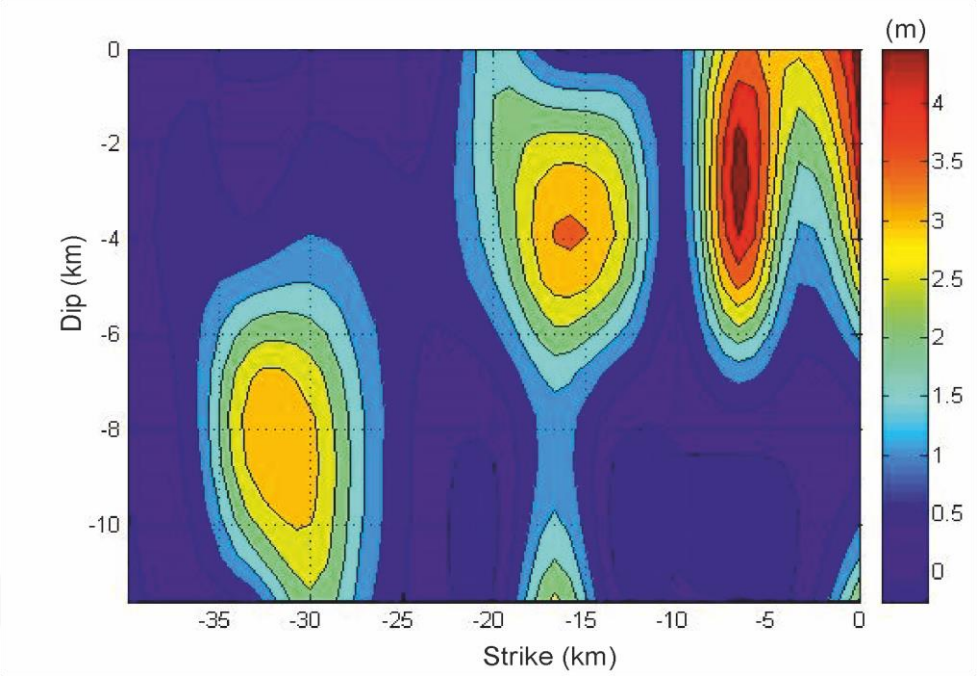

Figure 2.4. The slip distribution for the Duzce earthquake faulting area. A band-pass filter with 0.1-1.0 Hz applied to the to the observed data.

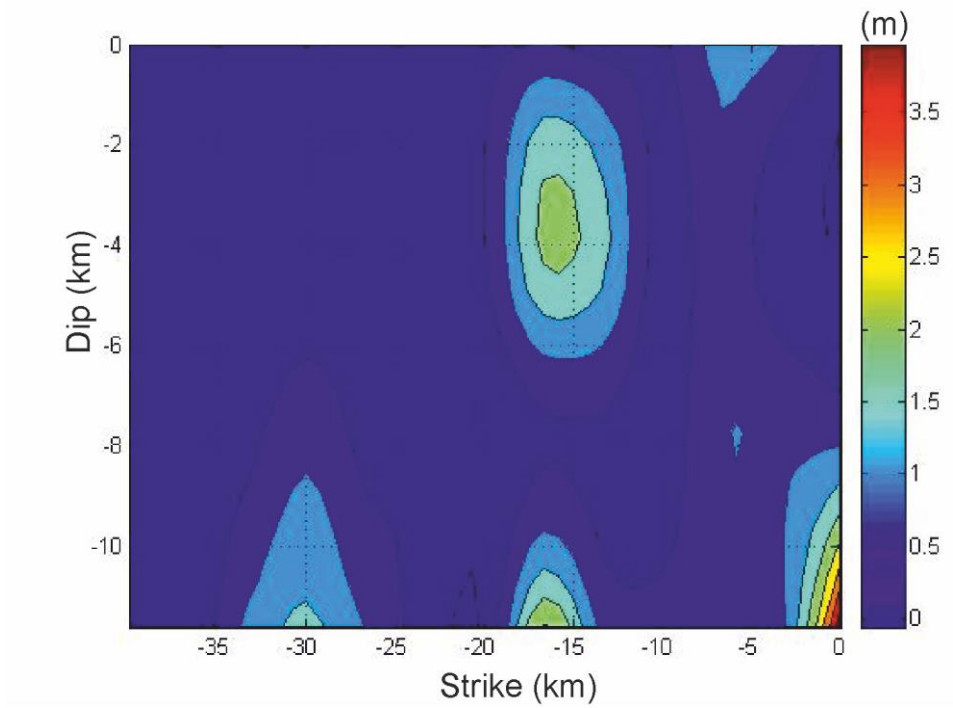

Figure 2.5. The slip distribution for the Duzce earthquake faulting area. A band-pass filter with 0.01-0.5 Hz applied to the to the observed data.

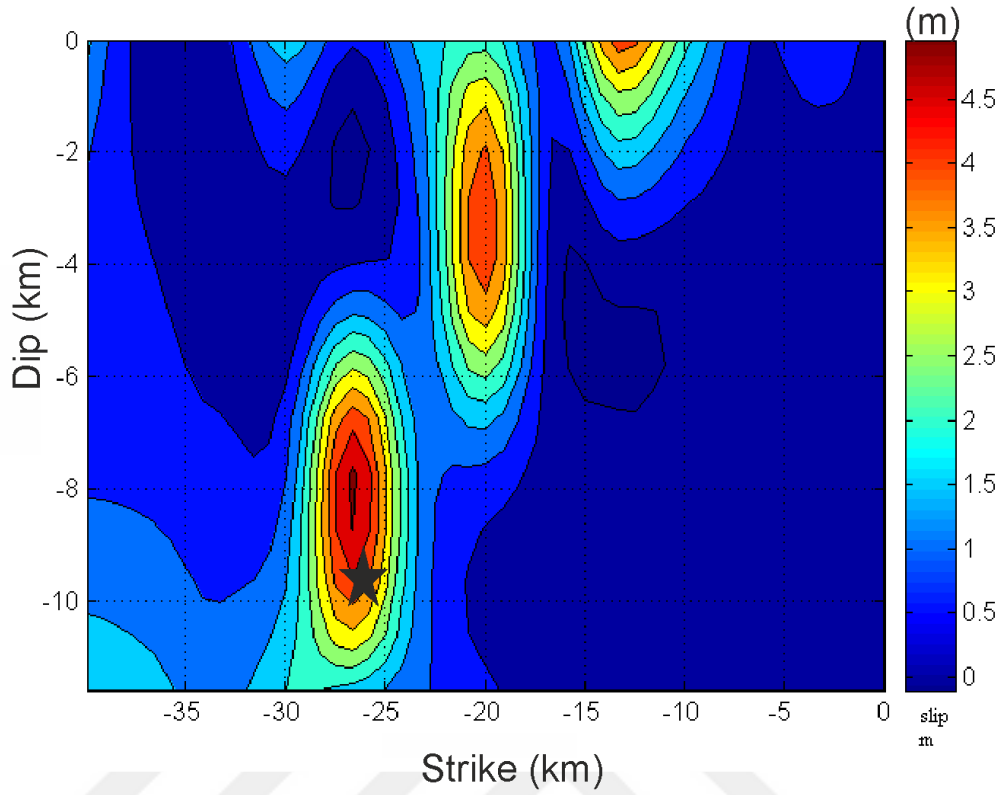

Figure 2.6. The slip distribution for the Duzce earthquake faulting area. A band-pass filter with 0.1-0.5 Hz applied to the to the observed data.

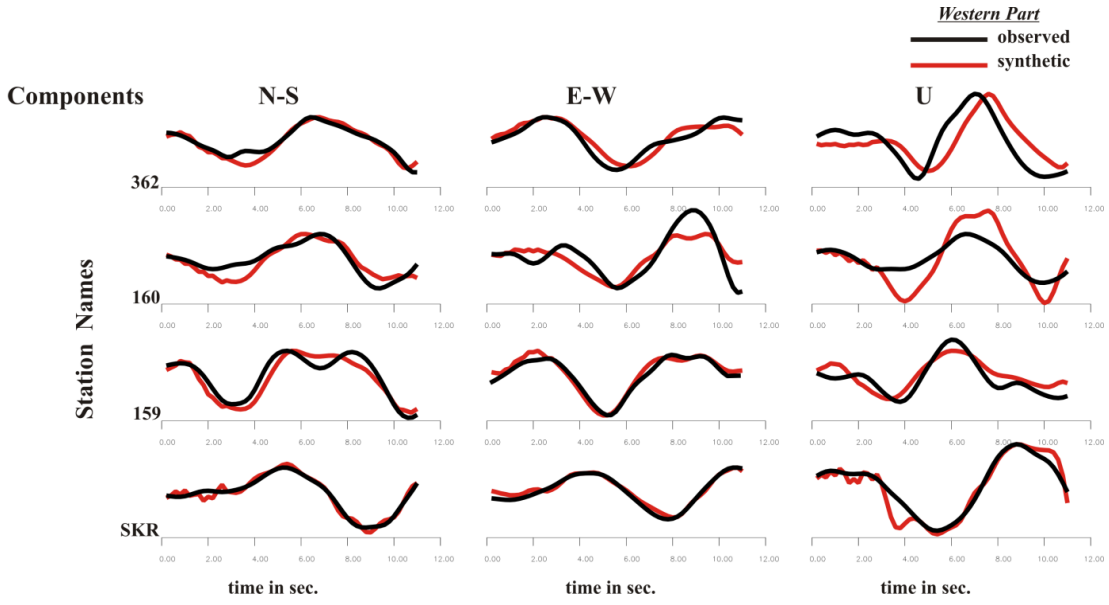

Figure 2.7. Observed (black) and calculated (red) velocity seismogram comparisons of each station placed at the western part of the hypocenter. (0.1-0.5 Hz.)

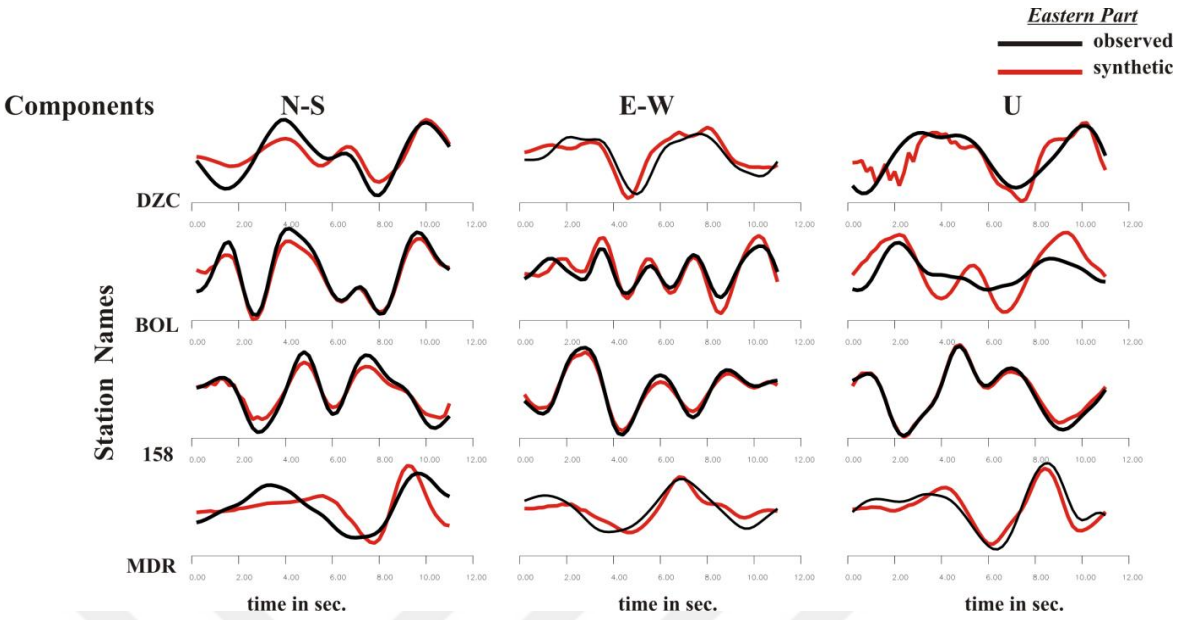

Figure 2.8. Observed (black) and calculated (red) velocity seismogram comparisons of each station placed at the western part of the hypocenter. (0.1-0.5 Hz.)

Asperity areas are appeared in Figure 2.4, 2.5 and 2.6 where high slip zones were observed. One of asperity is larger and found located very close to hypocenter, smaller one is in the eastern part of the fault plane and it extends to the free surface. A maximum 5 m of slip value was found near the hypocenter. Velocity seismogram comparisons are shown in figure 2.7 and 2.8 for the station UJF487 located at western part and the station CU1059 located at the eastern part of the hypocenter. Fitting results indicate that computed and observed seismogram are in well agreement each other.

The dynamic rupture process schedule of the Düzce earthquake was tested for three different frequency values. In obtaining the slip distribution from the process for 0.01-0.5 Hz frequency range, which was previously studied by Birgören et al. (2004), central asperity was not observed. In addition, maximum slip value was 2.3 m and three asperities were modeled on the slip distribution for 0.1-1.0 Hz frequencies. However, unrealistic asperity zone was observed at the corner of the fault area. This could be due to the kinematic inversion process.

3. RUPTURE PROCESS OF MODERATE SIZE EARTHQUAKES IN THE SOUTHERN MARMARA REGION

3.1. Introduction

The geometry and distribution of the active faults of NAFZ crossing the Marmara region has been a long standing issue in tectonics. Looking at the first evaluations, Pınar (1943) suggested that there are two strands tectonically characterized, namely northern and southern strands. The northern one going through the basins of northern Marmara and the southern one running through the Gemlik and Bandırma bays. Pfannestiel (1944) point out the importance of the NE-SW trending ridges in the northern Marmara Sea and included NE-SW faults in his model. Cramping and Evans (1986) interpreted northern Marmara as an E-W trending single graben. Barka and Kadinsky-Cade (1983) and Barka (1992) suggested that NAFZ has three branches continuous in the Marmara region. The northern segment has several pull-a-part stepping which forms the basin of the northern half of the Marmara Sea. Barka (1992) indicates that an E-W trending uplifted basement has been on the offshore seismic profiles between the Armutlu Peninsula and Marmara island. The elevation differences between this ridge and the Armutlu Peninsula is related to the fault kinematics, these uplifts are related to the hanging wall uplift of E-W trending normal faults forming northern and southern boundary of pull-apart systems, whereas, the high elevation of Armutlu, Biga Peninsula and Ganos are associated with the compressional component of the strike-slip patterns. Recent investigations utilizing high resolution seismic data and active source seismology (Karabulut et al., 2003), (Bekler and Gurbuz, 2008) indicate that it extends under the Sea of Marmara.

The southern branch (NAFSB) consists of Edincik, Kapıdağı and Bandırma-Mudanya uplifts which are located at the northern part of the branch. The Uludağ uplift and Söğütalan plateau are located at the southern part of the branch.

A general view of seismic activity during the period 1992 – 2017 exposed that Gemlik bay and its vicinity constitutes main active earthquake cluster zone. This zone is

essentially associated with the southern zone of the western extensions of the NAFZ. The most significant destructive and damaging historical earthquakes on the NAFSB are known to be the 1556, 1719, 1855 and 1894 earthquakes. After the transition to the instrumental period, 1953, 1957, 1964, 1969 (listed Table 3.1) earthquakes with magnitude larger than 6.0 were recorded in this region (Figure 3.1).

Table 3.1. Large ($Ms \geq 6.8$) Earthquakes in the Marmara Region over 4 centuries (Barka 1996, Ambreseys 2002). *Ms* : surface-wave magnitude.

E/Q No	**Year**	**Month**	**Day**	**Time** (UTC)	**Lat (N°)**	**Lon (E°)**	**Ms**	**Region**
1	1509	9	10	22:00	40.90	28.70	7.2	Marmara Sea
2	1556	5	10	0	40.60	28.00	7.1	Gönen
3	1625	5	18	0	40.30	26.00	7.1	Saros
4	1659	2	17	19:00	40.50	26.40	7.2	Saros
5	1672	2	14	0	39.50	26.00	7.0	Biga
6	1719	5	25	12:00	40.70	29.80	7.4	Izmit
7	1737	3	6	07:30	40.00	27.00	7.0	Biga
8	1752	7	29	18:00	41.50	26.70	6.8	Edirne
9	1754	9	22	01:30	40.80	29.20	6.8	Izmit
10	1766	5	22	05:00	40.80	29.00	7.1	Marmara Sea
11	1766	8	5	05:30	40.60	27.00	7.4	Ganos
12	1855	2	28	02:30	40.10	28.60	7.1	Bursa
13	1859	8	21	11:30	40.30	26.10	6.8	Saros
14	1893	2	9	17:16	40.50	26.20	6.9	Saros
15	1894	7	10	12:24	40.70	29.60	7.3	Izmit
16	1912	8	9	01:28	40.70	27.20	7.3	Ganos
17	1912	9	13	23:31	40.70	27.00	6.8	Ganos
18	1944	10	6	02:34	39.50	26.50	6.8	Edremit

Table 3.1. Large (*Ms* ≥ 6.8) Earthquakes in the Marmara Region over 4 centuries (Barka 1996, Ambreseys 2002). *Ms* : surface-wave magnitude (cont.).

E/Q No	Year	Month	Day	Time (UTC)	Lat (N°)	Lon (E°)	Ms	Region
19	1953	3	18	19:06	40.10	27.40	7.1	Gönen
20	1957	5	26	06:33	40.70	31.00	7.1	Abant
21	1964	10	6	14:31	40.10	28.20	6.8	Manyas
22	1967	7	22	1657	40.70	30.70	7.2	Mudurnu
23	1999	8	17	00:01	40.72	29.96	7.4	Izmit
24	1999	11	12	16:57	40.81	31.19	7.2	Düzce

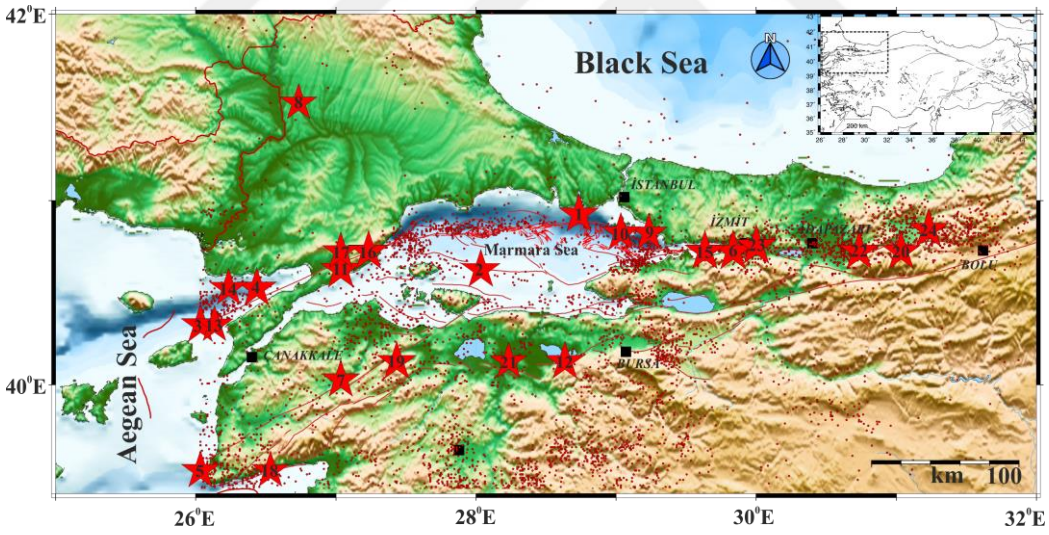

Figure 3.1. Recent seismicity and historical earthquakes and active fault map of the Marmara Region. Red dots indicate earthquake locations (1970- Present) taken from KOERI. Historical earthquakes of *Ms* ≥ 6.8 are for the period 1509 to 1999. Blue lines indicate active faults in the Marmara Region (Şaroğlu et al., 1992; Barka, 1996; Ambraseys, 2002; Armijo et al., 2005). Earthquakes of 6.8 ≤ *Ms* ≤ 7.4 and which ruptured faults of 30 to more than 100 km in length are indicated by red stars.

The Manyas, Gemlik and Ereğli Earthquakes of 20th, 24th October 2006, with Mw: 4.7, 4.8 and 7th June 2012 with Mw: 5.1 (listed Table 3.2) respectively, are the largest events that occurred on the NAFSB since 1999 Izmit earthquake (Figure 3.2). Even though there is no casualty or considerable structural damage caused by those event, investigation of their rupture characteristics is important for better understanding the seismotectonics of this region.

Table 3.2. The earthquake parameters.

Event	Coordinates	Mw	Strike/Dip/Slip/ (SDS) Depth (km)	Seismic moment, NM
Manyas Oct 20,2006	40.26N - 27.98E (KOERI)	4.7	244/84/-164/15 (KOERI)	1.73E+15
Gemlik Oct 26,2006	40.42N - 29.00E (KOERI)	4.8	14/71/-12/14 (Irmak, 2006)	3.43E+15
Ereğli June 07, 2012	40.85N-27.92E (KOERI)	5.1	55/80/-124/26 (KOERI)	4.99E+16

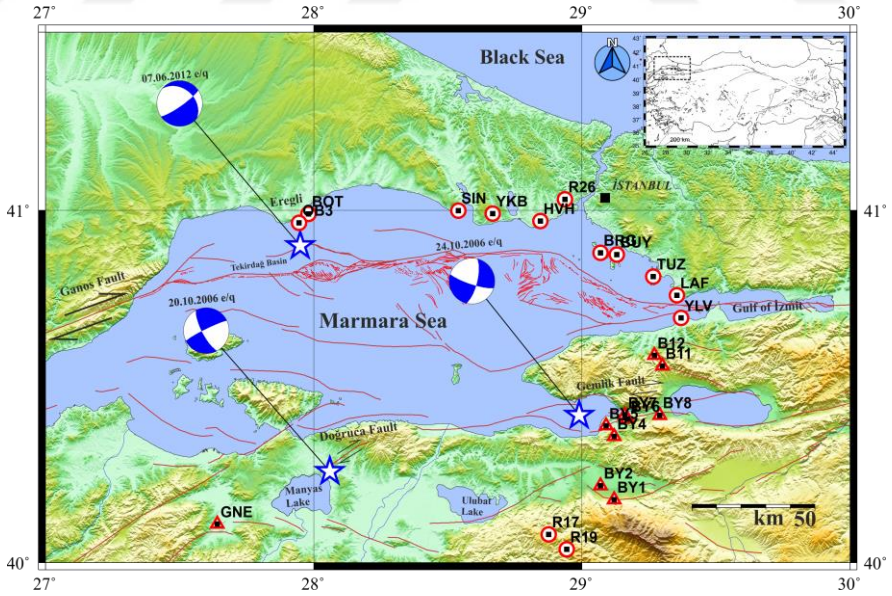

Figure 3.2. Location of the earthquakes and their fault plane solutions. The red triangles show the ERD station locations. The red circles show the KOERI station locations. Red lines indicate faults in the Marmara Region (Saroglu et al., 1992; Barka, 1996; Ambraseys, 2002; Armijo et al., 2005).

The 2016 Manyas Earthquake can be considered as a result of the Manyas graben extension bounded by its east-west depression basins, corresponding to the east boundary. The Manyas Earthquake occurred on Doğruca fault, which is possibly related with the 1953 Yenice-Gönen earthquake. The Doğruca fault is located in a NE-SW direction to the Manyas Lake and is separated from the Yenice-Gönen fault by depression basins. Slight damage to structures was observed at the village of Doğruca, 10 km south-east of Bandırma. The Gemlik Earthquake was located just north of the Gemlik Fault (Tsukuda, 1988) where the tectonic system is extremely complex. Different structures of a dextral type of motion join together in this region (Flerit el al., 2003). The Ereğli earthquake occurred near the Tekirdağ basin south of the Ganos Fault where strike slip deformation characterizes the North Anatolian Fault. The main strand of the Ganos Fault forms a 45 km long rectilinear segment between the Marmara and Aegean Seas (Okay et al., 1999).

Recent seismic profiles and tectonic data (Gurbuz et al., 2000; Karabulut et al., 2002; Bekler and Gurbuz 2008; Le Pichon et al. 2014) on the Armutlu Peninsula and Southern Marmara Region shows that the tectonic features of these regions are very complicated. The Doğruca and Gemlik Faults seem to be very quiet and have not produced even moderate size earthquakes for a long time. For that reason, rupture processes of these earthquakes are important in order to improve our understanding of the seismotectonics of this region. Due to the lack of strong motion stations in Turkey, the rupture characteristics that reflect sources of the earthquakes occurring in the Marmara region were not evaluated accurately until the 1970s. Hence, the recent Manyas, Gemlik and Ereğli earthquakes are extremely valuable for understanding the tectonic complexity of the region with respect to the source characteristics. Some authors who studied these earthquakes associated them with source mechanism and tectonic structure. Orgulu (2011) investigated source parameters of small scale earthquakes in the Marmara Region including both Manyas and Gemlik earthquakes using moment tensor inversion and first motion focal mechanisms.

This study stated that the Manyas event is located north of Manyas Lake and gives a strike-slip source (SDS; 68/75/-147, Mw=4.8, 6 km) with a northeast trending nodal plane, in close agreement with the Doğruca Fault. The latter Gemlik event (Srike/Dip/Slip; 127/62/-49, Mw=4.8, 6km) has the same mechanism solutions corresponding to a normal type faulting with a small strike-slip component and is related to the Gemlik fault

(Karabulut et al. 2011; Kinscher et al. 2013). In fact, all previous results are in agreement with the complex tectonics of the region which is extensional together with a transform regime (Kuscu et al. 2009). The main fault structures in Gemlik Bay area are right-lateral eastwest trending faults. However, there are also other secondary structures trending at oblique angles such as N-S extension (Irmak et al., 2007) or NW-SE direction (Kinscher et al., 2013).

The Ereğli earthquake occurred on the northern strand of NAF zone crossing though the Marmara Sea to the west close to Tekirdağ basin. ERD (General Directorate of Disaster Affairs of Turkey - now AFAD) reported that the focal mechanism solution indicates strike slip faulting with normal component (SDS; 100/21/-161, Mw=5.1, 14 km). Focal mechanisms and respective locations for the 20/10/06 (Manyas event), 26/10/06 (Gemlik event), and 07/6/12 (Ereğli) earthquakes are mapped in Figure 3.2.

In this thesis, the kinematic rupture characteristics of Gemlik, Manyas and Ereğli earthquakes are investigated by using the recordings of a dense SGM and KOERI array. The slip amplitude, slip rake, average rupture velocity and rise time of those events were determined through waveform fitting. The procedure basically was adapted from a study by Sekiguchi et al. (2000). The slip distributions on the fault planes were interpreted in terms of rupture complexities.

3.2. Data

For the waveform inversion, 8 SGM stations operated by ERD (listed Table 3.3) within 30 km epicentral distance were used for the Gemlik Earthquake (Figure 3.2). 4 SGM stations within 90 km epicentral distance were used for the Manyas Earthquake (Figure 3.2). 12 KOERI stations within 120 km epicentral distance were used for the Ereğli Earthquake. Original acceleration records were re-sampled with an interval of 0.01 s to avoid local site effect and high frequency effects, and integrated to velocity. Thus, waveform comparison was done by using low frequencies. S-wave portion from 1 sec before the S-wave onset were analyzed with total duration of 6 s. The velocity seismograms of both Manyas and Gemlik events were filtered in the 0.1-0.5 Hz range and seismograms of the Ereğli event were filtered in the by 0.1 – 0.6 Hz range.

Very low slip values are associated with observed larger part of the fault plane. This is case to eliminate the inconsistencies between the real and theoretical source time function. For this reason, a smaller fault plane was adopted. To eliminate the inconsistency between theoretical and real source time function durations, a smaller fault plane has been used due to the observation that a large part of the fault plane is characterized by very low slip values. Fault planes were chosen a priori as 2.5 km x 1.5 km for Gemlik, Manyas and Ereğli earthquakes. Among the crustal models, the model by Bekler and Gurbuz (2008) was adopted to calculate theoretical Green's function for the waveform inversion due to the lower misfit values.

Table 3.3. Name of the stations and their related information used during inversion of the waveforms.

Station Name	**Location**	**Epicentral Distance (km)**	**Operated by**
-BYT01-	40.18N-29.12E	27	ERD-Turkey
-BYT02-	40.22N-29.07E	21	ERD-Turkey
-BYT04-	40.36N-29.12E	11	ERD-Turkey
-BYT05-	40.39N-29.09E	7	ERD-Turkey
-BYT06-	40.41N-29.17E	14	ERD-Turkey
-BYT07-	40.42N-29.16E	13	ERD-Turkey
-BYT08-	40.42N-29.29E	24	ERD-Turkey
-BYT11-	40.56N-29.30E	30	ERD-Turkey
-GNE-	40.11N-27.64E	31	ERD-Turkey
-BLK-	39.65N-27.85E	68	ERD-Turkey
-R17-	41.02N-28.87E	82	KOERI
-R19-	41.03N-28.94E	88	KOERI
-R26-	41.03N-28.93E	87	KOERI
-BOTS-	40.99N-27.98E	16	KOERI
-BRGA-	40.87N-29.06E	96	KOERI

Table 3.3. Name of the stations and their related information used during inversion of the waveforms (cont.).

Station Name	Location	Epicentral Distance (km)	Operated by
-TUZL-	40.81N-29.26E	113	KOERI
-SINB-	40.99N-28.53E	54	KOERI
-LAFA-	40.75N-29.35E	121	KOERI

3.3. Velocity Model

Appropriateness of calculated waveforms is provided by the RMS misfit, which accounts for the crustal velocity model used for the inversion process. The more commonly used misfit criterion (Geller et al. 1995) is the RMS (root mean square) misfit defined by Equation 3.1.

$$RMSmisfit = \sqrt{\frac{\sum \left| S_{obs} - S_{syn} \right|^2}{\sum \left| S_{syn} \right|^2}} \qquad 3.1$$

where S_{obs} is the observed waveforms, S_{syn} is the synthetic waveforms, respectively.

The number of 5 different crustal structure velocity models to calculate theoretical Green's functions between each sub-fault node and stations until we get well-matched waveforms with also low RMS values. This crustal models (Figure 3.3) were selected from global to local references such as; PREM (Dziewonski and Anderson, 1981), IASP91, KOERI (earthquake location model) and local study (Bekler & Gurbuz, 2008). Those models were tested in order to get low RMS by comparison with each other. Bekler's local model gave more reliable with low RMS and ABIC value (Figure 3.4).

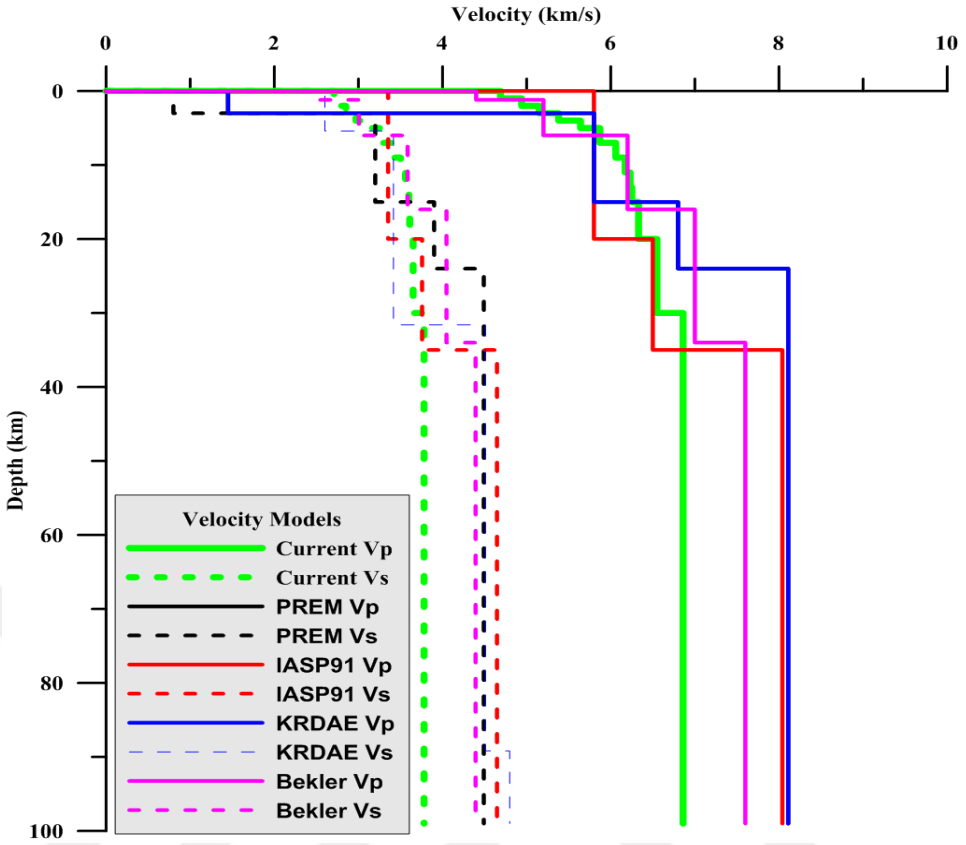

Figure 3.3. Crustal Vp and Vs velocity models tested to calculate theoretical Green's function in this study.

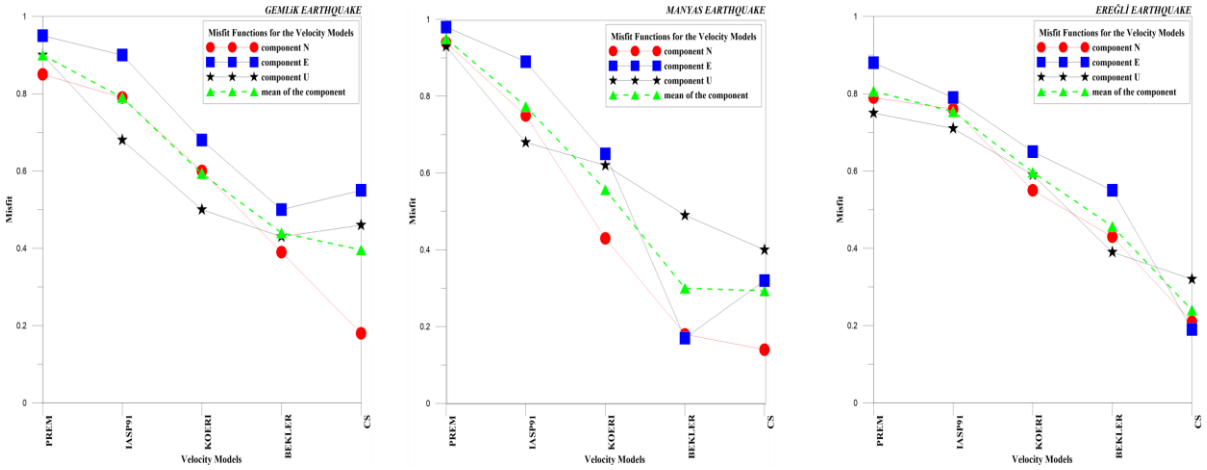

Figure 3.4. RMS misfits for two standard earth structure model for Gemlik, Manyas and Ereğli earthquakes. PREM, IASP91, KOERI, BEKLER (Bekler's explosion crustal model) and CS (Current Study).

3.4. Waveform Inversion

This thesis uses strong motion data in order to model three moderate earthquakes those are Manyas, Gemlik and Ereğli for kinematic process. Two steps constitute the basic principle of the applied methodology. The first is to carried out source processing by filtering the data in the range of 0.1-0.6 Hz and applying the scheme of multi time window linear inversion to estimate total slip duration (Sekiguchi et al., 2000). The later step is to calculate Green's functions for an initial crustal model. In addition, the distribution of slip values generated from each sub-fault for a specific time windows, and seismic moment release vector were estimated through controlling observed and calculated seismogram matching each other. Hartzell and Heaton (1983) generally stated how this procedure would be followed. Two time windows were used to represent the slip velocity time functions in each sub-fault, which had a rise time of 0.14 s (Manyas and Gemlik events) and 0.16s (Ereğli event). For the all events, velocity of rupture (triggers the rupture of the first time window) front propagation was chosen as 2.7 km/s. This is almost 60% of the S-wave velocity, where the rupture initiated at depth of focus. On the hand, this velocity is 72% slower than the mean rupture velocity associated with results of Geller (1976).

Slip distribution shows complex pattern yielded from kinematic model. Furthermore, this complexity statistically reduces misfit value (ABIC value) compared to the smooth model obtained for a smaller fault plane is considered. Eugenio et al. (2013) carried out kinematic inversion for synthetic data and suggested that if there is poor station coverage and a small fault plane, distribution of rupture velocity could not be resolved well. In such case, rupture velocity is considered as constant. The rupture velocity with minimum misfit of Eugenio et al. (2013) was selected as 2.8 km/s among the different velocity range values.

The theory based on Akaike (1980) uses non-negative constraints. This method was applied to limit the rake angle 180 ± 45 degrees (Akaike, 1980). Undesirable slips were not regarded by applying smoothing constraints. Synthetic seismogram calculations (theoretical Green's function) uses the reflection-transmission matrix method of Kennett and Kerry (1979) and discrete wave number method of Bouchon (1981) for each sub-fault and seismic station pairs in 1D crustal structure model. Akaike's Bayesian information

criterion (ABIC) is the criteria in order to check the best match among the seismograms during the calculating the Greens's functions between each sub fault and seismic station. For this purpose, number iterations were carried out by perturbing the smoothing constraints. In addition, fault plane solutions and centroid depths obtained from previous studies were also tested. Band-pass filtering is an effective data processing step having a good match between the observed seismograms and synthetics. Estimation of the earthquake source rupture properties is one of main objective with respect to the slip distribution and seismic moment. Multi-time window linear waveform inversion needs ground motion data recorded at almost near source area. One main target of this study is to estimate the earthquake source characteristics from the recorded ground motions by means of slip distributions and seismic moment using on low frequency ground motion in the near source area. Observed and computed velocity waveforms are shown in Figure 3.5 for the Manyas event. Synthetic seismograms and observed data are subjected to the same filters. Comparison between the converted velocity seismogram and the synthetic generated by the inversion inputs indicates a better fit for the Gemlik event (Figure 3.6). Figure 3.7 shows the observed and the calculated waveforms for the Ereğli event at 12 stations with satisfactory matched seismograms.

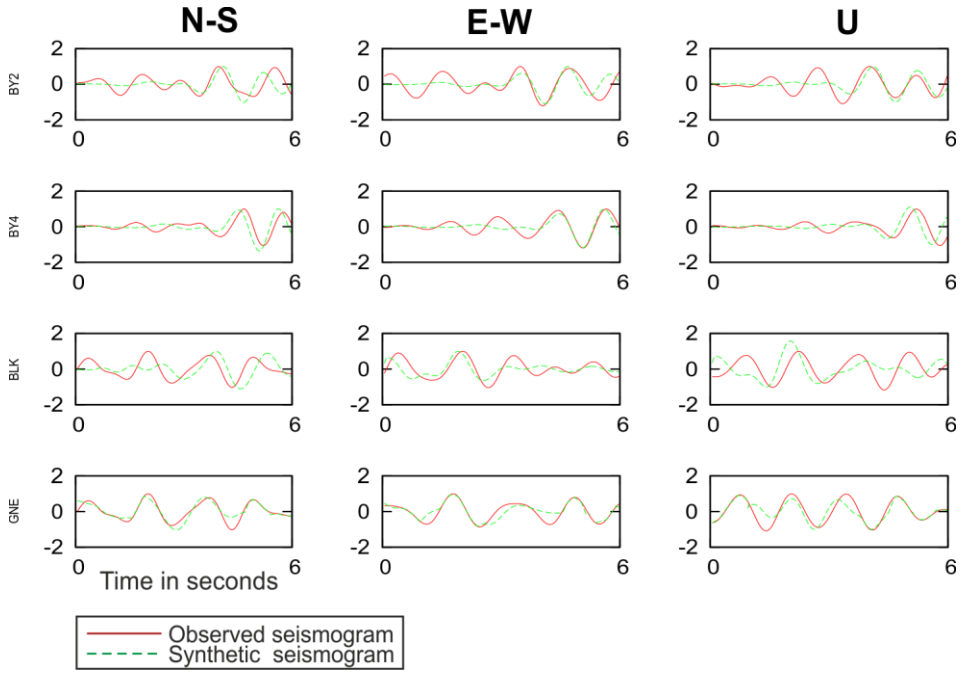

Figure 3.5. Observed (red) and computed (green) velocity seismogram comparisons are performed for the Manyas earthquake.

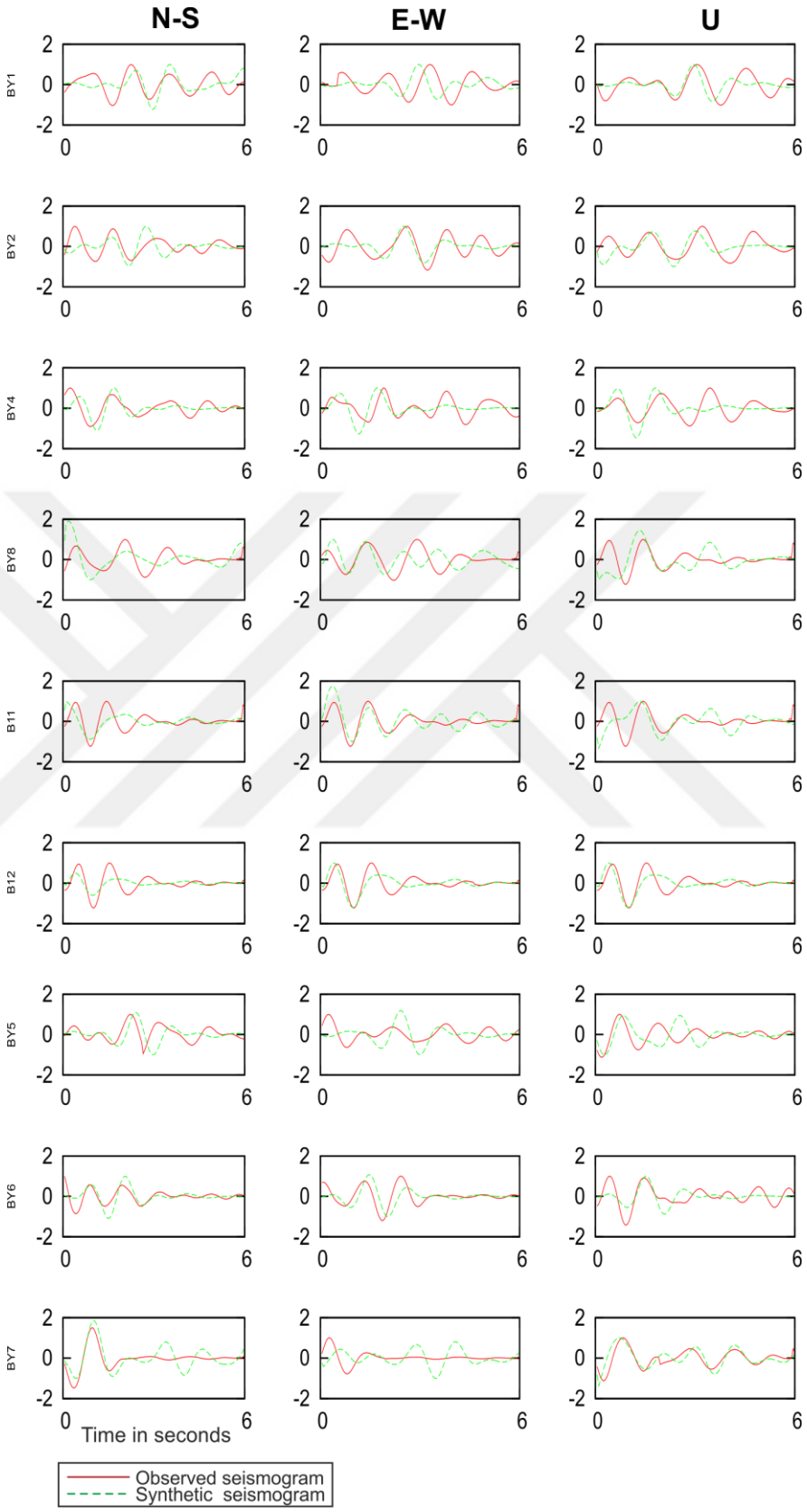

Figure 3.6. Observed (red) and computed (green) velocity seismogram comparisons are performed for the Gemlik earthquake.

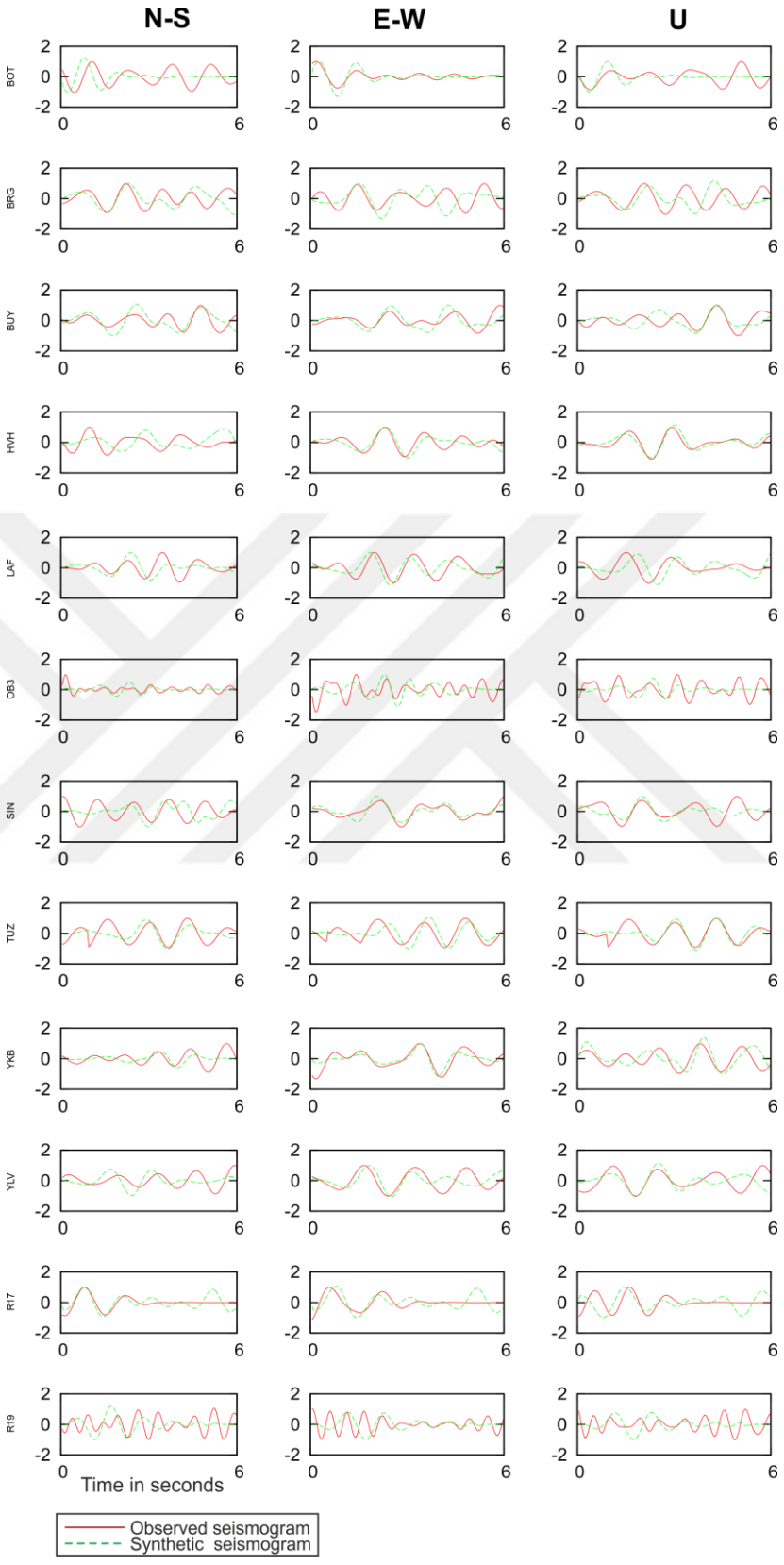

Figure 3.7. Observed (red) and computed (green) velocity seismogram comparisons are performed for the Ereğli earthquake.

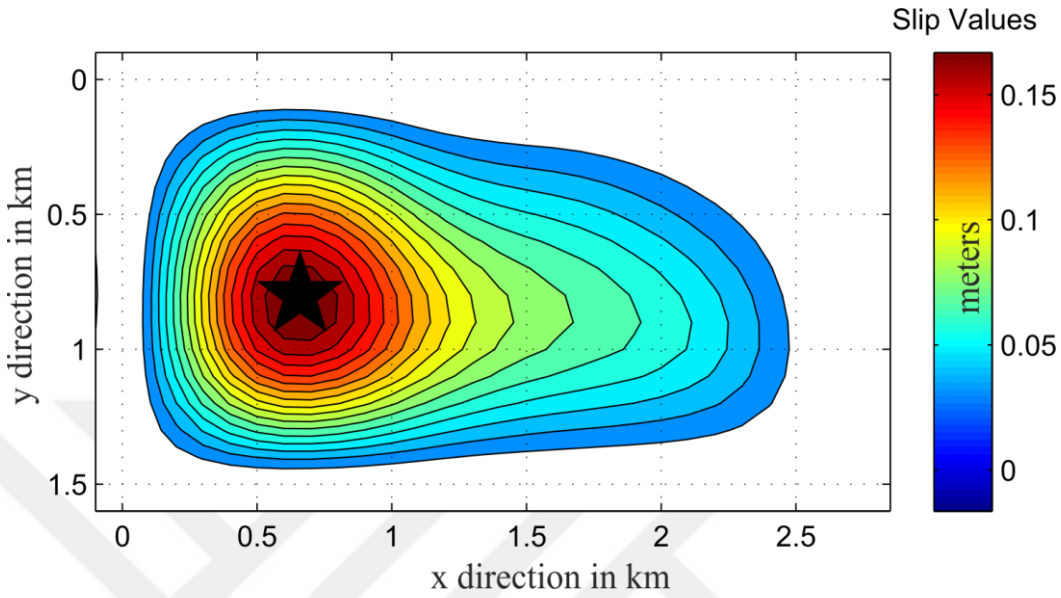

Figure 3.8. The slip distribution of Manyas earthquake. The location of the source is represented by star symbol.

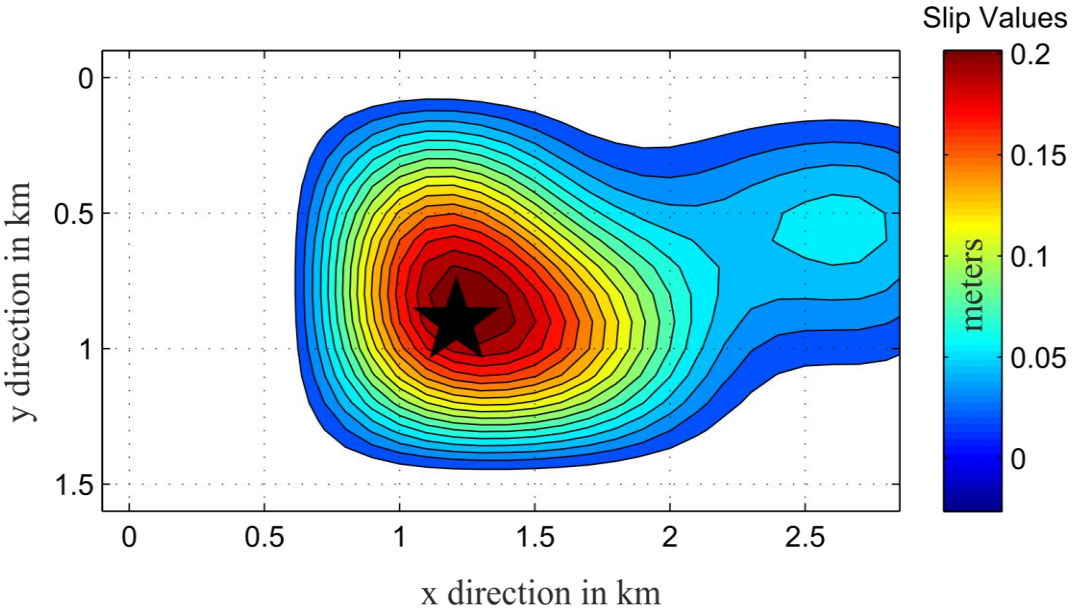

Figure 3.9. The slip distribution of Gemlik earthquake. The location of the source is represented by star symbol.

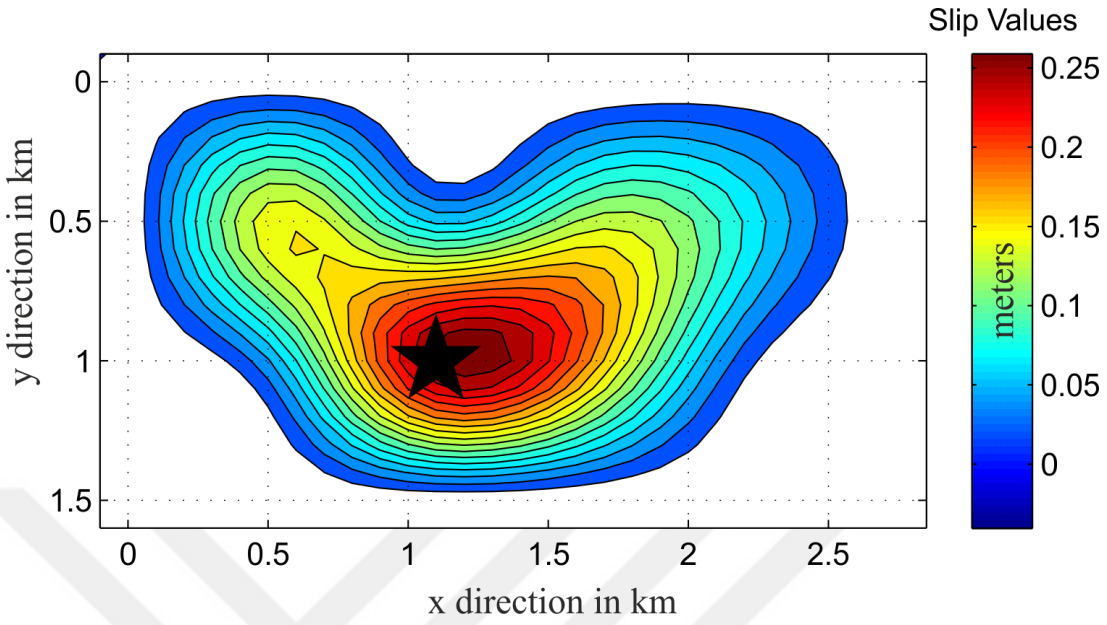

Figure 3.10. The slip distribution of Ereğli earthquake. The location of the source is represented by star symbol.

Table 3.4. The slip values and stress drop.

Event	Seismic moment (E15Nm)	Fault Plane (kmxkm)	Max Slip (cm)	Stress drop (Mpa)
Manyas	05.40	2.5x1.5	16	8
Gemlik	09.70	2.5x1.5	18	12
Ereğli	52.05	2.5x1.5	25	13

3.5. Estimation of Spectral Source Parameters for Local Earthquakes in Southern Marmara Region

Elastic rebound theory in tectonics briefly explains how energy is released during earthquakes. In rigid body mechanics particles are usually modelled as completely undeformable. On the other hand, the essence of seismology is the study of the relation between the deformation of material and the forces generated by that deformation. The simplest possible theory for the fracturing of rocks predicts failure on the plane of maximum shear stress. Rigid materials as rocks in the brittle crust that are under the

pressure (stored strain) also bend, break, and snap back. A fault is rupture in rocks along which rocks have dislocated. When the rupture occurs, energy is released and stress drop occurs. In recent years, especially the number of seismological studies carried out in this respect have been increased. As a pioneer Brune (1970) revealed and suggested some basic definitions in order to model source parameters by using near and far field displacement spectrums. Abercombie and Leary (1993) contributed to source parameters studies. Another source parameter calculation was carried out by Sharma and Wason (1994) for the earthquakes occurred near Himalayan region.

The current study is aimed to estimate source parameters for Manyas, Gemlik and Ereğli earthquakes those were recorded by KOERI stations. Observed displacement spectrum is basically defined as in equation (3.1),

$$U(w) = S(w).G(w).R(w).I(w) \tag{3.1}$$

where;

S(w) is source spectra, G(w) is geometrical propagation that includes wave propagation pattern and attenuation affects and R(w) represents local site amplification and I(w) represents instrumental response. At first, the instrument responses were removed from used KOERI broadband stations. Later, in order to get SH wave rotation of each seismogram horizontal components were carried out while vertical component merely used for P wave onset. For the three studied earthquakes occurred in the Southern Marmara region, waveforms from 37 stations were analyzed after converted broadband time series into acceleration ones.

An example spectrum of the three earthquakes whose recorded by ADVT station is presented in figure 3.11. The Brune (1970) source model imposes specific variations in slope at higher frequencies than corner frequency. To avoid those kinds of variations at higher frequencies, Brune (1983) suggested a 2^{nd} order Butterworth filter for both acceleration and displacement spectrum. A cut-off frequency defines as fmax (Hanks, 1982). Brune (1970) introduced a theory related with acceleration and displacement source spectrums (3.2 and 3.3),

$$A(R,f) = \frac{C\omega^2\Omega_0}{1+(\frac{f}{f_c})^2} \quad (3.2)$$

$$D(R,f) = \frac{C\Omega_0}{1+(\frac{f}{f_c})^2} \quad (3.3)$$

Frequency values observed at higher grade slopes are called as f_c and f_{max} from the acceleration spectrum. In this case frequency determination in the acceleration spectrum is much easier.

For the f_c value, the frequency at which the spectrum amplitude increase is abruptly selected and for the value of f_{max}, the frequency value at which the curve enters a tendency to fall again after continuing smoothly along a band is selected. From these definitions, f_c, f_{max} and Ω_0 (cut-off, maximum frequency and displacement spectral level) were manually determined.

At the next step, for the region that covers the 3 Southern Marmara earthquakes, frequency dependent seismic Q value by was examined as $Q_{sh}=113.445f^{0.47}$ for far distances and as $Q_{sh}=60.97f^{1,42}$ for near distances. An assumption of $Q_p=2,25Qs$ (Gajewski et al., 1990, Kurtulmuş and Akyol, 2013) was used by using P-wave phase. The spectral curves of Brune's source model calculated from equations 3.2 and 3.3 using the selected f_c, f_{max} and Ω_0 spectral parameters were superposed with observed spectrums.

Using the spectral parameters determined by the trial and error method of the synthetic model. Seismic moment, strain and source radius are some of those parameters could be calculated from the equations as below;

$$M_0 = \frac{4\pi\rho\beta^3 R\Omega_0}{R_{\theta\varphi}S_a} \quad (3.4)$$

where;

shear velocity is indicated by β, seismic moment is represented by M0, the average value of propagation pattern is represented by $R_{\theta\varphi}$, distance to focus is R and S_a represents site amplification at free surface.

Hanks and Kanamori (1979) introduced the relationship between the Mw and M_0 as following equation 3.5;

$$Mw=0.66\log(M_0) + 10.7 \quad (3.5)$$

The equations 3.6 and 3.7 give radius of source and stress drop, respectively as below;

$$S_r = \frac{K\beta}{2\pi f_c} \quad 3.6)$$

$$\Delta\sigma = \frac{7M_0}{16{s_r}^3} \quad (3.7)$$

The constant K value used in the calculation of the source radius were selected as 2.33 using SH phase. From the study of Sivaram et al., (2013).the value of K from P pahse is selected as 1.91.

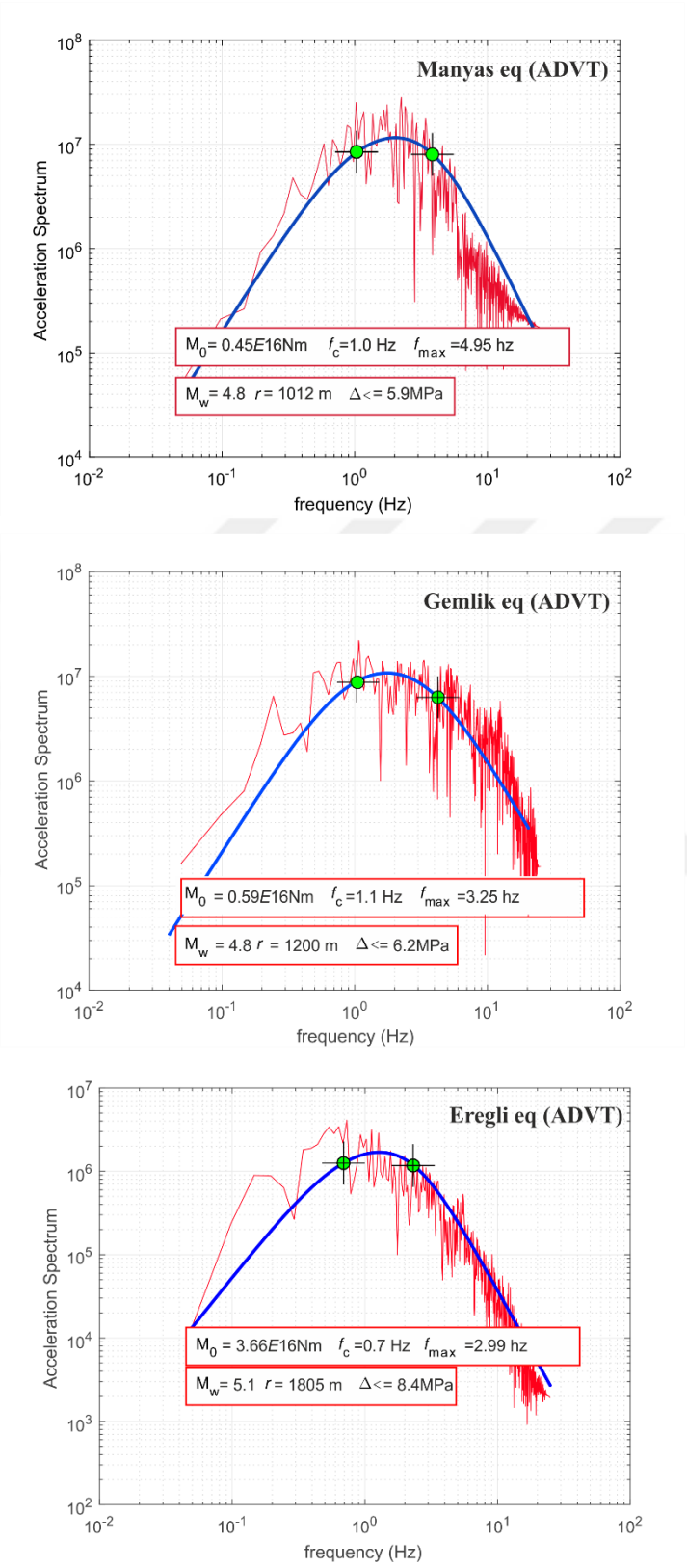

Figure 3.11. An example of SH spectrum of broadband time history of earthquake recorded at ADVT on broadband instrument along with fitted source model.

Table 3.5. The average values of spectral parameters of studied 3 earthquakes. M_0, Mw, f_c, f_{max}, S_d, S_r and N_{sta} are seismic moment, moment magnitude, cut-off frequency, maximum frequency, stress drop, radius of source and number of stations, respectively.

Event	**M_0**	**Mw**	**f_c (Hz)**	**f_{max} (Hz)**	**S_d (Mpa)**	**S_r(m)**	**N_{sta}**
Manyas Oct 20,2006	0.45	4.8	1.00	4.95	5.90	1012	6
Gemlik Oct 26,2006	0.59	4.8	1.10	3.25	6.20	1200	7
Ereğli June 07 2012	3.66	5.1	0.70	2.92	8.40	1805	24

Earthquake spectral source parameters such as corner frequency, f_{max}, stress drop and source radii are key parameters defining the characteristics of an earthquake source. In the present study, source parameters of 3 local events (Manyas, Gemlik and Ereğli earthquakes) have been estimated (table 3.5). A database of broadband recordings of those moderate earthquakes has been examined by the seismic network of KOERI. The displacement and acceleration spectrums including P and SH phases of waveforms were analyzed according to Brune's (1970) source model. A total of 37 waveforms were analyzed for the 3 local events and multi-station spectral characteristics of each event were determined manually. Each source parameter was calculated by averaging according to number of used seismic station for each event. Observed spectrums were corrected for attenuation effects using a pre-existing regional estimate of the quality factor Qs. The obtained seismic moments range from 1.60×10^{16} to 5.25×10^{16} Nm ($4.7 \leq Mw \leq 5.1$) with corner frequency range between 0.35 and 2.60 Hz. The source radii values are between 690 and 2400 meters and stress drop values vary between 2 and 13 Mpa with respect to station conditions. The results indicate that there are no significant variations at stress drop values computed from kinematic results and source spectrum. In our estimates of stress drop we use the method of Madariaga (1976) which is modified from Brune (1970) from SH-wave corner frequencies. Results obtained from median stress drop values and shear stress drop values are consistent with each other. The faulting type and the moderate size of the studied earthquakes may explain this consistency.

3.6. Discussion

Slip distribution models on the fault plane indicate a simple circular rupture pattern with decreasing slip values. Figures 3.8, 3.9 and 3.10 show final slip distribution models for Manyas, Gemlik and Ereğli earthquakes, respectively. For the Manyas earthquake, the rupture area was found to be 2.5 km along strike and 1.5 km along dip. The mean slip over this area is 0.16 m (figure 3.8). The stress drop using this rupture area and slip is 8 MPa. The slip concentrates in an almost circular distributed pattern. Similar homogeneous slip distribution was inferred for the Gemlik earthquake and the best-fitting slip distribution from different parametric models is characterized by an average slip of about 0.18 m (Figure 3.9) corresponding to a seismic moment of 9.70E15 Nm with 12 Mpa stress drop. We modelled two asperities; one is larger asperity near the hypocenter and another is smaller and located to the deeper part of the fault plane towards the east. The maximum slip is estimated is 0.25 m near the hypocenter and total seismic moment found as 5.20E16 Nm that is slightly bigger than other two earthquakes occurred in southern Marmara region The static stress drop was calculated as 13 Mpa associated with strike slip faulting the Ereğli earthquake (Figure 3.10).

The maximum slip is found to be close to the hypocenter with a value of 0.25 m. The total moment is calculated as 5.20×10^{16} Nm which is slightly bigger than that of the above mentioned studies. The static stress drop was calculated as 13 Mpa associated with strike slip faulting (Table 3.4). We noticed that mean slip values are in agreement with the results of Iio (1986). Based on the slip values static stress drops are calculated through a global empirical relationship (Lay and Wallace, 1995) and given in Table 3.4 for strike-slip fault types. Moment magnitude–rupture area scaling is influenced by the assumption of whether the stress drop from smaller to larger magnitude earthquakes can be considered constant or not.

According to results Marsan (2005) and Helmstetter et al. (2005), while the large earthquakes deserve much attention in terms of energy release, small quakes collectively have the same influence as larger ones with respect to the stress changes caused by seismic spatial clustering. Therefore, information about the stress drop values estimated from the rupture process give insight about how small earthquakes affect earthquake triggering.

Previous studies of Ichinose et al., (1997), Wells and Coppersmith (1994), Rebollar et al., (2001), Abdel-Fattah (2002), Somerville et al., (1999) are given in Table 3.6. Earthquake source information of moderate earthquakes occurred in the world and studied in this thesis are listed as for comparison.

Table 3.6. The earthquake source information used in to create an empirical relationship.

Date	**Location**	**Magnitude**	**Seismic Moment (10^{26} dyne-cm)**	**Rupture Length**	**Rupture Width**	**Disp. Dmax**
23.01.1975	Brawley,California	4.6(Ms)		10.4*	4*	0.20*
31.05.1975	Galway Lake,California	5.2(Ms)		6.8*	3*	0.02*
15.03.1979	Homeastead Val., California	5.6(Ms)		3.9*	4*	0.10*
06.08.1979	Coyoto Lake, California	5.7(Ms)		14.4*	10*	0.15*
30.03.1986	Marryat Creek,Australia	5.8(Ms)		13*	3*	1.3*
11.06.1983	Coalinga, California	5.4(Ms)		3.3*	6.5*	0.64*
29.10.1989	Chenoua, Algeria	5.7(Ms)		4.0*	10*	0.13*
13.09.1986	Kalamata,Greece	5.8(Ms)		15*	14*	0.18*
17.05.1993	Eureka Valley, California	5.8(Ms)		4.4*	7*	0.02*
14.10.1998	Umbria,Italy	5.7(Ms)		12*	2-3*	0.8*
21.03.1934	South Izu, Japan	5.5(Ms)§	0.095	7!	4!	
9.10.1965	Antioch,USA	4.9(Ml)§		3	6	
27.02.1972	Bear Valley, USA	4.7(Ml)§	0.008	3.8	2.5	
10.03.1972	San Juan Bautisla	4.8(Ml)§	0.016	4.3	2.5	
23.01.1975	Brawley, USA	4.6(Ms)§		9	4	0.20
08.02.1975	Horse Canyon, USA	4.7(Ml)§	0.035	2	2	
11.03.1978	South Puget Sound, USA	4.8 (Ml)§		2.5	4	
01.01.1979	Malibu, USA	4.7(Ms)§		5	5	
19.08.1979	Charlevoix,Canada	4.5(Ms)§	0.015	2	2	
26.12.1979	Carlisle,England	4.8(Ml)§		4	3	
25.02.1980	Anza, USA	4.7(Ms)§	0.041	2.5	2.5	
29.02.1980	Arudy,France	4.9(Mb)§	0.064	3.8	3.5	
27.7.1980	Sharpsburg, USA	4.7(Ms)§	0.043	4	5	
14.02.1981	Elk Lake, USA	4.8(Ms)§	0.1	6	7	
15.06.1982	Anza, USA	4.8 (Ml)§	0.017	2.5	3	
31.03.1983	Popayan,Columbia	4.9(Ms)§	0.35			0.01
11.08.1983	Liege,Belgium	4.3(Ms)§	0.016	5	3	
10.07.1984	North Wales, Great Britan	4.7(Ms)§	0.01	3	3.2	
05.04.1986	Cuzco,Peru	4.6(Ms)§	0.077			0.1
28.05.1987	Kameoka,Japan	4.9(Ml)§		1.4	1.8	

Table 3.6. The earthquake source information used in to create an empirical relationship (cont.).

Date	**Location**	**Magnitude**	**Seismic Moment (10^{26} dyne-cm)**	**Rupture Length**	**Rupture Width**	**Disp. Dmax**
10.06.1987	Wabash Valley, USA	4.4(Ms)§	0.031	1.7	3	
02.08.1987	Xunwu,China	4.8(MI)§	0.036	4	4	
10.10.1986	San Salvador	5.4(Ms)§	0.45	6	7.5	
13.09.1986	Kalamata,Greece	5.8(Ms)§	0.89	15	14	0.18
25.09.1987	Lakeside, USA	4.6	0.038	5.5	6	
03.12.1988	Pasadena, USA	4.2	0.031	4.5	2.5	
28.06.1992	Landers, California	7.2(Mw)£	7.5	69.0	15.0	7.94
16.09.1978	Tabas,Iran	7.1(Mw)£	5.8	95.0	45.0	2.13
17.10.1989	Loma Prieta,California	6.95(Mw)£	3.0	40.0	18.0	4.96
17.01.1995	Kobe,Japan	6.9(Mw)£	2.4	60.0	20.0	3.48
28.10.1983	Borah Peak,Idaho	6.87(Mw)£	2.3	48.75	26.4	1.47
23.12.1985	Nahanni, Canada	6.75(Mw)£	1.5	34.67	16.49	5.16
17.01.1994	Northridge,California	6.66(Mw)£	1.1	18.0	21.0	2.86
05.10.1985	Nahanni,Canada	6.63(Mw)£	1.0	29.33	13.92	3.83
09.02.1971	San Fernando,California	6.53(Mw)£	0.7	13.36	12.03	3.00
15.10.1979	Imperial Valley, California	6.43(Mw)£	0.5	36.0	10.0	1.80
24.11.1987	Superstition Hills, California	6.33(Mw)£	0.35	20.0	8.05	1.86
24.04.1984	Morgan Hill, California	6.18(Mw)£	0.21	26.0	11.5	1.00
07.08.1986	NorthPalmSprings,California	6.14(Mw)£	0.18	20.0	13.3	0.45
1.10.1987	Whittier Narrows, California	5.97(Mw)£	0.1	10.0	10.0	0.90
08.06.1979	Coyote Lake,California	5.66(Mw)£	0.035	5.5	4.57	1.20
20.10.2006	Manyas Earthquake,Turkey	4.7(Mw)~	0.00174	1.50	1.0	0.12
24.10.2006	Gemlik Earthquake, Turkey	4.8(Mw)~	0.00343	1.50	1.0	0.18

*:Source parameters estimated from theoretical relationship between certain source parameters (Mohammadioun, B., and Serva, L. 2001).

§: Source parameters taken from Wells and Coppersmith, 1994.

!: Estimated from body and surface wave studies.

Ms: Indicates Surface wave magnitude, Ml: Indicates Local magnitude, Mw: Indicates Moment magnitude.

£: List of earthquakes and source parameters taken from Somerville et al., 1999.

~: Source parameters obtained from this study.

Rupture area and seismic moment of those collected events as well as the results of this thesis are presented in Figure 3.12. Exponential fit to this data yields ln(y)=0.71*ln(x)+4.91. In general, rupture area of moderate sized events is overestimated by Somerville et al., (1999).

The results obtained from the empirical scaling relations are compared with the big earthquakes occurred worldwide. Rupture models from kinematic inversion of the earthquakes produce non-unique solution. For this reason, two type of constraints were used to get rid of unwanted slip distribution due to the underdetermined parameters of rupture models until well matched observed and calculated waveforms were obtained. From the first findings the rupture area was calculated as ~6 km^2 and maximum slip value as ~8 cm. The results are proportional to scaling relation for larger events studied by Somerville et al. (1999).

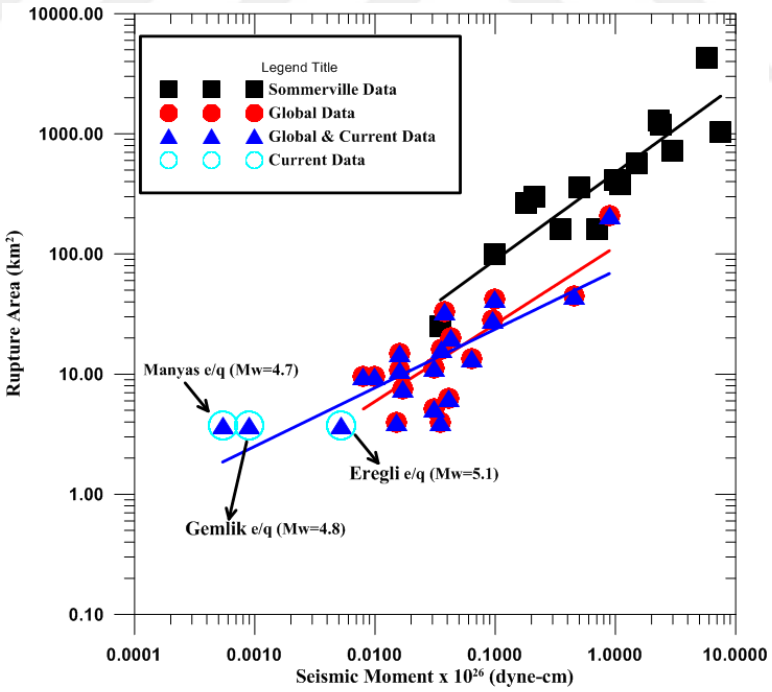

Figure 3.12. Rupture Area-Seismic Moment relation. Red-filled circles indicate source parameters estimated from theoretical relationship between certain source parameters taken from (Global Data) Mohammadioun and Serva (2001) and Wells and Coppersmith (1994). Black filled squares indicate, source parameters taken from Somerville et al., study (1999).

Open circles indicate the source parameters obtained from this study, source parameters obtained from this study and Global Data are presented by triangles.

In this study, not only SGM but also broadband data were intended to be used in order to enhance model resolution. Broadband (BB) data were not combined with the SGM data since the BB station distribution did not provide sufficient azimuthal coverage at reliable offsets. On the other hand, none of the band-pass filter intervals made the BB data suitable in this study. One of the findings arising from this study is that investigation of moderate size earthquakes requires good quality near-field SGM records. Because of that reason, some of SGM records at far distances were not used. Definitely, the regression models show a large amount of scattered data. This of course affects the accuracy of the empirical relationship for a confidence model. The accuracies of the fits are related with a tectonic setting, data quality and magnitude evaluation criteria of any earthquake solution, such as fault typing and especially for moderate earthquakes.

4. DYNAMIC RUPTURE PROCESS: DATA and METHODS

4.1. Introduction

The basic principle of dynamics of mechanical system is based force system. There is relationship between energy balance and motion that is governed by those force system (Aki and Richard, 2002). In literature, many researchers are involved in the issue of rupture process by using several analysis techniques. Kostrov (1966) is the first researcher who simulated shear crack propagation, spontaneously. Andrews (1976) and Das and Aki (1977b) studied on simulated spontaneous rupture propagation. Their target model was slip weakening one as a friction law of the fault. Researches by Mikumo and Miyatake (1978), Day (1982a, 1982b), Virieux and Madariaga (1982), Cochard and Madariaga (1994), Fukuyama and Madariaga (1998), Inoue and Miyatake (1998) and Madariaga et al., (1988) can be address in relation to this topic.

Although a few of studies on simulation of ground motion associated with dynamic models, some of these studies have made considerable contributions to dynamic modeling. For example, Olsen et al. (1997) used finite difference method technique and make some simulations of rupture by using ground motion data of 0.1 – 0.5 Hz in the frequency range. He simulated 1992 Landers, California earthquake. Inoue and Miyatake (1998) used synthetics ground motion data exhausted from a strike-slip fault in order to perform a rupture process. They performed 3D finite difference approach for frequencies up to 2 Hz. Similarly, Dalguer et al. (2001a,2001b) aimed to simulate rupture propagation of Chi-Chi earthquake occurred in 1999 at Taiwan. The simulated rupture process of the Chi-Chi earthquake gave numerous invaluable inputs in order to understand the complexity of damaged distribution caused by this event. According to theirs results, the northern portion the fault rupture spreads to the surface with low values (about velocity of 1.2 km/s). Distinctively, in the southern portion, rupture propagation speed is about 3.0 km/s, higher than the opposite site. Dalguer and Irikura (2003a) focused on 1999 the Kocaeli earthquake to simulate shear dynamic rupture process. They used the 3D staggered-grid finite difference method to realize this study.

Results showed that at the east and west part of the fault, the highest strength excesses (around 10MPa) and dynamic stress drop (around 30Mpa) were found, suggesting barriers that were broken during the earthquake (asperities zone). At the central band of the fault, from the hypocenter to the east-forward direction the relative strength has very low values, (about 0.2 to 1.0 MPa) suggesting weakness zone and probably broken region before the earthquake. During the dynamic rupture propagation, this zone broke with super-shear rupture velocity, as predicted by the kinematic model.

Dalguer et al., (2003b) realized 3D dynamic rupture process for Tottori, Japan earthquake occurred in 2000. Fracture zones of surface rupture makes this earthquake to be interested. They also used discrete element method. Interval new crack are the attractive properties of this rupture area. They consider that those cracks propagate under tensile stress due to the dynamic process shear dislocation. Slip-weakening is simply a model that uses friction law on the fault for the shear rupture propagation. Important dynamic parameters such as critical slip, strength excess, dynamic stress drop were found by used kinematic source parameters.

Aochi and Madariaga (2003) ran another simulation study. They used boundary integral equation method to simulate dynamic rupture propagation along a number of different irregular fault geometries of the 1999 Kocaeli earthquake. In addition to this, they investigated the effect of frictional parameters and the initial stress field.

Somerville (2003) and Kagawa et al. (2004) examined on differences between buried and surface rupture by processing ground motion data. They noticed that larger asperities of surface rupture events are located in the shallower part than approximately 5 km. However, for the buried rupture of earthquakes, big slip areas located at deeper than 5 km over the depth. Another striking result of this study is that the total rupture area for the buried sources is 1.5 times smaller than the surface rupture of earthquakes, even both events has same seismic moments. Moreover, deeper asperities yield more stress drops than the shallow ones, again slip velocities have high values due to asperities located at deeper parts. Zhang et al. (2004) to study stress distribution of the fault plane, friction law for rupture and to specify dynamic parameters of this earthquake source analyzed 1999 Chi-Chi earthquake. Zhang et al. (2003) reported that, in the majority of the points on the

fault, the relationship between stress and shear is consistent with the slip-friction law in the rupture process. On the other hand, consistency with the observed velocity-weakening law between stress and shear velocity is not clear. To summarize, large slip areas produce high stress drop. There are some deductions from this work. For example, when the shear stresses reach the level of the fault strength, calculated strength excesses are small before the main shock. It means, the aftershocks are related with the spatial distribution of dynamic parameters of seismic source. Moreover, these aftershocks where concentrated near the fault plane have larger critical slip-weakening distance values.

Zhang et al. (2004) study shows the complexity of dynamic rupture process. Unlike the kinematic model, starting time of the rupture distribution is more heterogeneous pattern. They noticed that, the regions with a large strength excess on the fault surface delayed the rupture propagation. When the rupture front faces the high strength excess regions, rupture fronts jumps from high strength excess zones to low strength excess zones, namely leaving the un-ruptured source areas behind which subsequently rupture.

4.2. Comparison between Kinematic and Dynamic Rupture Simulations

There are two earthquake source processing models those provide powerful approach in order to understand the rupture phenomena and earthquake mechanism near the hypocenter. Rupture discontinuity modeling approaches are different in processing steps. A fault slip assumption is considered in kinematic model. In this model, slip function is based on space and time. In the dynamic model, the fault rupture is taken as a physical model. The former associates the earthquake with prescribed slip events, without taking into account the physics involved in the rupture, but the latter is an earthquake physics model and the kinematic slip model involves a solution dynamically.

4.2.1. Kinematic Model

Earthquake kinematic approach is quite effective in rupture modeling on fault plane area with a few of seismic source related parameters. These parameters can be determined from analysis of the resulting seismic radiation. A typical set of input parameters used to characterize a kinematic model includes: slip at each sub-fault on the fault, rupture velocity

Vr and the permanent slip D and rise time, defining the slip velocity function, which is usually chosen to have a convenient parametric form. The output of these models is the earthquake ground motion on the free surface. Once a kinematic model is obtained, it is possible to calculate the ground motion at any point using an appropriate Green's function. The calculation of this ground motion has its basis in the well-known representation theorem (Eq. 3.2 of Aki and Richard 2002) that can be solved numerically.

The form of the slip velocity function is an essential assumption. Usually this function is prescribed as a function of position and time, which is specified using either: (i) an assumed functional form, sometimes with guidance from simple theory, subject to empirically-guided adjustments, and/or (ii) multiple time windows, where one can ideally obtain the shape from solving for the shape of the function. However, for the case of near-field data, Cohee & Beroza (1994) have shown that the multiple time window approach does worse for estimating the rupture velocity, and slip distribution (See Konca & Bouchon 2014 for discussion of these two approaches).

For the predetermined shape of slip velocity functions, commonly used ones include the boxcar Haskell (1964), Brune's function (Brune, 1970), Kostrov- like function (Hisada, 2000), and others. Then, if the slip functions of these kinematic models are well represented, they may provide quite detailed descriptions of earthquakes. From the inversion of the observed ground motions, slip distribution and the rupture history over time can be modelled (Kohketsu, 1985). In this thesis, in addition to kinematic analysis of Düzce earthquake, the slip distributions of three moderate sized occurred at southern Marmara are determined by using weak and strong motion data. Recently improved inverse solution methods allow to understand the kinematic behavior of earthquake source in detail (Yoshida 1995). Multiple-time window linear waveform inversion uses Aki and Richards (1980) representation theorem. In this methodology, displacement due to moment release on the fault surface is defined as;

$$Un(x,t) = \int d\tau \int\int_{\Sigma} \left[u_i(\xi,\tau)\right] C_{ijkl}(\xi) n_j G_{nk,l}(x, t-\tau; \xi, 0) dS \qquad (4.1)$$

where

$$[u_i(\xi,\tau)] = u_i(\xi,\tau) + -u_i(\xi,\tau) \quad (4.2)$$

where $u_n(\mathbf{x},t)$ is the displacement at point **x** at time *t;* G*nk,l*(**x**,*t*;ξτ) is the spatial derivative of Green's function, where on a plane normal to the *l* direction at position ξ, the Green's function is the *n*th displacement component at point **x** to due to a point dislocation in the *k*th direction.*;* ∑ is the fault surface; n_j is the *j*th component of **n**, the vector normal to fault surface; c_{ijkl} is the elasticity tensor, and $[ui(\xi,t)]c_{ijk}ln_j$ is the total moment tensor (Asano et al., 2005; www.seismo.ethz.ch).

One advantage of kinematic models is their simplicity and straightforward application for macro-scale earthquake simulation, especially when propagation effects in complex geologic structure are dominant. In fact, kinematic models have contributed substantial advances in understanding of geological effects on ground motion, e.g.: basin amplification, energy channeling and focusing by sedimentary waveguides, hazard curves based on physics of wave-propagation (CyberShake: Graves et al., 2006) using detailed broadband scenarios.

4.2.2. Dynamic Model

When compared the kinematic models, studying the dynamic model involves physical characteristic definition of the rupture. A dynamic determination of slip due to the fault kinematics is needed to solve elasto-dynamic equations first with respect to the frictional slipping. In seismology heterogeneity and the complex dynamic rupture process of an earthquake source make the solution of the fault behavior limited. Some researchers like Ohnaka et al. (1987), Ruina, 1983, Dieterich, 1979 worked on laboratory experiments of sample rocks. They observed important clues on nature of the constitutive, which produce fault plane sliding during earthquakes, namely friction phenomena. The earthquake rupture is characterized as dynamically continuous shear dislocation on a frictional fault plane covers elastic continuum.

This is very useful for analyzing natural earthquakes (Andrews, 1976; Das and Aki, 1977a; Day, 1982a, and Day, 1982b; Olsen et al., 1997). The main disadvantage of the dynamic models is the lack of information to realistically parameterize the strain of the friction model and the crust. Efforts to make proper earthquake records using dynamic models help fill this void, but these efforts are extremely non-unique.

3D dynamic calculations are quite challenging in terms of computer resources. Simulation of large earthquakes requires a large amount of memory and processor power. This computational intensity is disadvantageous for dynamic modeling, but advances in high-performance computing are mitigating this limitation. Kinematic models attempt almost reasonable outline for integrating observational constraints into the earthquake source. However, there are no physical constraints on causal source physics. Generally speaking, it is more difficult to integrate observational constraints into dynamic models, but dynamic models nonetheless have greater potential for addressing science question that bear directly on strong motion simulation, especially where source processes are dominant.

4.2.3. Numerical Comparison Between Kinematic and Dynamic Rupture Simulation

Dalguer and Day (2006) studied on Japan-Tottori earthquake in year 2000 by performing dynamic and kinematic rupture simulation. The dynamic model was developed assuming the simple slip weakening friction model (Andrews 1976). They adjusted dynamic parameters of stress such as strength excess, stress drop, critical slip distance for the slip weakening as shown in Figure 4.1, calculated in the METI (2004) project. Originally these parameters were estimated by Dalguer et al (2002, 2003a) using the kinematic source model derived from the kinematic source inversion of Iwata and Sekiguchi (2002). Trial and error scheme was done until getting the dynamic parameters. They indicate that e final slip of the dynamic rupture simulation was approximately equivalent to the final slip of the kinematic models of Iwata and Sekiguchi (2002), as shown in Figure 4.2.

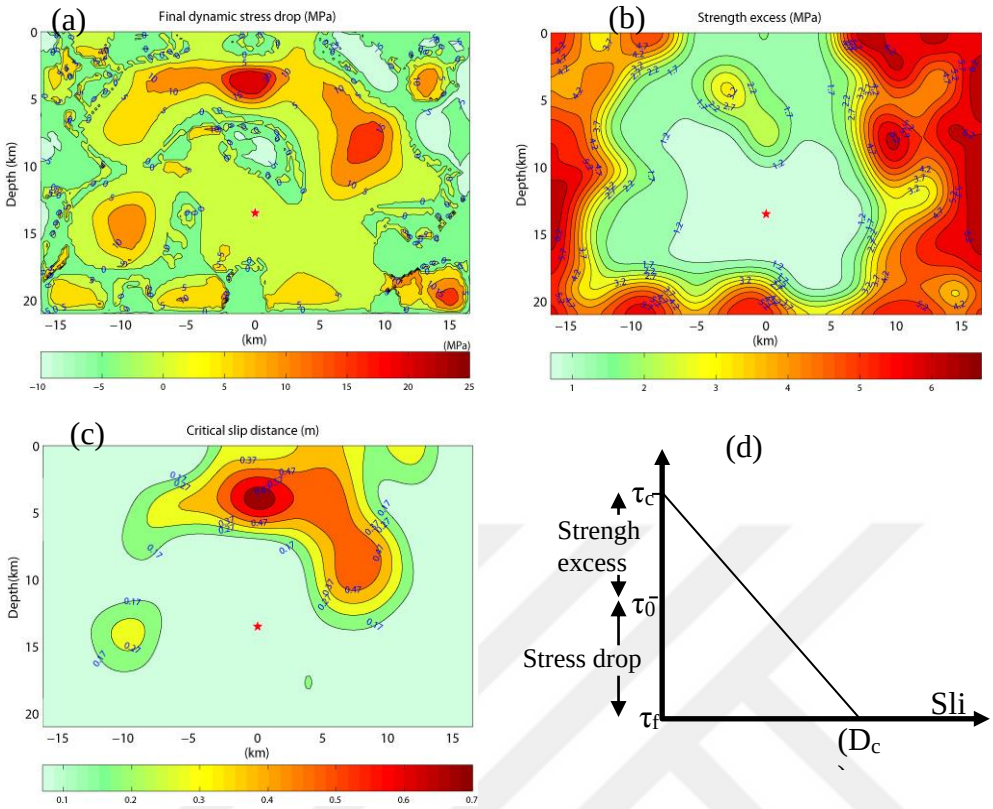

Figure 4.1. Dynamic parameters of the 2000 Tottori earthquake presented in the METI (2004) project: (a) Dynamic stress drop distribution; (b) strength excess distribution and (c) critical slip distance distribution. The start indicates the hypocenter location. (d) Slip weakening friction model; where τ_c is the static yielding stress, τ_0 the initial stress, τ_f final stress and D_c the critical slip distance.

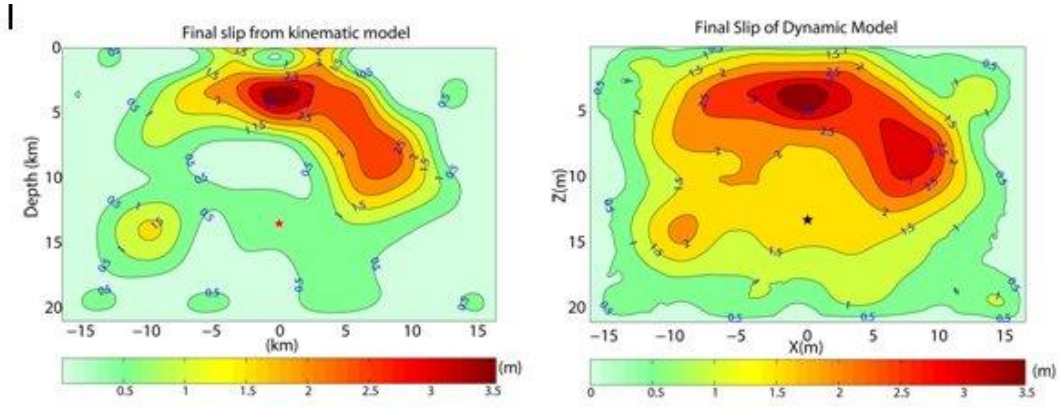

Figure 4.2. Final slip distribution of the 2000 Tottori earthquake of the kinematic model of Iwata and Sekiguchi (2002) (left), and the dynamic model (right).

Dalguer and Day (2006, 2007) first mentioned the staggered-grid split node fault model then developed the model by implementing finite difference code. This process takes lots of time and needs multi-processors (Dalguer et al., 2006) in order to make dynamic rupture simulation.

Kinematic and dynamic rupture propagation of models is another well-defined difference between these two models. Figure 4.3. shows the rupture front progress for these two models. The kinematic rupture propagates without any physical constraint; however, the rupture for the corresponding dynamic model propagates in response to the stress state and friction model.

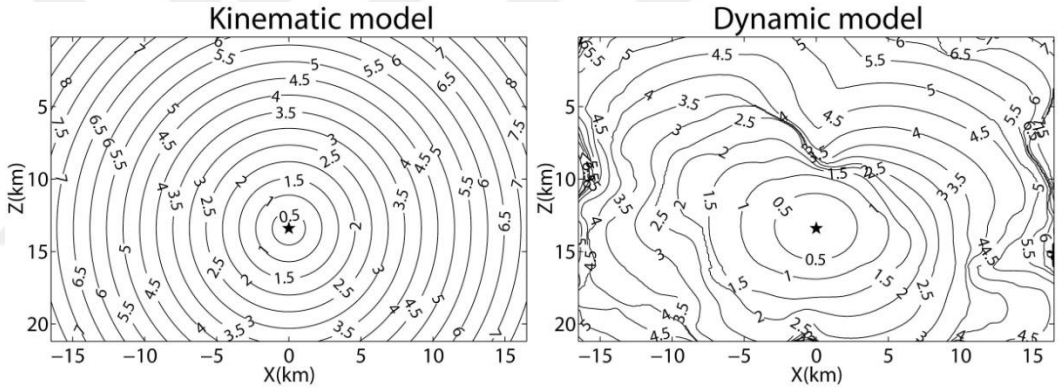

Figure 4.3. Contour plot of the rupture front of the 2000 Tottori (Japan) earthquake from kinematic (left) and dynamic (right) rupture models.

4.3. Slip Weakening Behavior

According to constitutive law, the maximum frictional strength can be formulized (Dieterich, 1994) associated with basic constitutive parameters as below,

$$\tau = f(u, \dot{u}, \sigma_n^{eff}, c_e, \lambda_c, T, \Psi) \tag{4.3}$$

where

u is the slip,

$\dot{u}$ is the slip velocity,

σ_n^{eff} *is* the effective normal stress,

Here pore fluids effect the σ_n^{eff} value,

c_e is the chemical effect of the fluid pressure,

$\lambda_{c,}$ defines fault surface geometry,

T is the temperature,

Ψ is the state variable.

On the other hand, there is relationship between state variable g_i ;

$$\frac{d}{dt}\psi_i = g_i(u, \dot{u}, \sigma_n^{eff}, c_e, \lambda_c, T, \boldsymbol{\Psi}) \tag{4.4}$$

The function g_i actually depends on the constitutive parameters. The equation 4.4 is known as evolution equations. Slip weakening and friction law, which depends on rate and state are the main constitutive relations in order to work on crack dynamic.

4.3.1. The Slip−Weakening Law

There are many problems with ideas for example; analysis of rupture is only true if the fault is formed by the present stress field. In particular, when a fault predates stress field, analysis is more complicated. Nevertheless, the discussion is a simple introduction to the concepts involved in rupture dynamic process.

Three main steps are responsible of an earthquake occurrence scheme, namely, rupture initiation, frictional sliding and rupture ending. Since frictional sliding is more complicated, the relationship between shear stress applied on a body and sliding dislocation is irregular (Zhang et al., 2003). The one of the stage is more affective that is constitutive friction laws. This controls the rupture process directly and defines the fault characteristics. For the examining the source rupture process, the friction law is a vital key to dynamic simulation. Of course, each earthquake has different source rupture process due to the source complexity. This complexity and the disparities of material properties may control rupture evaluation for each different events. The investigating of friction laws and

related parameters is very important in the understanding and study of earthquake source process.

Material of the rocks become weaker during the friction with increasing slip then those materials have stable sling model. This can be called as slip weakening. Zhang et al., (2003) point out that some of rocks display an inverse reliance of friction on slip velocity. Hence, this is the basic background definition of velocity weakening. There are two known friction laws; Ida (1972), Andrews (1976) and Day (1982a) used slip-weakening law. Carlson and Langer (1989), Fukuyama, and Madariaga (1995, 1998) prefer to work on slip and velocity weakening law. In addition, some researchers like Dieterich (1978), Dieterich et al. (1978), Okubo and Dieterich, (1984), Ohnaka, (1990) and Ohnaka and Shen (1999) worked on some laboratory studies based on material friction in which sliding is considered as slip of a fault. Stress measurements could be only done at shallow depths near a fault, so it is very difficult to correlate these results with one of the friction laws. Another study was carried out by Okubo (1989). He implied that the use of a rate- and state-dependent friction was related with dynamic traction.

Nevertheless, those of researchers mentioned above performed their experiments limited in small scale such as laboratory conditions. This could not be compared with a large and real faulting area with respect to the natural earthquake. Results have indicated that studies done at both laboratory conditions and fault area are theoretical ones. Zhang et al. (2003) emphasized that a slip−weakening law is sufficient when the rupture process will be reproduced during an earthquake. If the physical mechanic properties of a fault during its activity behavior is evaluated, a rate and state frame that describes state of stress on the rupture plane well can be obtained.

The equation 4.3.3 gives the slip weakening law

$$\begin{cases} D = 0 & for\ \sigma < \sigma_y \\ \sigma = \sigma_y + (\sigma_s - \sigma_y)\frac{D}{Dc} & for\ 0 < D \leq Dc \\ \sigma = \sigma_y & for\ D > Dc \end{cases} \qquad (4.5)$$

where

σ_y is strength excess,

σ_s is the level of static stress,
Dc is distance to critical slip weakening.

The amount of Dc is a good identifier that allows to mark the cohesive zone. This defines a region where seismic energy is going to be released. The slip value of any point at fault sliding surface is zero until the total value of shear stress (σ) has maximum (yield stress, σ_y) level (peak value) from its initial stress (σ_0). When the yield stress (σ_y) is obtained once, the slip value (D) at any point on the fault has a starting value zero then this slip increases then it becomes a shear stress. This shear stress (σ) decreases to level of static stress linearly. Figure 4.4 indicates the relationship between slip and stress based on slip weakening law.

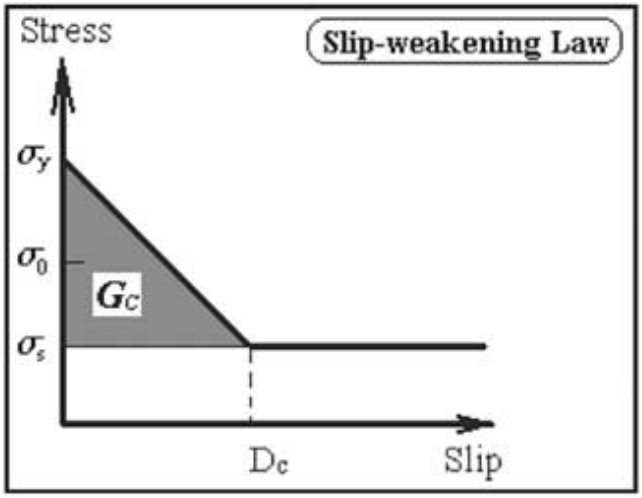

Figure 4.4. A graph of slip versus stress by means of weakening friction model.

4.3.2. Rate and State-Dependent Friction Laws

Friction is represented as rate−and state−dependent laws. This is generalized usage of constitutive relations when it compares with slip−weakening law. Figure 4.5 summarizes this explanation. The main feature of these laws is their slip-rate sensitivity. It is assumed that friction increases when slip rate decreases, which controls the way slip heals. According to the laws, slip rate ($\dot{u}$), state variable (Ψ,•) and normal stress (σ_n^{eff}) are the main keys of the friction (Bizzari et al. 2001). The rate and state dependent constitutive

law can be explained in several ways. The best known is slowness laws (the Dieterich–Ruina), which used to have observations on friction of rock materials in laboratory conditions. The Dieterich–Ruina's version is stated as,

$$\tau = \left[\mu - \alpha \ln\left(\frac{v_*}{v} + 1 \right) + b \ln\left(\frac{\Phi v_*}{L} + 1 \right) \right] \sigma_n^{eff}$$
$$\frac{dy}{dt} \Phi = 1 - \frac{\Phi v}{L} \qquad (4.6)$$

where,

τ is shear stress,

σ_n^{eff} is normal stress (effective) : normal stress- pore pressure,

V is known as slip velocity,

α and b material dependent parameters,

V_* is reference velocity,

μ is the friction of steady-state condition at $V=V_*$,

L is the distance of critical slip,

Φ is the variable of state and this variable increase linearly over time and occurring re-strengthening process.

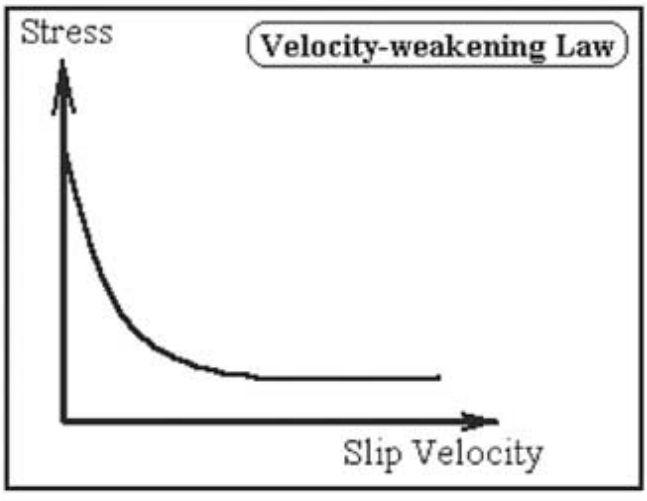

Figure 4.5. A graph of exponential relationship between stress and slip velocity according to a typical rate-dependent friction law (velocity-weakening).

4.4. SORD - A Support-Operator Method for Viscoelastic Wave Modeling in 3D Heterogeneous Media

Recently developed methods have examined the dynamic rupture simulation in heterogeneous medium. For example, Aagaard (1999) and Oglesby et al. (2000) studied on the simulation by using finite element method. Festa (2004) and Vilotte et al. (2005) worked also on this subject by using spectral element methods. In addition to those performances, finite volume techniques (Benjemaa et al., 2007) and revised finite element method users (Cruz-Atienza et al. 2007; Kase and Day, 2006; Zhang et al., 2006) realized the simulation algorithms. In order to resolve rupture simulation procedure, high spatial sampling is the most required considerable calculation step. Adaptive local optimization is a required working path if someone must use unstructured grid pattern. The problem in constructing the adaptive grid pattern (meshing system) is to generate grids. Unfortunately, adaptation for parallel computation is difficult and efficiency would be low. A model with a regular structured mesh pattern is sampled according to 'brute force' approach. It is more convenient way to get parallelizable algorithms. Considered method of 'support operator' based on generalized finite element schemes of Samarskii et al. (1981, 1982) and Shashkov (1996). Ely et al. (2008) performed the 'support operator' technique and applied to elastic wave propagation in three-dimensional case then he initiated to adapt this application for spontaneous rupture.

4.4.1. Theoretical Formulation

Day and Dalguer (2005) defines faulting which is form of a plane model such as internal surface ($\sum$) where displacement is occurred. This is the discontinuity of displacement during a rupture. Let say $\hat{n}(x)$ is unit normal includes points one sitem (Σ^-) to other (Σ^+) side of the surface. In equation 4.4.1, u^- and u^+ are limits of displacement at the surface,

$$u^{\mp}(x,t)=\lim_{\epsilon \to 0} u(x \pm \epsilon \hat{n}(x),t) \qquad (4.7)$$

From the equation 4.7 both sides can be separated by not interpenetrating. Then, the normal displacement can be written as;

$$\hat{n}.(u^{+}\text{-}u^{-}) \geq 0 \tag{4.8}$$

The normal displacement will be positive.

In the case of displacement, slip is expressed as,

$$s = (I - \hat{n}\hat{n}).(u^{+}\text{-}u^{-}) \tag{4.9}$$

Equation 4.4.4 gives 'traction' and traction depends on unit normal and continuous stress.

$$\tau = \sigma.\hat{n} \tag{4.10}$$

The shear component traction is given in equation 4.11,

$$\tau_s = (I - \hat{n}\hat{n}).\tau \tag{4.11}$$

There is a boundary condition for the rupture that depends on frictional strength (τ_c) and absolute value of shear traction. Equation 4.12 presents this boundary conditions as;

$$|\tau_s| \leq \tau_c \tag{4.12}$$

If frictional strength less than shear traction, slip occur and $\sum$ is visible to elastic waves. On the other hand, when a shear traction equals to frictional strength then slip occurs. Equation 4.13 gives the relationship between the shear traction and slip velocity.

$$\tau_c.\dot{s} = |\dot{s}|\tau_s \tag{4.13}$$

The slip weakening model changes as function of the slip propagation length. A path integration specifies this equation with respect the slip velocity.

$$l = \int_0^t |\dot{s}| dt \quad .$$

(4.14)

The frictional strength is given in equation 4.15 equal to the product of the normal traction and a coefficient of friction;

$$\tau_c = -\tau_n \mu_f(l) \tag{4.15}$$

where,

$\mu_f(l)$ is friction coefficient and τ_n is the normal traction. Friction coefficient can be expressed as function of slip propagation length;

$$\mu_f(l) = \begin{cases} \mu_s - (\mu_s - \mu_d) l/d_0 & l \leq d_0 \\ \mu_d & l > d_0 \end{cases} \tag{4.16}$$

where,

μ_d and μ_s dynamic and static friction coefficients, respectively,

d_0 is the critical slip-weakening distance.

The normal stress has negative value (not tensional) during rupture, and hence positive τ_c value is observed.

The methodological aspects of the complexity is actually based on rate- and state-dependent equations. In equation 4.16, if the shear traction is zero then there would be distinction between τ and $\tau_c$disappears. Here, initial state (τ_0) will be called as traction. It is possible solve the equation either from an initial stress field (σ_0) or directly strike and dip (Fig. 4.4.1). Generally speaking, the first solution approach is more suitable for specifying tractions in case of regional tectonic burden. The other is more traditional and local frictions on the fault yield initial traction on the fault. Combination of those approaches can be expressed as;

$$\tau_0 = \sigma_0 . \hat{n} + \tau_n \hat{n} + \tau_{s1} \hat{s}_1 + \tau_{s2} \hat{s}_2 \tag{4.17}$$

where ,

$\hat{s}_1$ is the strike

$\hat{s}_2$ is the dip.

Those normal of dip and strike can be expressed with respect to a downward pointing unit normal ($\hat{d}$).

$$\hat{s}_1 = \hat{n} \times \hat{d} \tag{4.18}$$

$$\hat{s}_2 = \hat{s}_1 \times \hat{n}. \tag{4.19}$$

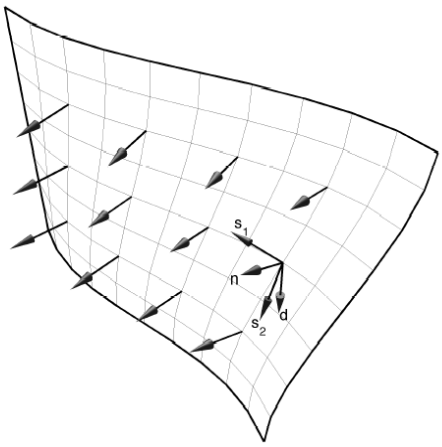

Figure 4.6. Slip vectors on a non-planar fault. Instead of classical source representation, vectors (unit normal $\hat{n}$) downward unit vector ($\hat{d}$) specify the strike and dip in coordinate system ($\hat{s}_1, \hat{s}_2 \times \hat{n}$).

4.4.2. Numerical Method

Analytical solutions to problems can sometimes be limited. In this case, under the above mentioned boundary conditions, numerical approximations are essential. Most of recent numerical algorithms use Support Operators method (SOM) introduced by Ely et al. (2008). The method uses a hexahedral, logically rectangular mesh in time domain. Ely et al. (2008) defined two type of spatial functions; one is nodal functions (H^N) those have

hexahedra vertices and the other is cell functions (H^c) those have hexahedra volumes. Discrete variables constitute the mesh structure with the same names

Some parameters are included in equation 4.20 for numerical stabilization. A discretization is needed for a staggered spatial pattern on the nodes. Except for stress tensor

(σ), kinematic variables (u,v), additional parameters were defined Ely et al. (2008), named stiffness (Y) and viscosity (β). by On the nodes; Hourglass viscosities β and Y, used for numerical stabilization;

$$(\rho, \gamma, \beta, x, u, v, a, g) \in H^N \text{ ve } (\lambda, \mu, \mathrm{Y}, \sigma) \in H^c \tag{4.20}$$

Function spaces with second-order exact D and $\mathcal{D}$ operators are shown in equation 4.21.

$$\mathrm{D} : \mathrm{H^N} \rightarrow \mathrm{H^C} \text{ ve } \mathcal{D} : \mathrm{HC} \rightarrow \mathrm{H^N} \tag{4.21}$$

Details of the definitions and more are explained in the paper of Ely et al. (2008). The discretized the equation of motion (summarized in the paper of Ely et al. (2008) with Δt is designated by a superscript;

$$g_{ij} = D_j\left(u_i^n + \gamma v_i^{n-1/2}\right) \tag{4.22}$$

$$\sigma_{ij} = \Lambda \delta_{ij} g_{kk} + M\left(g_{ij} + g_{ji}\right) \tag{4.23}$$

$$a_i = RD_j\sigma_{ij} - \tau_k Y Q_k\left(u_i^n + \check{\beta} v_i^{n-1/2}\right) \tag{4.24}$$

$$v_i^{n+1/2} = v_i^{n-1/2} + \Delta t a_i \tag{4.25}$$

$$u_i^{n+1} = u_i^n + \Delta t v_i^{n+1/2} \tag{4.26}$$

$$\Lambda = \frac{\lambda}{V^C} \tag{4.27}$$

$$M = \frac{\mu}{V^C} \tag{4.28}$$

$$R = \frac{1}{\rho V^N} \tag{4.29}$$

where,

V^C and $V^N$is cell and node valumes, respectively.

In this system stable cell distance (Δx) and time interval (Δt):

$$1 < \frac{\Delta t}{\Delta x}\sqrt{\frac{3(\lambda + 2\mu)}{\rho}} \tag{4.30}$$

Andrew (1999) and Day and Dalguer (2005) specified split node method investigating the fault boundary conditions. The modified acceleration can be identified as indicate in equation 4.31.

$$\tilde{\mathbf{a}}_{\pm}^{n} = \mathbf{a}_{\pm}^{n} \pm A R_{\pm}(\boldsymbol{\tau} - \boldsymbol{\tau}^{0}) \tag{4.31}$$

where A is the part of fault surface with respect the each computed node. The boundary conditions for the fault model impressed in equations (4.12), (4.16), (4.17), and (4.18) are to construct the traction. The trial traction can be emphasized as seen in equation 4.32. This equation tell that the traction is needed to have zero relative velocity among the double nodes at following time steps.

$$\tilde{\boldsymbol{\tau}} = \boldsymbol{\tau}^{0} + \frac{(\mathbf{v}_{+}^{n-1/2} - \mathbf{v}_{-}^{n-1/2}) + \Delta t\,(\mathbf{a}_{+}^{n} - \mathbf{a}_{-}^{n})}{\Delta t\; A(R_{+} + R_{-})} \tag{4.32}$$

Then the trial traction is ($\tilde{\tau}_i^{\,s}$) is found as;

$$\tilde{\tau}_i^{s} = \tilde{\tau}_i - \hat{n}_i \sum_{j=1}^{3} \hat{n}_j \tilde{\tau}_j \tag{4.33}$$

The normal traction (Eq. 4.34) has a trial value in getting zero relative dislocation.

$$\tilde{\tau}^n = \sum_{i=1}^{3} \hat{n}_i \left[\tilde{\tau}_i + \frac{(u_i^+ - u_i^-)}{\Delta t^n A (R^+ + R^-)} \right] \quad (4.34)$$

Finally, the tensile stress (traction) on the fault can be expressed as;

$$\tau_i = \tau^n \hat{n}_i + \tau^s \frac{\tilde{\tau}_i^s}{|\tilde{\tau}^s|} \quad (4.35)$$

4.4.3. Perfectly Matched Layer

It is necessary to limit the calculation domain wave modeling in spaced materials. Some theories approach to do this. So that, Perfectly Matched Layers method is the mostly preferred one and introduced by Berenger (1994, 1996) applying for electromagnetic waves. Marcinkovich & Olsen (2003) defined boundary conditions for absorbent layer to perform elasto-dynamics outputs such control velocity and stress. The program SORD, which is defined and used within this thesis, has almost similar theoretical background.

The SORD is required to make some modifications, which yield in damping of the spatial velocity damping and stress. The advantageous of this modification reduces the computational storage and off course multiplications will be reduced. So, the changed explanation is;

$$\dot{g}_{ij} + d(x_j) g_{ij} = \partial_j v_i \quad (4.36)$$

$$\dot{\sigma}_{ij} = \lambda \delta_{ij} \sum_k \dot{g}_{kk} + \mu(\dot{g}_{ij} + \dot{g}_{ik}) \quad (4.37)$$

$$\dot{p}_{ij} + d(x_j) p_{ij} = \partial_j \sigma_{ji} \quad (4.38)$$

$$\dot{v}_i = \frac{1}{\rho} \sum_j \dot{p}_{ij} \quad (4.39)$$

where;

xj is the distance between cell (node) and PML interface for x, y or z domain.

Indices repetitions are not implied in the summation formula in 4.39. Note that PML interface must be vector to Cartesian coordinate axis (x, y or z). Corners of the model and damping in any one direction are overlap with PML zones.

Modified formations are proper to storage velocity and stress values of elastic state for numerical schemes. Developed form stores the velocity and displacement is re-arranged. The equations presented above can be re-written as;

$$\dot{g}_{ij} + d(x_j) g_{ij} = \partial_j v_i \tag{4.40}$$

$$\sigma_{ij} = \lambda \delta_{ij} \sum_k g_{kk} + \mu (g_{ij} + g_{ik}) \tag{4.41}$$

$$\dot{p}_{ij} + d(x_j) p_{ij} = \partial_j \sigma_{ji} \tag{4.42}$$

Equation 4.43 is for the damping profile within the PML zone of Marcinkovich & Olsen (2003).

$$d(x) = \frac{3.5Vs}{w} \left(\frac{x}{w} \right)^2 \left(\frac{8}{15} n - \frac{3}{100} n^2 + \frac{1}{1500} n^3 \right) \tag{4.43}$$

where ,

w is the thickness of MPL, n is the number of grid nodes, and Vs is the harmonic mean of the S-wave velocities of minimum and maximum values presented in the physical model.

4.5. Dynamic Rupture Process

4.5.1. Model Parameters for Dynamic Rupture Process

The rupture zone of 1999 Duzce Earthquake was built as a single plane dipping to the north (strike 265^0, dip 65^0) with the fault dimension of 40.95 km x 12.6 km (Birgören et al., 2004). The fault plane was divided into 52 sub-faults, each 3.15 km x 3.15 km size. Since the dynamic rupture simulation requires much finer grid of source points, before

applying the SORD procedure, an interpolation to the kinematically obtained slip values has been performed. The interpolated slip values and initial stress drop of the Düzce earthquake is given in figure 4.8 and figure 4.9. In this study, the original source area was interpreted as 105 km x 20 km x 70 km size. The interpolated length of each element was 172 m in modeling. Crustal velocity structure from Mindevalli and Mitchell (1989) was adopted. The interpolated new source area is also bent so as to be consistent with the dipping angle of the fault plane. The absorbing boundary condition was applied from the sides and bottom of the medium. Fault plane geometry is given figure 4.10. The fault plane shows simply slip distribution with maximum 5 m offset that close to the hypocenter. Slip distribution was adopted from Birgören et al. (2004). Birgören et al. (2004) found that the best-fitting source model is obtained when the rupture velocity is increased to supershear velocities. Kinematic slip model from Birgören et al. (2004) was used as a reference in order to calibrate our dynamic source parameters so that similar slip distribution and rupture velocity is obtained. To initiate the rupture procedure, stress excess parameter (*Se*) is needed. Since strength excess distribution is not available, hypocenter and its vicinity (3 x 3 km area) is represented as -1 MPa and selected as 6 MPa in the rest of the fault plane. Thus, the initial shear stress is selected which is higher than the initial static fracture, so rupture will be initiated at hypocenter. The outputs *Se* and Dc distributions have been corrected to remove artificial numerical site affects as higher unrealistic asperities at closer free surface. Namely, to prevent the previous unrealistic surface rupture, the Se value has been set equal to 2 MPa in the first 2 km of the shallow part.

The method of Dalguer and Day (2007) SGSN (staggered grid split nodes) was also tested in the beginning which gave more reliable results in studying the faults have 90 degrees of slope. However, this method was not preferred since network structure used for fault with slopes (as seen on Düzce earthquake) which has a defined free surface plane. Instead, SORD was used in this study. Associated software Mpich2 and Phantom, supported by ETH-Zurich, were installed in order to run the main code.

During early stage of the thesis, Andrew code (1980) was adopted to compute initial stress distribution at a fault plane. $\Delta\sigma$ is assumed as the static stress drop for the initial values. While computed stress distribution are compatible with displacement distribution after having run the calculating process, stress values were found.

There are some steps in order to compute stress drop by Andrew (1980) code; first, the total slip distribution values for a defined fault geometry is an input for slip interpolation from the kinematic inversion output. Then, the interpolated strike and dip slip values are going to be input parameters for a Matlab code. This code prepares static stress drop along the strike and down dip components for a given also other input parameters, namely, fault dimension (sampling in x,z) rigidity, and Lame's constant). This program is basically based on Andrews (1980) concept. The final step will be obtain static stress drop in MPa before the SORD procedure. The schematic flow chart is given in Figure 4.7.

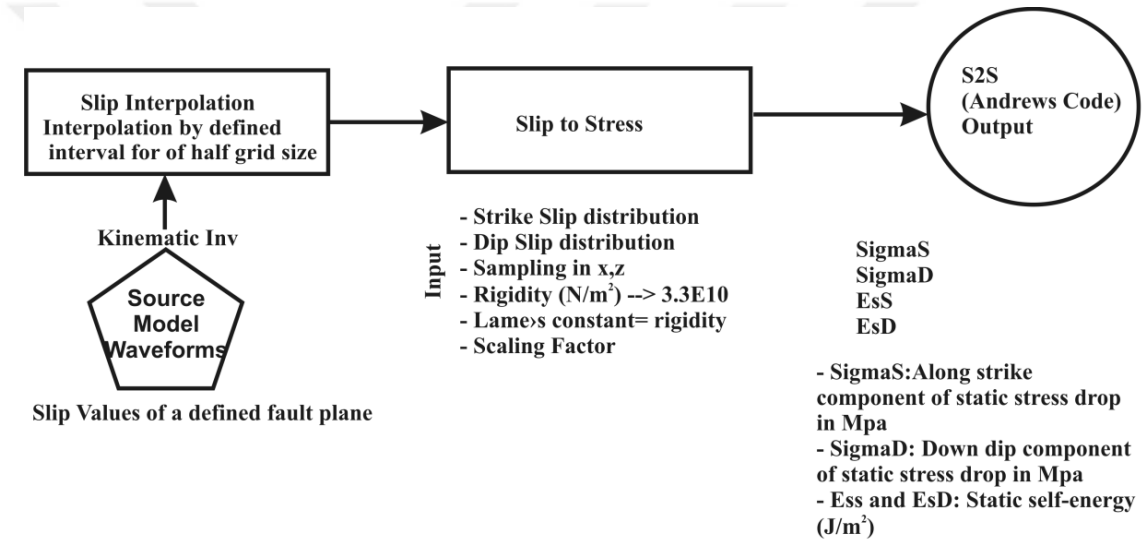

Figure 4.7. Schematic diagram to prepare SORD input.

The rupture is conceded following linear slip dependent friction decrement criteria. The rupture is also initiated spontaneously when an enough amount of energy accumulated and rupture velocity is variable. The initial slip strain, which is of 2% of stress drop at the region defined a 1 km diameter area around the hypocenter was higher than the initial static rupture strain. There by rupture was started at focus. The length of element was 172 m in modeling. The cumulative slip distribution map at the fault plane was obtained after running code SORD by several iterations by also interpretations of the code input and output and changing the input amplitudes. Each run is performed for 40 sec rupture form at computer with 27 processors and a computer with 8 processor bought from project facilities.

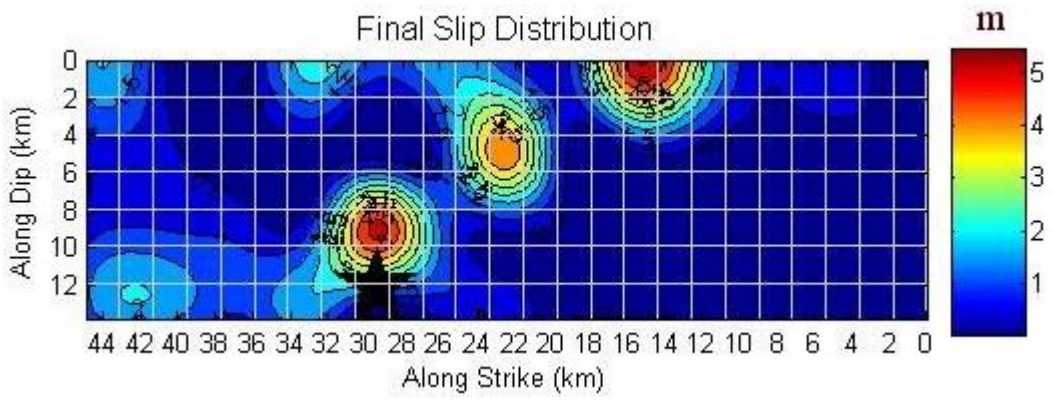

Figure 4.8. Interpolated final slip distribution of Düzce Earthquake.

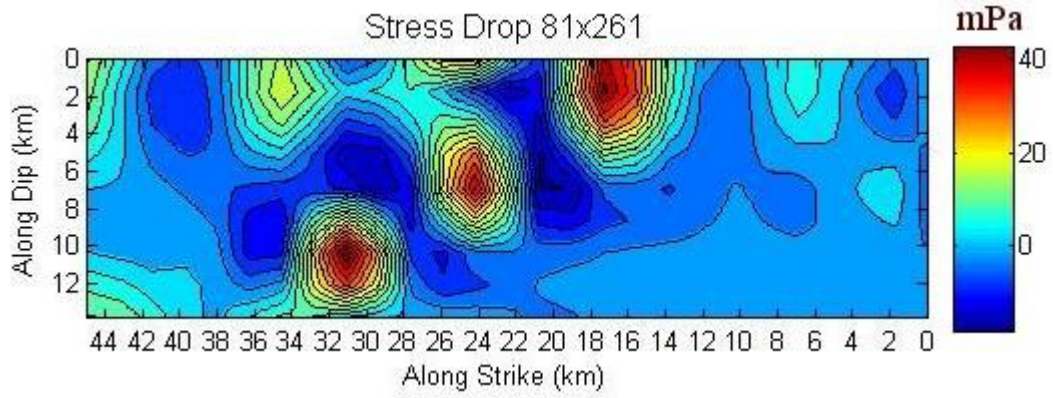

Figure 4.9. Interpolated initial stress drop of Düzce Earthquake.

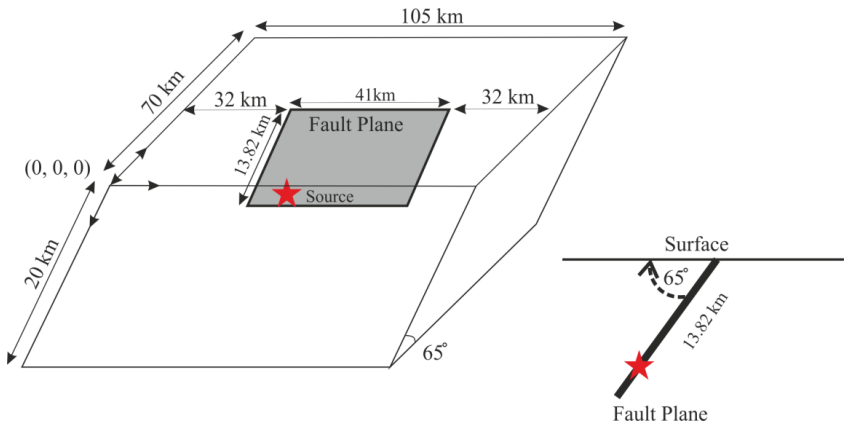

Figure 4.10. Schematic presentation of a fault plane geometry.

Table 4.1. Model Parameters of the underground structure for the SORD (model based on Mindevalli and Mitchell (1989).

Depth (m)	V_p (m/sec)	V_s (m/sec)	Density (kg/m^3)	Q_p	Q_s
0	4690	2710	2430	200	100
1000	4780	2760	2450	200	100
2000	4940	2850	2490	400	200
3000	5150	2970	2530	400	200
4000	5380	3110	2580	500	250
5000	5640	3250	2630	500	250
7000	5870	3390	2670	600	300
9000	6060	3500	2720	600	300
11000	6170	3560	2750	800	400
13000	6230	3600	2770	800	400
15000	6250	3610	2780	800	400
20000	6330	3650	2800	800	400
25000	6550	3780	2860	800	400

Before running SORD, input parameters given were as follows: initial stress (ta0) is ~ 72 Mpa, dynamic friction coefficient μ_d is variable along the fault plane and critical slip distance (Dc) is constant at 0.4 m, while static friction coefficient is 0.6. The parameters Dc is used for the numerical calculations in rupture modeling. The initial slip and stress distribution derived from kinematic model are shown in figure 4.8 and 4.9. At the beginning of the process, (Dkinematic/Ddynamic) *Stressdrop is calculated and the program was run again. A number of dynamic rupture models were used iteratively by trial and error until dynamic slip distribution resembles that of kinematic model (KI). Initial dynamic and model parameters used in SORD processing shows in table 4.1 and table 4.2.

Table 4.2. Initial dynamic parameter used in SORD processing.

	μ_s	μ_d	τ_o	σ_n	D_c	$\Delta\sigma$
Fault Plane	0.6	variable	$\tau_d + \Delta\sigma$	120	0.4	variable

σ_n = Normal stress (Mpa)
D_c = Critical slip distance (m)
μ_s = Static friction coefficient
μ_d = Dynamic friction coefficient
τ_o = Shear Stress (MPa)
$\Delta\sigma$ = Stress Drop (Mpa)

Estimation parameter of stress drop is calculated by iterative dynamic rupture simulation as follow;

Step 1.- Assume an initial stress drop distribution $\Delta\sigma_i$.

Step 2.- Then a dynamic slip distribution (Dd) is calculated from dynamic rupture simulation.

Step 3.- Correct the assumed stress drop $\Delta\sigma_i$ using kinematic slip distribution (Dk)

$$\Delta\sigma_{new} = \Delta\sigma_i \frac{Dk}{Dd}$$

Step 4.- Repeat the procedure (2) and (3) using the new stress drop distribution ($\Delta\sigma_{new}$) by iterative dynamic rupture simulation until Dk/Dd ≈ 1 in areas of large slip.

The initial stress drop distribution of Step 1 is estimated by one of the two following criteria; the one is a kinematic approach, that is, from the entire spatial-temporal kinematic source model calculate the spatial-temporal stress-time function, solving the elasto-dynamic equations of motion. From this stress-time function dynamic stress drop ($\Delta\sigma_i$) can roughly be estimated. The later one assumes arbitrary uniform stress drop distribution. This criterion is adopted when the first criterion fails, that is, when it is not possible to distinguish the dynamic stress drop from kinematic approach. Rupture on the fault plane was achieved by following the linear slip-dependent friction weakening criterion. Rupture initiates as spontaneous when sufficient energy accumulates and the rupture velocity is

variable. The rupture is conceded following linear slip dependent friction decrement criteria. The rupture is also initiated spontaneously when an enough amount of energy accumulated and rupture velocity is variable. The initial slip strain, which is of 2% of stress drop at the region defined a 1 km diameter area around the hypocenter was higher than the initial static rupture strain. There by rupture was started at focus. The length of element was 172 m in modeling. The cumulative slip distribution map at the fault plane was obtained after running code SORD by several iterations by also interpretations of the code input and output and changing the input amplitudes.

4.6. Discussions

In this section, the results of the 1999 Düzce Earthquake simulations based on dynamic rupture methodology to study the properties of dynamic source rupture is discussed. This analysis leads to an efficient investigation of the structural damage pattern caused by the earthquake. The success of the dynamic process substantially depends on parameterization of the model input, which is described by the friction law and stress condition on a fault. For the dynamic processing, these parameters control the full dynamic rupture simulation code, namely SORD.

In the first run; strength excess value was taken as 6 Mpa at the fault area and -1 Mpa around hypocenter to initiate rupture process physically. These parameters did not initiate a rupture as observed from the slip distribution and total rupture time map.

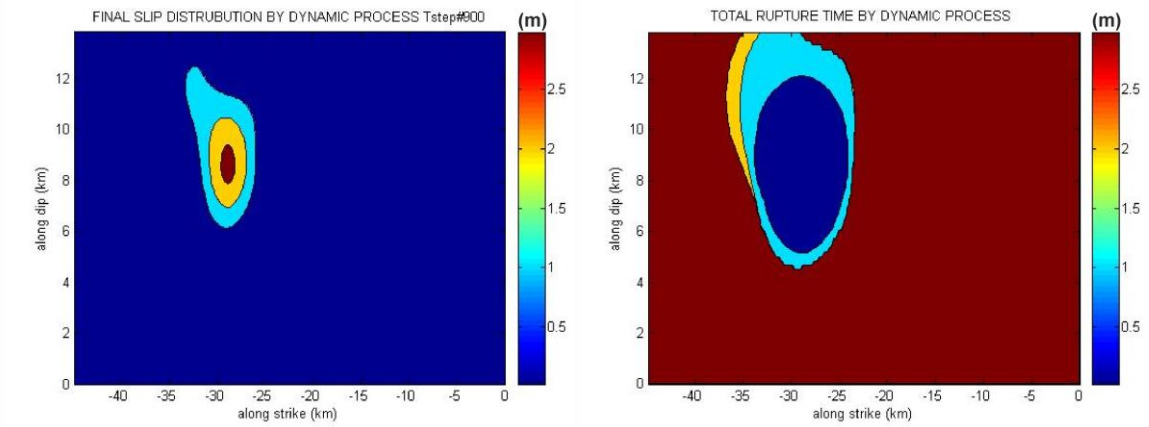

Figure 4.11. Slip distribution and total rupture time by dynamic rupture process for the first process.

In the second run; the slip values from kinematic inversion those smaller than 0.4 m were equalized to 0.4 m. Stress drop values are obtained by a Matlab script, which are then used as the input to SORD to obtain input parameters for the other Matlab script to produce slip distribution and rupture time process.

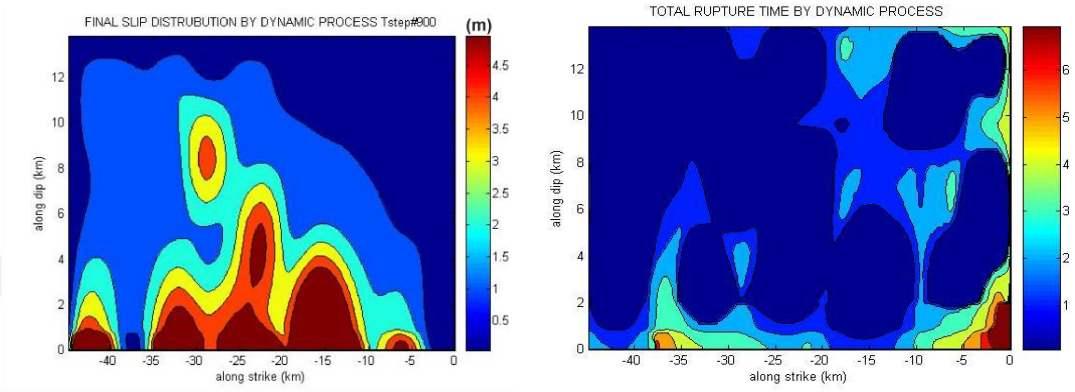

Figure 4.12. Slip distribution and total rupture time by dynamic rupture process for the second process.

In this run strength excess was selected 6 Mpa in the fault plane except hypocenter -1 Mpa. Stress drop values for the first 2 km part of the fault plane from the surface have been selected lower than remaining part of the fault plane.

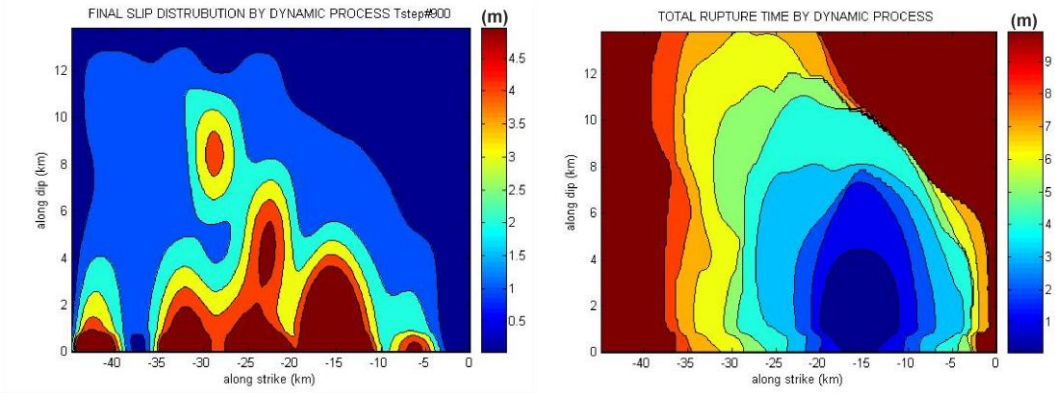

Figure 4.13. Slip distribution and total rupture time by dynamic rupture process for the third process.

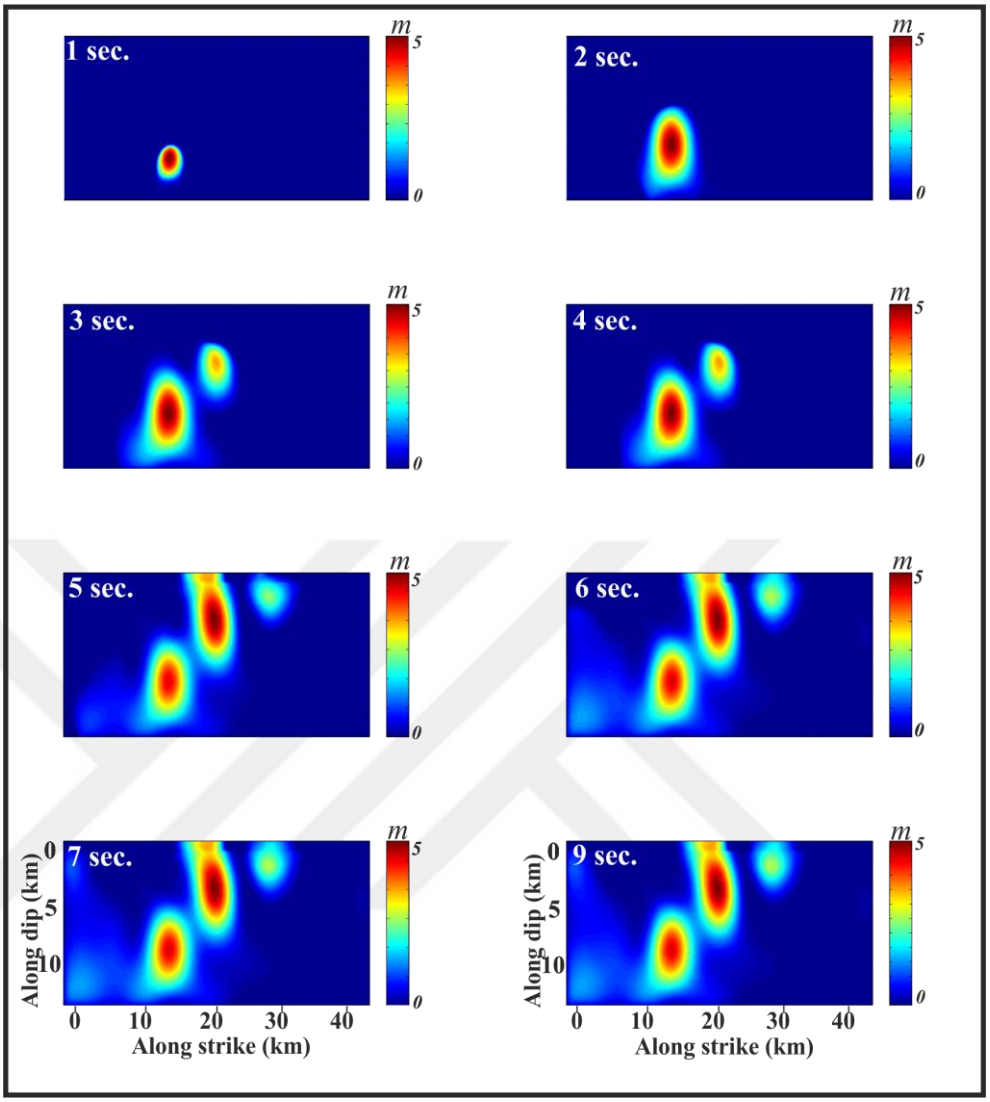

Figure 4.14. Snapshots of dynamic slip distribution.

In the last run; (Dk/Dd)*Stressdrop has been calculated and run again with Dc:0.4 m. Following is the SS and T_{rup}. After the last run, unrealistic asperity areas disappeared and slip values in the hypocenter were found to be smaller. In figure 4.14 the snapshots of accumulated slip on the fault plane are shown at 1s time steps for the rupture simulation of the Düzce earthquake. Each map represents the slip distribution at the time step indicated in each snapshot. The last snapshot in the bottom-right corner is the final slip distribution obtained from the dynamic simulation. Results of the prior kinematic study (Birgören et al., 2004) suggests that there are 3 main slip areas. The first one is a large slip area near the hypocenter. From our dynamic rupture model, the maximum stress drop was estimated about ~ 40 Mpa. Figure 4.15d illustrates the final slip distribution of the fault plane. The

results also show, the largest slip occurred at the ~ 6 km local depth and the high stress drop zone that is presented in Figure 4.15 has been defined as the asperity zone. Total rupture time was found ~ 9 sec (Figure 4.16a). The total earthquake moment is modelled as 1.455E19 Nm which is consistent with kinematic results and Tanırcan et al., (2017), Birgören et al., (2004).

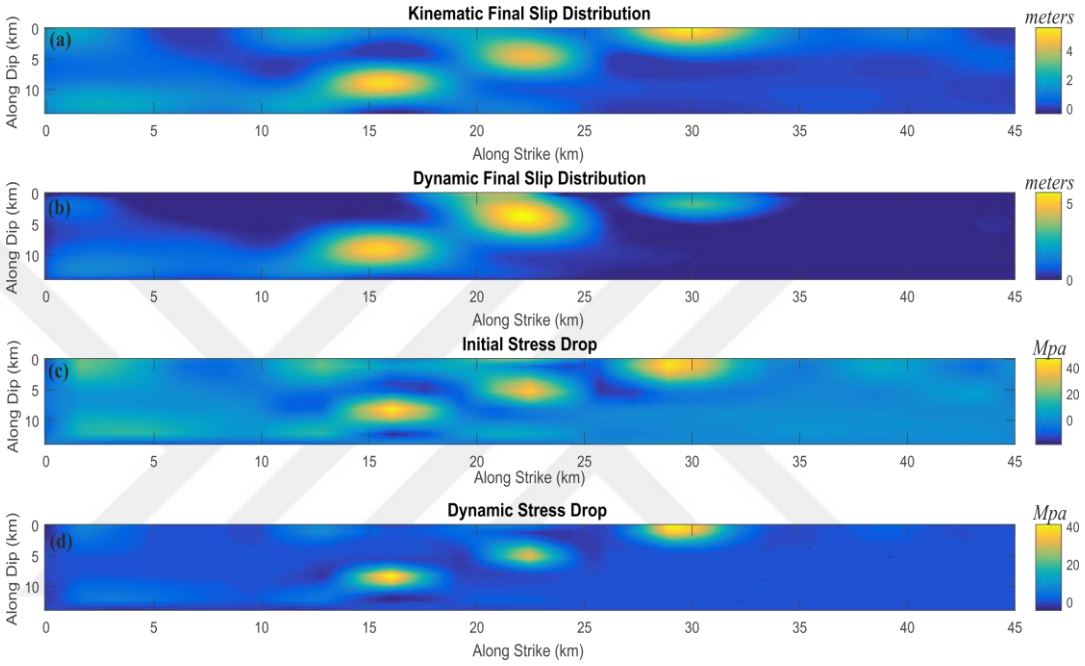

Figure 4.15. Comparison between kinematic (a) and dynamic (b) slip patterns. On the other hand, almost similar distributions between initial stress drop (c) and dynamic stress drop (d) are presented.

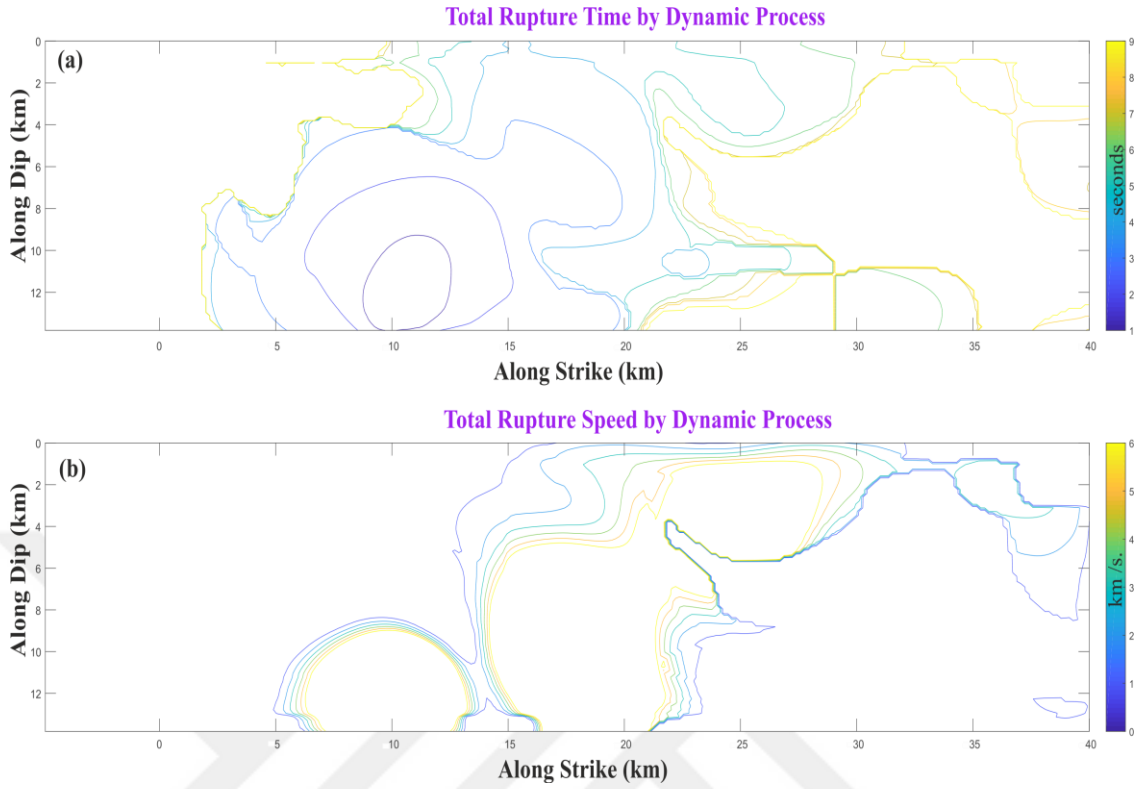

Figure 4.16. Total rupture time (a) and total rupture speed (b) obtained from dynamic process.

Figure 4.16a indicates that the total rupture time distribution from presented dynamic rupture model. According to this outcome, rupture initiates to propagate bilaterally, and then rupture becomes unilateral patters towards the eastern part of the hypocenter. In addition, Figure 4.16b indicates the rupture speed pattern on the fault plane. Initially rupture speed is below mean S-wave velocity, however it seems to be a supershear near the asperities and at the shallow zones.

One major difference between the kinematic and dynamic model is that the rupture velocity is not given a priori for a dynamic model. However, it is possible to modify the parameters such as stress drop and fracture energy (Ma et al., 2008). In this case, by modifying the stress drop, the slip distribution obtained from the kinematic inversion can also be obtained successfully. In addition, the higher rupture velocity toward east naturally comes out of the dynamic rupture simulation. The dynamic rupture simulation shows a very sharp increase in rupture velocity toward east as estimated by prior kinematic models

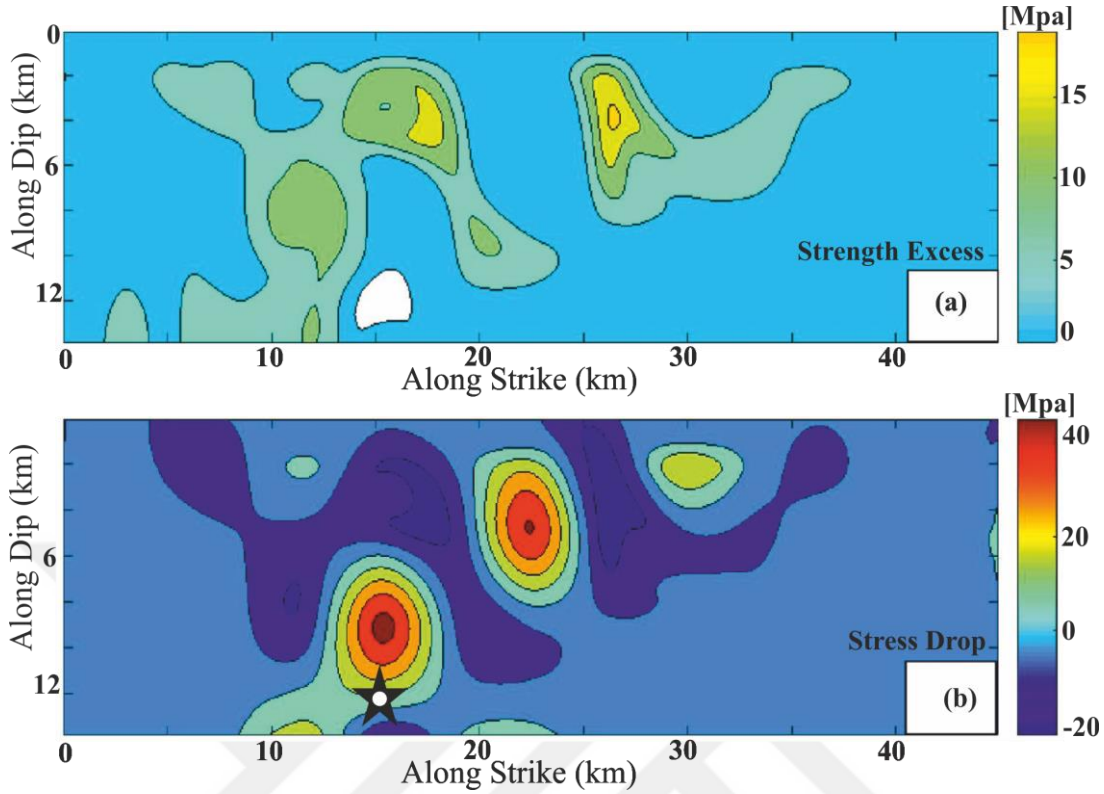

Figure 4.17. Final dynamic rupture model. Strength excess distribution (a) and stress drop distribution (b) (Modified from Tanırcan et al., 2017).

Figure 4.17 shows that, although the dynamic slip distribution and stress drop distributions have a fairly simple homogenous pattern, the rupture time and rupture speed distributions are highly complex. Tanırcan et al. (2017) announced that rupture propagation for Düzce earthquake is crossing the high strength excess zones. For those zones, this pattern can be interpreted as the overloaded asperities can cause ruptured. High slip distribution (asperity) areas and their remaining areas can be expressed as a barrier. (High strength excess area).

Rupture speed and rupture time distributions are compatible with asperity area. Rupture propagate towards the asperity area. High stress drop areas are compatible with asperity areas. There are negative stress drop regions near the edges of asperity area. The finally modelled a distribution map of stress drop and strength excess those can define mainly three asperities for the Düzce earthquake fault plane. Maximum strength excess was found as 19 Mpa at barriers between the asperities and stress drop is about 40 Mpa.

5. CONCLUSIONS

When the examination of the rupture characteristics of the two major earthquakes in 1999 in Turkey (Kocaeli and Düzce events, Mw=7.4 and Mw=7.2, respectively) reveals that these earthquakes propagated at supershear velocity towards east of hypocenter. In this thesis, rupture propagation behavior of the 1999 Düzce earthquakes that reflects the source features of the North Anatolian Fault zone (NAFZ).

The Düzce earthquake was simulated using dynamic rupture approach in order to reveal the effects of dynamic source rupture. Results may assist in the examination of the structural damage pattern due to this earthquake. Birgören et al. (2004) states that friction and stress conditions on the fault plane is defined based on dynamic model parameterization. In this state of art, waveform inversion calculations use near field strong motion data in order to understand slip distribution on the fault plane. These input parameters are used for a dynamic code. A full dynamic rupture simulation code, SORD has been employed for the dynamic rupture processing.

Supershear rupture velocity is dominant particularly at the eastern propagation presented by (Birgören et al., 2004). Western shallower parts of the fault plane were not ruptured during the simulation. The most remarkable output of the dynamic simulation, a rupture was not occurred towards the north-west of the fault plane. In the simulation, it is determined that the western and near-surface section of the fault plane is not ruptured (speed is almost 0). This result can be interpreted as the complete or partial breakage of the region during the Kocaeli Earthquake that took place approximately three months before the Düzce Earthquake. This finding also supports the results of Düzce Earthquake surface displacements (Konca et al., 2010) calculated by SPOT analysis.

Another noteworthy result is that the rupture time toward the eastern at the shallow hypocenter is greater than at the west. Final parameters obtained from dynamic model are consistent with kinematic model with respect to the slip distribution. The dynamic rupture pattern indicates that, from the hypocenter, it appears that, although the initial rupture

seems to be homogeneous, the rupture spreads towards the east for about 2.5 seconds. Rupture becomes unilateral with complex propagation, namely. It is noticed that from the models three asperities were ruptured and the rupture reached the ground within 5–7 s towards the eastern side of the fault plane. The unruptured shallow zone in the western part of fault plane was possibly already (partly or fully) broken before during the August 17, 1999 earthquake. When the rupture velocity in the entire fault plane is calculated, it is seen that the local supershear rupture velocities are reached in the 2nd and 3 asperities close to the surface following fracture of the asperity at hypocenter. Although these speeds are up to 5.6 km/s, the average velocity is found to be around 4.0 km/s.

The slip values of the 1999 Düzce earthquake determined by also kinematic waveform inversion method and dynamic rupture process were obtained by using strong motion records. Slip distribution models on the fault plane indicate a simple circular rupture pattern with decreasing slip values for Manyas, Gemlik and Ereğli earthquakes, respectively. For the Manyas earthquake, the rupture area was estimated to be 2.5 km along strike and 1.5 km along dip zone with an average slip of 0.16 m which matches to a static stress drop of about 8 MPa. The slip concentrates in an almost circular distributed pattern. Two asperities were modeled; for the Gemlik earthquake. One is larger asperity near the hypocenter and another is smaller and located to the deeper part of the fault plane towards the east. The best fitting slip distribution from different parametric models is defined by an average slip of about 0.18 m corresponding to a seismic moment of 9.70E15 Nm with 12 Mpa stress drop. The result shows almost homogenously elongated asperities were modeled during the Ereğli earthquake. For this earthquake, an asperity very close to the hypocenter was observed. On the other at the deeper parts of the fault plane we observe almost smaller asperity in the eastern segment of the plane. We calculated the maximum slip as 0.25 m just near the source and seismic moment as 5.20E16 Nm, which is slightly bigger than that of the above mentioned studies. The static stress drop was calculated as 13 Mpa associated with strike slip faulting.

Earthquake spectral source parameters such as corner frequency, f_{max}, stress drop and source radius are key parameters defining the characteristics of an earthquake source. In the present study, source parameters of 3 local events (Manyas, Gemlik and Ereğli earthquakes) have been estimated A database of broadband recordings of those moderate

earthquakes has been examined by the seismic network of KOERI. The obtained seismic moments range from 1.60×10^{16} to 5.25×10^{16} Nm ($4.7 \leq Mw \leq 5.1$) with corner frequency range between 0.35 and 2.60 Hz. The source radii values are between 690 and 2400 meters and stress drop values vary between 2 and 13 Mpa with respect to station conditions. The results indicate that there are no significant variations at stress drop values computed from kinematic results and source spectrum. Stress ($\Delta\sigma$) drop calculations based on Brune (1970) and Madariaga (1976) indicate that median stress drop values and shear stress drop values are consistent with each other. The faulting type and the moderate size of the studied earthquakes may explain this consistency.

REFERENCES

Aagaard, B. T., 1999, "Finite-element simulations of earthquakes", Technical Report EERL-99-03, California Institute of Technology, *Earthquake Engineering Research Laboratory,* Pasadena, CA.

Abdel-Fattah, A.K, 2002, Source characteristics of a moderate earthquake (M 4.9) using empirical Green's function technique, *Annals of Geophysics*, Vol. 45, No. 5, pp. 575-586

Abercrombie, R. and L. Peter, 1993, "Source parameters of small earthquakes recorded at 2.5 km depth, Cajon Pass, southern California: Implications for earthquake scaling", *Geophysical Research Letters,* Vol. 20, No. 14, pp. 1511-1514.

Aochi, H. and R. Madariaga**,** 2003, "The 1999 Izmit, Turkey, earthquake: Non-planar fault structure, dynamic rupture process, and strong ground motion", *Bulletin of the Seismological Society of America,* Vol. 93, pp. 1249-1266.

Akaike, H., "*Likelihood and the Bayes procedure, in Bayesian Statistics*", edited by J. M. Bernardo et al., pp. 143– 166, Univ. Press, Valencia, Spain, 1980.

Ambraseys, N. N., 2002, "The seismic activity of the Marmara Sea region over the last 2000 years", *Bulletin of the Seismological Society of America,* Vol. 92, No. 1, pp. 1–18.

Ambraseys N.N. and C.F., Finkel, 1991, "Long-term seismicity of Istanbul and the Marmara Sea region, *Terra Nova,* Vol. 3, pp. 527-539.

Ambraseys, N.N. and Finkel, C.F., *Seismicity of Turkey and Adjacent Areas, A historical Review,* 1500-1800. Eren Yayincilik ve Kitapcilik Ltd., 1995.

Aki K. and P.G. Richard, *Quantitative Seismology, Theory and Method,* 2nd. Ed W.H. Freeman and Co., San Francisco, 2002.

Akyuz, H. S., R. Hartleb, A. Barka, E. Altunel, G. Sunal, B. Meyer, and R. Armijo,2002, "Surface rupture and slip distribution of the 12 November 1999 Düzce Earthquake (M 7.1), North Anatolian fault, Bolu, Turkey", *Bulletin of the Seismological Society of America*, Vol. 92, pp. 61– 78.

Alsan, E., L. Tezucan, and M. Bath, *An earthquake catalogue for Turkey for the interval 1913-1970,* Common Report No. 7-75 of Kandilli Observatory, Turkey and Seismic Institute, Uppsala, Sweden, 1975.

Andrews, D.J, 1976, "Rupture velocity of plane-strain shear cracks", *Journal of Geophysical Research,* Vol. 81, pp. 5679-5687.

Andrews, D. J., 1980, "A stochastic fault model: 1. Static case", *Journal of Geophysical Research,* Vol. 85, pp. 3867 – 3877.

Andrews, D. J., 1999, "Test of two methods for faulting in finite-difference calculations", *Bulletin of the Seismological Society of America* 89, No. 4, pp. 931–937.

Archuleta, R., A., 1984, "Faulting model for the 1979 Imperial Valley earthquake", *Journal of Geophysical Research,* Vol. 89, pp. 4559–4589.

Armijo, R., N. Pondard, M. Meyer, G. Uçarkuş, B.M.D. Lépinay, J. Malavieille, S. Dominguez, M.A. Gustcher, S. Schmidt, C. Beck, N. Çağatay, Z. Çakir, C. İmren, K. Eriş, B. Natalin, S. Özalaybey, L. Tolun, I. Lefèvre, L. Seeber, L. Gasperini, C. Rangin, Ö. Emre and K. Sarikavak, 2005, "Submarine fault scarps in the Sea of Marmara pullapart (North Anatolian Fault): implications for seismic hazard in Istanbul", *Geochemistry Geophysics Geosystems,* Vol. 6, pp. Q06009.

Asano, K., T. Iwata, and K. Irikura. 2005, "Estimation of Source Rupture Process and Strong Ground Motion Simulation of the 2002 Denali, Alaska,

Earthquake". *Bulletin of the Seismological Society of America* ,95, No. 5, pp 1701–1715.

Barka, A. and K. Kadinsky-Cade, 1988, "Strike-Slip fault geometry and its influence on earthquake activity", *Tectonics*, Vol. 7, pp. 663-684.

Barka, A., 1992, "The North Anatolian Fault Zone", *Annales Tectonicae,* Vol. 6, pp. 164-195.

Barka, A. A., 1996, "Slip distribution along the North Anatolian fault associated with the large earthquakes of the priod 1939- to 1967", Bulletin *of the Seismological Society of America,* Vol. 86, No. 5, pp. 1238-1254.

Bekler, T. and C. Gurbuz, "Insight into the crustal structure of the Eastern Marmara Region, NW Turkey", *Pure Applied Geophysics*, Vol. 165, No. 2, pp. 295–309.

Benjemaa, M., N. Glinsky-Olivier, V. M. Cruz-Atienza, J. Virieux and S. Piperno, 2007, "Dynamic non-planar crack rupture by a finite volume method", *Geophysical Journal International*, Vol. 171, No. 1, pp. 271—285.

Berenger, J. P., 1994, "A perfectly matched layer for the absorption of electromagnetic waves", *Journal of Computational Physics*, Vol. 114, No. 2, pp. 185–200.

Berenger, J.P., 1996, "Three-dimensional perfectly matched layer for the absorption of electromagnetic waves", *Journal of Computational Physics*, Vol. 127, No. 2, pp. 363–379.

Birgoren, G., H. Sekiguchi, and K. Irikura, 2004, "Rupture model of the 1999 Düzce, Turkey, earthquake deduced from high and low frequency strong ground motion data", *Geophysical Research Letter,* Vol. 31, pp. L05610.

Bizzarri, A., M. Cocco, D.J. Andrews, and E. Boschi E., 2001, "Solving the dynamic rupture problem with different numerical approaches and constitutive laws", *Geophysical Journal International*, Vol. 144, pp. 656 – 678.

Bouin, M.P., M. Bouchon, H. Karabulut, and M. Aktar, M., 2004, "Rupture process of the 1999 November 12 Düzce (Turkey) earthquake deduced from strong motion and Global Positioning System measurement", *Geophysical Journal International*, Vol. 159, No. 1, pp. 207-211.

Bouchon, M., 1981, "A simple method to calculate Green's functions for elastic layered media", *Bulletin of the Seismological Society of America*, Vol. 71, pp. 959–971.

Bouchon, M., M. Bouin, H. Karabulut,M. N. Toksoz, M. Dietrich, and A. J. Rokasis, 2001, "How fast is rupture during an earthquake? New insight from the 1999 Turkey earthquakes", *Geophysical Research Letter*, Vol. 28, pp. 2723– 2726.

Brune, J., 1970, "Tectonic stress and the spectra of seismic shear waves from earthquakes", *Journal of Geophysical Research*, Vol. 75, pp. 4997–5009.

Bürgmann, R., S. Ergintav, P. Segall, E.H. Hearn, S. McClusky, R.E. Reilinger, H. Woith, and J. Zschau, 2002, "Time-dependent afterslip on and deep below the Izmit earthquake rupture", *Bulletin of the Seismological Society of America*, Vol. 92, pp. 126–137.

Carlson, J. and J. Langer, 1989, "Mechanical model of an earthquake fault", *Physical Review A*, Vol. 40, pp. 6470– 6484.

Cochard, A. and R. Madariaga, 1994, "Dynamic faulting under rate-dependent friction", *Pure Applied Geophysics*, Vol. 142, pp. 419– 445.

Crampin, S. and B. Üçer, 1975, "The seismicity of Marmara Sea Region of Turkey", *Geophysical Journal of Royal Astronomical Society*, Vol. 40, pp. 269–288.

Crampin, S. and R. Evans, 1986, "Neotectonics of the Marmara Sea region of Turkey", *Geological Society of London,* Vol. 143, pp. 343-348.

Cruz-Atienza, V.M., J. Virieux, and H. Aochi, 2007, "3D finite-difference dynamic-rupture modelling along non-planar faults", *Geophysics*, Vol. 72, No. 5, pp. 123–137.

Dalguer, L.A., K. Irikura, J.D. Riera, and H.C. Chiu, 2001a, "Fault dynamic rupture simulation of the hypocenter area of the thrust fault of the 1999 Chi-Chi (Taiwan) earthquake", *Geophysical Research Letter*, Vol. 28, No. 7, pp. 1327-1330.

Dalguer, L. A., K. Irikura, J. D Riera, and H. C. Chiu, 2001b, "The importance of the dynamic source effects on strong ground motion during the 1999 Chi-Chi, Taiwan, Earthquake: Brief interpretation of the damage distribution on buildings", *Bulletin of the Seismological Society of America*, Vol. 91, No. 5, pp. 1112-1127.

Dalguer, L. A., K. Irikura, and W. Zhang, 2002, "Distribution of dynamic and static stress changes during 2000 Tottori (Japan) earthquake: Brief interpretation of the earthquake sequences; foreshocks, mainshock and aftershocks", *Geophysical Research Letter*, Vol. 29, p. 16.

Dalguer, L.A., K. Irikura, and J.D. Riera, 2003a, "Simulation of tensile crack generation by three-dimensional dynamic shear rupture propagation during an earthquake", *Journal of Geophysical Research*, Vol. 108, No. B3, p. 2144.

Dalguer, L. A., K. Irikura, and J. D. Riera, 2003b, "Generation of new cracks accompanied by the dynamic shear rupture propagation of the 2000 Tottori (Japan) earthquake", *Bulletin of the Seismological Society of America*, Vol. 93, No. 5, pp. 2236-2252.

Dalguer, L. A. and S. M. Day, 2006, "Comparison of fault representation methods in finite difference simulations of dynamic rupture", *Bulletin of the Seismological Society of America, Vol.* **96**, pp. 1764–1778.

Dalguer, L., A. and S. M., Day, 2007, "Staggered-grid split-node method for spontaneous simulation", *Journal of Geophysical Research,* Vol. 112, pp. B02302.

Das, S. and K. Aki., 1977a, "Fault planes with barriers: a versatile earthquake model", *Journal of Geophysical Research,* Vol. 82, pp. 5648–5670.

Das, S. and K. Aki, 1977b, "A numerical study of two-dimensional spontaneous rupture propagation", Geophysical *Journal of Royal Astronomical Society,* Vol. 50, pp. 643–668.

Day, S. M., 1982a, "Three-dimensional finite difference simulation of fault dynamics: rectangular faults with fixed rupture velocity", *Bulletin of the Seismological Society of America, Vol.* 72**, pp.** 705–727.

Day, S. M., 1982b, "Three-dimensional simulation of spontaneous rupture: the effect of nonuniform prestress", *Bulletin of the Seismological Society of America*, Vol. 72, **pp.** 1881– 1902.

Day, S., M. and L.A. Dalguer, 2005, "Comparison of finite difference and boundary integral solutions to three-dimensional spontaneous rupture", *Journal of Geophysical Research,* Vol. 110, pp. B12307.

Dieterich, J. H., 1978, "Preseismic fault slip and earthquake prediction", *Journal of Geophysical Research,* Vol. 83, pp. 3940– 3946.

Dieterich, J.H., 1979, "Modeling of Rock Friction 1. Experimental Results and Constitutive Equation", *Journal of Geophysical Research, Vol.* 4, pp. 2161-2168.

Dieterich, J. H., D.W. Barber, G. Conrad, and Q. A. Gorton, " Preseismic slip in a large scale friction experiment", Proceedings *US Rock Mechanics*/Geomechanics *Symposium,* Vol. 19, pp. 110–117, 1978.

Dieterich, J., 1994, "A constitutive law for rate of earthquake production and its application to earthquake clustering", *Journal of Geophysical Research: Solid Earth*, Vol. 99, pp. B2c 2018.

Dziewonski, A. M. and D. L. Anderson, 1981, "Preliminary Reference Earth Model", *Physics of the Earth and Planet Interior*, Vol. 25, pp. 297-356.

Ely, G. P., S. M. Day, and J. B. Minster, 2008, "A support-operator method for visco-elastic wave modeling in 3d heterogeneous media", *Geophysical Journal International*, Vol. 172, No. 1., pp. 331–344.

Ergin, K., U. Güçlü, and Z. Uz, *Türkiye ve civarının deprem kataloğu (Milattan Sonra 11 yılından 1964 sonuna kadar*, İTÜ, Maden Fakültesi, Arz Fiziği Enstitüsü Yayınları, No: 24, pp. 169, Istanbul, 1967.

Eugenio M.S.T., B. Selouis, A. Emolo, and A. Zollo, 2013, "Combining strong-motion, InSAR and GPS data to refine the fault geometry and source kinematics of the 2011, M w 6.2, Christchurch earthquake (New Zealand)", *Geophysical Journal International*, Vol. 194, No. 3, pp. 1766-1777.

Eyidoğan, H. and J.A. Jackson, 1985, "Seismological study of normal faulting in the Demirci, Alaşehir and Gediz earthquakes of 1969-70 in western Turkey: implification for the nature and geometry of deformation in the continental crust", *Geophysical Journal of Royal Astronomical Society*, Vol. 81, pp. 569-607.

Eyidoğan, H., 1988, "Rates of crustal deformation in western Turkey as deduced from major earthquakes", Tectonophysics, Vol. 148, pp. 83–92.

Festa, G., *Fault dynamics with spectral elements and slip imaging by isochone back projection*, Ph.D. thesis, Alma Mater Studiorum - Università di Bologna, 2004.

Flerit, F., R. Armijo, G.C.P. King, B. Meyer, and A. Barka, 2003, " Slip partitioning in the Sea of Marmara pull-apart determined from GPS velocity vectors", *Geophysical Journal International*, Vol. 154, pp. 1–7.

Fukuyama, E., and R. Madariaga 1995," Integral equation method for planar crack with arbitrary shape in 3D elastic medium", *Bulletin of the Seismological Society of America*, Vol. 85, pp. 614 – 628.

Fukuyama, E. and R. Madariaga, 1998, "Rupture dynamics of a planar fault in a 3D elastic medium: Rate-and slip-weakening friction", *Bulletin of the Seismological Society of America*, Vol. 88, pp. 1– 17.

Gajewski, D., R. Stangl, K. Fuchs, and K. Sandmeier, 1990, "A new constraint on the composition of the topmost continental mantle: Anomalously different depth increases of P and S velocity", *Geophysical Journal International*, Vol. 103, pp. 497-507.

Geller, R. J., 1976, "Scaling relations for earthquake source parameters and magnitudes", *Bulletin of Seismological Society of America*, Vol. 66, pp. 1501-1523.

Graves, R. et al., 2006, "SCEC CyberShake Platform: incorporating deterministic 3D waveform modeling into probabilistic seismic hazard curves", Seismological *Research Letters*, Vol. 33, p. 302.

Gürbüz C., M. Aktar, H. Eyidoğan, A. Cisternas, H. Haessler, A. Barka, M. Ergin, N. Türkelli, O. Polat, B. Üçer, H.S. Kuleli, S.Barıs, B. Kaypak, T. Bekler, E. Zor, F. Biçmen, and A. Yörük, 2000, "The seismotectonics of the Marmara Region (Turkey): Results from a microseismic experiment", *Tectonophysics*, Vol. 316, pp. 1–17.

Hanks, T.C.,1982, "fmax," *Bulletin of the Seismological Society of America*, Vol. 72, pp. 1869-1879.

Hanks T.C. and H. Kanamori, 1979, “A Moment Magnitude Scale”, Journal of Geophysical Research, Vol. 84, No. B5, pp. 2348-2350.

Haskell, N., 1964, “Total energy and energy spectral density of elastic wave radiation from propagating fault”, *Bulletin of the Seismological Society of America*, Vol. 54, pp. 1811-1842.

Hartzell, S. H. and T. H. Heaton, 1983, “Inversion of strong ground motion and teleseismic waveform data for the fault rupture history of the 1979 Imperial Valley, California earthquake”, *Bulletin of the Seismological Society of America*, Vol. 73, pp. 1553–1583.

Helmstetter, A., Y.Y. Kagan, and D. D. Jackson, 2005, “Importance of small earthquakes for stress transfers and earthquake triggering. Journal of Geophysical Research, Vol. 110, pp. B05S08.

Hisada, Y., 2000, “A theoretical square model considering the spatial variation in slip and rupture velocity”, *Bulletin of the Seismological Society of America*, Vol. 90, pp. 387400.

Ichinose, G. A., D.S. Kenneth, and J.G. Anderson, 1997, “Source Parameters of the 15 November 1995 Border Town, Nevada, Earthquake Sequence”, *Bulletin of the Seismological Society of America*, Vol. 87, No. 3, pp. 652-667.

Ida, Y., 1972, “Cohesive force across the tip of a longitudinal-shear crack and Griffith’s specific surface energy”, *Journal of Geophysical Research*, Vol. 77, pp. 3796 – 3805.

Ikeda, Y., Y. Suzuki, E. Herece, F. Saroglu, A.M. Isikara, and Y. Honkura, 1991, “Geological evidence for the last two faulting events on the North Anatolian fault zone in the Mudurnu Valley, western Turkey”, *Tectonophysics*, Vol. 193, pp. 335–345.

Inoue, T. and T. Miyatake, 1998**, "**3D simulation of near-field strong ground motion based on dynamic modeling", *Bulletin of the Seismological Society of America,* Vol. 88, No. 6, pp. 1445-1456.

Iwata, T., H. Sekiguchi, H. Miyake, W. Zhang W, and K. Miyakoshi, 2004, "Dynamic source parameters and characterized source model for strong motion prediction", *13 th world conference on earthquake engineering Vancouver, B.C.,* Canada August 1-6, pp. 2392.

Kagawa, T., K. Irikura, and P. Somerville, 2004, "Differences in ground motion and fault rupture process between surface and buried rupture earthquakes", *Earth, Planets and Space,* Vol. 56, pp. 3-14.

Kaneko, Y., J.P. Avouac, and N. Lapusta, 2010, "Towards inferring earthquake patterns from geodetic observations of interseismic coupling", *Natural Geosciences,* Vol. 3, pp. 363–369.

Karabulut, H., M. P. Bouin, M. Bouchon, M. Dietrich, C. Cornou, and M. Aktar, 2002, "The seismicity in the Eastern Marmara Sea after the 17 August 1999 Izmit Earthquake", *Bulletin of the Seismological Society of America,* Vol. 92, No. 1, pp. 387–393.

Karabulut, H., S. Ozalabey, T. Taymaz, A. Aktar, O. Selvi, and A, Kocaoglu, A., 2003, "A tomographic image of the shallow crustal structure in the Eastern Marmara", *Geophysical Research Letters,* Vol. 30 pp. 2277.

Karabulut, H., J. Schmittbuhl, S. Özalaybey, O. Lengliné, A. Kömeç-Mutlu, V. Durand, M. Bouchon, G. Daniel, and M.P. Bouin, 2011, "Evolution of the seismicity in the eastern Marmara Sea a decade before and after the 17 August 1999 Izmit earthquake", Tectonophysics, Vol. 510, pp. 17–27.

Kase, Y. and S. M. Day, 2006, "Spontaneous rupture processes on a bending fault", *Geophysical Research Letters,* Vol. 3, p. L10302.

Kennett, B. L. N. and N. J Kerry, 1979, "Seismic waves in a stratified half-space", *Geophysical Journal Royal Astronomical Society*, Vol. 57, pp. 557–583.

Kinscher, J., F. Krüger, W. Woith, B. Lühr, E., Hintersberger, T. Irmak, and S. Baris, 2013, "Seismotectonics of the Armutlu peninsula (Marmara Sea, NW Turkey) from geological field observation and regional moment tensor inversion", *Tectonophysics*, Vol. 608, pp. 980-995.

Kohketsu, K., 1985, "The extended reflectivity method for synthetic nearfield seismograms", *Journal of the Physics of the Earth*, Vol. 33, pp. 121-131.

Kostrov, B.V., 1966, "Unsteady propagation of longitudinal shear cracks", *Journal of applied Mathematics and Mechanics*, Vol. 30, pp. 1241–1248.

Konca, A. O., S. Leprince, J. F Avouac, and D. V, Helmberger, 2010, "Rupture Process of The 1999 Mw=7.1 Düzce Earthquake from Joint Analysis of SPOT, GPS, INSAR, Stong Motion and Teleseismic Data: A Supershear Rupture with Variable Rupture Velocity", *Bulletin of the Seismological Society of America*, Vol. 100, No. 1, pp. 267-288.

Kurtulmuş, T.Ö. and N. Akyol, 2013, "Crustal attenuation characteristics in western Turkey", *Geophysical Journal International*, Vol. 195, No. 2, pp. 1384-1394.

Kuşçu, I., M. Okamura, H. Matsuoka, K. Yamamori, Y. Awata, and S. Özalp,2009, "Recognition of active faults and step over geometry in Gemlik Bay, Sea of Marmara, NW Turkey", *Marine Geology*, Vol. 260, pp. 90–101.

Lawson C. L. and Hanson RJ, *Solving Least Squares Problems*, Prentice Hall, Englewood Cliffs, NJ, 1974.

Le Pichon, X., C. İmren, C. Rangin, C., A.M.C. Şengör, and M. Siyako, 2014, "The South Marmara Fault", *International Journal of Earth Sciences*, Vol. 103, No. 1, pp. 219–231.

Ma, S. and S. Custodio, R.J. Archuleta and P. Li, 2008, "Dynamic modeling of the 2004 Mw 6.0 Parkfield, California", *Journal of Geophysical Research*, Vol. 113, pp. 1-16.

Madariaga, R., 1976, "Dynamics of an expanding circular fault", *Bulletin of the Seismological Society of America*, Vol. 66, pp. 639–666.

Madariaga, R., K. B. Olsen, and R. J. Archuleta., 1998, "Modeling dynamic rupture in a 3-D earthquake fault model", *Bulletin of the Seismological Society of America*, Vol. 88, pp. 1182– 1197.

Makropoulos, K.C. and Burton, P.W., 1981, "A catalogue of Seismicity in Greece and the Adjacent Areas", *Geophysical Journal of Royal Astronomical Society*, Vol. 65, pp. 741-762.

Marcinkovich, C. and K. Olsen, 2003, "On the implementation of perfectly matched layers in a three-dimensional fourth-order velocity-stress finite difference scheme", *Journal of Geophysical Research*, Vol. 108, No. B5, p. 2276.

Marsan D., 2005, "The role of small earthquakes in redistributing crustal elastic stress", *Geophysical Journal International*, Vol. 163, pp. 141-151.

METI, 2004, "Final report of METI's project".

Mikumo, T. and T. Miyatake, 1978, "Dynamical rupture process on a three-dimensional fault with non-uniform frictions, and near-field seismic waves," *Geophysical Journal of Royal Astronomical Society*, Vol. 54, pp. 417-438.

Mindevalli, O. Y. and B. J. Mitchell, 1989, "Crustal Structure and Possible Anisotropy in Turkey from Seismic Surface Wave Dispersion", Geophysical Journal International, Vol. 98, pp. 93-106.

Mohammadioun, B. and L. Serva, 2001, "Stress Drop, Slip Type, Earthquake Magnitude, and Seismic Hazard", *Bulletin of the Seismological Society of America* Vol. 91, pp. 694-707.

Ohnaka, M., Y.K. Kuwahara, and K. Yamamoto, K., 1987, "A constitutive law for the shear failure of rock under lithospheric conditions"**,** *Tectonophysics,* Vol. 144**,** p. 10.

Ohnaka, M., 1990, "Nonuniformity of crack-growth resistance and breakdown zone near the propagating tip of shear crack in brittle rock: A model for earthquake nucleation to dynamic rupture", *Canada Journal of Physics,* Vol. 68, pp. 1071–1083.

Ohnaka, M. and L. F. Shen, 1999, "Scaling of the shear rupture process from nucleation to dynamic propagation: Implications of geometric irregularity of the rupturing surfaces", *Journal of Geophysical Research,* Vol. 104, pp. 817–884.

Oglesby, D. D., R.J. Archuleta, and S.B. Nielsen, 2000, "The three-dimensional dynamics of dipping faults", *Bulletin of the Seismological Society of America*, Vol. 90, No. 3, pp. 616–628.

Olsen, K. B., R. Madariaga, and R. Archuleta, 1997, "Three dimensional dynamic simulation of the 1992 Landers earthquake", *Science, Vol.* 278**, pp.** 834–838.

Okay, I.A., E. Demirbağ, H. Kurt, N. Okay, and İ. Kuşçu, 1999, "An active, deep marine strike-slip basin along the North Anatolian fault in Turkey", *Tectonics,* Vol. 18, No. 1, pp. 129-147.

Okubo P. G., 1989, "Dynamic rupture modeling with laboratory − derived constitutive relations", *Journal of Geophysical Research,* Vol. 94, No. B9, pp. 12321 – 12335.

Okubo, P. G., and J. H. Dieterich, 1984, "Effects of physical fault properties on frictional instabilities produced on simulated faults", *Journal of Geophysical Research*, Vol. 89, 5817–5827.

Örgülü, G., 2011, "Seismicity and source parameters for small-scale earthquakes along the splays of the North Anatolian Fault (NAF) in the Marmara Sea", *Geophysical Journal International*, Vol. 184, pp. 385-404.

Peyrat, S., K. Olsen, and P. Madariaga, 2001, "Landers earthquake", *Journal of Geophysical Research*, Vol. 106, No. 26, pp. 467– 26,482.

Pfannenstiel, M., 1944, "Diluviale Geologie des Mittelmeergebietes: Die diluvialen Entwicklungsstadien und die Urgeschichte von Dardanellen, Marmarameer und Bosporus. Ein Beitrag zu den klimatisch bedingten eustatischen Spiegelschwankungen des Mittelmeeres", *Geologische Rundschau*, Vol. 34, pp. 334–42.

Pınar, N., *Marmara Denizi Havzasinin Sismik Jeoloji ve Meteorolojisi*" PhD Thesis. Institut de Géologie, Institut de Physique Générale de l'Université d'Istanbul, Kenan Matbaasi, Istanbul, p. 64., 1943.

Pınar, N. and E. Lahn, 1952, "Türkiye depremleri izahlı katoloğu", *Bayındırlık Bakanlığı, Yapı ve İmar İşleri Reisliği Yayınları*, Vol. 6, No. 36, p. 153.

Rebollar C.J., L. Quintanar, R. Castro, S. Day, J. Madrid, J.N., Brune, L. Astiz, and F. Vernon, 2001, "Source characteristics of a 5.5 magnitude earthquake that occurred in the transform fault system of the Delfín Basin in the Gulf of California", *Bulletin of Seismological Society of America*, Vol. 91, pp. 781-791.

Reilinger R.E., S.C. McClusky, B.J. Souter, M.W., Hamburger, M.T. Prilepin, A. Mishin T. Guseva, and S. Balassanian, 1997, "Preliminary estimates of plate convergence in the Caucasus collision zone from global positioning system measurements", *Geophysical Research Letters*, Vol. 24, pp. 1815–1818.

Ruina A. L., 1983, “Slip instability and state variable friction laws”, *Journal of Geophysical Research,* Vol. 88, pp. 10359-10370.

Sekiguchi, H., K. Irikura, and T. Iwata, 2000, “Fault geometry at the rupture termination of the 1995 Hyogo-ken Nanbu earthquake”, *Bulletin of the Seismological Society of America*, Vol. 90, pp. 117– 133.

Sekiguchi, H. and T. Iwata, 2002, “Rupture process of the 1999 Kocaeli, Turkey, earthquake estimated from strong notion waveforms”, *Bulletin of the Seismological Society of America*, Vol. 90, pp. 300–311.

Sellami, S., N. Pavoni, D. Mayer-Rosa, S. Mueller, H. Eyidogan, M. Aktar, C. Gurbuz, S. Baris, O. Polat, and N. Yalcin, *Seismicity And Seismotectonics Of The Bursa Region, In: Active Tectonics Of Northwestern Anatolia*-The Marmara Poly-Project, (Eds. Shindler, C. And Pfister, M.) (Hochschulverlag Ag An Der Eth Zurich-Swiss, 1997) P. 449–486, 1997.

Samarskii, A., V. Tishkin, A. Favorskii, and M. Shashkov, 1981, “Operational finite difference schemes”, *Differential Equations,* Vol. 17, pp. 854–862.

Samarskii, A., V. Tishkin, A. Favorskii, and M. Shashkov, M., 1982, “Employment of the reference-operator method in the construction of finite difference analogs of tensor operations”, *Diff. Equations*, Vol. 18, pp. 881–885.

Sharma M. L. and H.R. Wason, 1994, “Occurrence of Low Stress Drop Earthquakes in the Garwal Himalayan Region”, *Physics of the Earth and Planetary Interiors*, Vol. 85, No. 3-4, pp. 265-272.

Shashkov, M., *Conservative Finite-Difference Methods on General Grids*, CRC Press, Boca Raton, FL., 1996.

Sivaram, K., D.D. Kumar, and S.S. Teotia, 2013, "Source parameters and scaling relations for small earthquakes in Kumaon Himalaya", *Journal of Seismol*, Vol. 17, pp. 579.

Somerville, P.G., K. Irikura, R. Graves, S. Sawada, D. Wald, N. Abrahamson, Y. Iwasaki, T. Kagawa, N. Smith, and A. Kowada, 1999, "Characterizing crustal earthquake slip models for the prediction of strong ground motion", *Seismological Research Letters*, Vol. 70, pp. 59-80.

Somerville, P.G., 2003, "Magnitude scaling of the near fault rupture directivity pulse", Physics of the Earth and Planetary Interiors, Vol. 137, pp. 201-212.

Sosyal, H., S. Sipahioğlu, D. Kolçak, and Y., Altınok, *Türkiye ve Çevresinin Tarihsel Deprem Kataloğu, (M.O. 2100 - M.S. 1900)*, TÜBİTAK Proje No:TBAK-341, İstanbul, 1981.

Stein, R. S., A. A. Barka, and J. D. Dieterich, 1997, "Progressive failure on the North Anatolian fault since 1939 by earthquake stress triggering", *Geophysical Journal International*, Vol. 128, pp. 594-604.

Straub, C., *Recent crustal deformation and strain accumulation in the Marmara Sea region, NW Anatolia, inferred from GPS measurements*, PhD. Thesis, Institut für Geodesie und Photogrammetrie, Mitteilungen Nr. 58, Zürich, 1996.

Straub, C., H. G. Kahle, and C. Schindler, 1997. "GPS and geological estimates of the tectonic activity in the Marmara Sea region, NW Anatolia", *Journal of Geophysical Research*, Vol. 102, No. 27, pp. 587-27.

Swiss Seismological Service, SED, 2006, ETH Zurich, http://www.seismo.ethz.ch

Şaroğlu, F., Ö. Emre, and İ. Kuşçu, Active *Fault Map of Turkey at Scale 1:1 000 000*, Mineral Research and Explorations Institute of Turkey Publication, Ankara, 1992.

Tanırcan, G., L. Dalguer, F.N. Bekler, and N.M. Özel, 2017, "Dynamic Rupture Modelling of the 1999 Düzce, Turkey Earthquake", *Pure and Applied Geophysics*, Vol. 174, pp. 3343-3355.

Taymaz, T., J.A. Jackson, and D. McKenzie, 1991, "Active tectonics of the north and Central Aegean Sea", *Geophysical Journal International*, Vol. 106, pp. 433-490.

Taymaz, T., *Symposia On Seismotectonics of the North-Western Anatolia-Aegean and Recent Turkish Earthquakes*, Scientific Activities - 2001, Istanbul Technical University, Faculty of Mines, May 8, 2001, ATLAS DBR -Offset Printing House, Istanbul, Turkey, 113, 2001.

Tsukuda, E., E. Herece, and İ. Kuşçu, 1988, "*Some geological evidence on activity of the Western Anatolian Fault, Geyve, Iznik, Gemlik area",* ITIT Project: 8513, 68-91.

Umutlu, N., K. Koketsu, and C. Milkerit, 2004, "The rupture process during the 1999 Düzce, Turkey, erathquake from joint inversion of teleseismic and strong ground-motion data", *Tectonophysics*, Vol. 391, pp. 315-324.

Utkucu, M., S. Nalbant, J. McCloskey, S. Steacy, and Ö. Alptekin, 2003, "Slip Distribution and Stress Changes Associated with the 1999 November 12, Düzce (Turkey) Earthquake (Mw=7.1)", *Geophysical Journal International*, n ,Vol. 153, pp. 229-241.

Üçer, B., *Marmara Bölgesinin deprem etkinliği ve aktif tektonikle ilişki*, Doktora Tezi, İstanbul. Üniversitesi, 1990.

Yagi, Y. and M. Kikuchi, 1999. "Source rupture process of the Kocaeli, Turkey, earthquake of August 17, 1999, obtained by joint inversion of near-field data and teleseismic data". *Geophysical Research Letter*, Vol. 27, pp. 1969– 1972.

Yoshida, S., K. Koketsu, B. Shibazaki, T. Sagiya, T. Kato, and Y. Yoshida, 1996, "Joint inversions of near-and far-field waveforms and geodetic data for the rupture

process of the 1995 Kobe earthquake", *Journal of Physics of the Earth*, Vol. 44, pp. 437– 454.

Yoshida, S., 1995, "Waveform Inversion Methods for the Earthquake Source", *Journal of Physics of the Earth,* Vol. 43, pp. 183-209.

Vilotte, J., G. Festa, and R. Madariaga, 2005, "Spectral element simulations of rupture dynamics along kinked faults", *Eos Trans. AGU*, Vol. 86, No. 52, Fall Meeting.

Virieux, J. and R. Madariaga., 1982, "Dynamic faulting studied by a finite difference method, *Bulletin of the Seismological Society of America,* Vol. 72, pp. 345-369.

Wald, D. J. and T. H. Heaton, 1994, "Spatial and temporal distribution of slip for the 1992 Landers, California, Earthquake", *Bulletin of the Seismological Society of America*, Vol. 84, pp. 668– 691.

Wells, D. L. and K. J. Coppersmith, 1994, "New empirical relationships among magnitude, rupture length, rupture width, rupture area, and surface displacement", *Bulletin of the Seismological Society of America*, Vol. 84, pp. 974-1002.

Zhang, W., T. Iwata, K. Irikura , A. Pitarka, and H. Sekiguchi, 2003, "Dynamic rupture process of the 1999 Chi-Chi, Taiwan, earthquake", *Geophysical Research Letter,* Vol. 31, p. L10605.

Zhang, W., H. Sekiguchi, and M. Bouchon, 2004, "Heterogeneous distribution of the dynamic source parameters of the 1999 Chi-Chi, Taiwan, earthquake" *Journal of Geophysical Research,* Vol. 108, p. B5, 2232.

Zhang, W., T. Iwata, and K. Irikura, 2006, "Dynamic simulation of a dipping fault using a three-dimensional finite difference method with nonuniform grid spacing", *Journal of Geophysical Research,* Vol. 111, p. B05301.